Evaluation of the Effect of a Modified Wedge Geometry on the Behavior of Mono-Strand Post-Tensioning Anchorages

By

Patrick Charles McAlpine

Thesis
Submitted to Department of Civil Engineering
College of Engineering
Villanova University
In partial fulfillment of the requirements
For the degree of

MASTER OF SCIENCE
In
Civil Engineering

August, 2014

Villanova, Pennsylvania

Statement by the Author

This thesis has been submitted in partial fulfillment of requirements for an advanced degree at the Villanova University and is deposited in the University Library to be made available to borrowers under rules of the Library.

Brief quotations from this thesis are allowable without special permission, provided that accurate acknowledgment of source is made. Requests for permission for extended quotation from or reproduction of this manuscript in whole or in part may be granted by the head of the major department or the Associate Dean for Graduate Studies and Research of the College of Engineering when in his or her judgment the proposed use of the material is in the interests of scholarship. In all other instances, however, permission must be obtained from the author.

Acknowledgements

This research was all made possible by Villanova University. I would specifically like to acknowledge my advisor, Dr. Eric Musselman, for being a critical partner and guide throughout this research. I would also like to acknowledge my second reader Dr. Shawn Gross. Additionally, I owe the Villanova Structures Lab employees, George Pappas and Jeff Cook, thanks for all of their help setting up and running my tests. Finally, thanks are owed to Dr. David Dinehart for his guidance starting in my undergraduate career that led me to this point.

I would also like to acknowledge Hayes Engineering for providing all of the testing material and allowing me to work with their wedges. They were extremely supportive of this research and were a great resource.

Dedication

To my family and my friends, you have always kept me motivated and on track. Without you I would not have been able to persevere in the way I have.

Table of Contents

Abstract

The objective of this study is to create and evaluate if finite element modeling is a feasible approach to modeling different wedge geometries of post tensioned systems by comparing the experimental data from two wedges to analytical data. The motivation to develop an accurate finite element model of a wedge, tendon, and anchor system is to better understand the internal stresses the system is subjugated to and the interactions between components. By not fully understanding what is occurring within the anchor, the most efficient anchor cannot be designed. This can lead to premature failures of the strand which can result in total collapse of the structure. In recent years the applications of post tensioned strands have grown rapidly. Some of these applications require the strand to withstand higher strains than can currently be reached. An example of one of these applications is a shear rocking wall in earthquake prone areas. To date there is some experimental data on strand testing, but very little research has been conducted examining a modified geometry wedge. There is even less in depth literature on finite element modeling of the interactions between the components. One reason for this lack of research is because of the great variability in anchor and wedge configurations. Therefore, the focus of this research is to develop the interaction laws for one type of anchorage from one manufacturer. Once these laws are established and considered scientifically sound, the most efficient anchor wedge mechanism can be designed.

This thesis presents one of the stepping stone models needed to help converge on the interaction laws. The experimental component of this report evaluated two different wedge geometries. In the experimental trials the modified wedges preformed more efficiently than the standard wedges. The modified wedges were able to reach much higher strains. These geometries were modeled in a finite element program and the experimental results were

replicated by adjusting the interaction relationships. The starting point for the relationships were based off of the studies found in the literature review. The results from analytical model of the standard wedges matched the experimental results very accurately. The analytical model of the modified wedge requires refinement. The results of the analytical model did not match the experimental observations as well as they should. However, the results still support the theory that the computer software can differentiate between standard and modified wedge geometries.

List of Tables

List of Figures

List of Variables

V = Voltage

σ = Stress

Δ_g = Relative Displacement of Grip

ε_o = Original Strain

σ_o = Original Stress

σ_T = True Stress

Δ_w = Wedge Seating

$\mu\varepsilon_{rg}$ = Micro Strain Relative Grip

Δ_a = Anchor Displacement

Δ_f = Frame Displacement

Δ_{f*} = Adjusted Frame Displacement

$\mu\varepsilon_{fin}$ = Final Strain

Δ_a = Anchor Displacement

$m_{(a,w)}$= Slope (Anchor, Wedge)

b = Intercept

x_x = x Variable

y_y = y Variable

P = Load

$\mu\varepsilon_f$ = Micro Frame Strain

$\mu\varepsilon_0$ = Micro Zeroed Strain

0_{fac} = Zero Factor

Chapter 1: Introduction

1.1 Overview

Post tensioning systems have multiple applications. They can be used in slabs, shear walls and even beams. Generally post-tensioning is carried out to increase the strength of the member by reducing the tension within the concrete. These strands can be used individually or in a bundle, which is known as a multi-strand system. The steel strands are subjected to extreme tensile forces. Being anchored at the ends, it is the part of the strand that interacts with the anchorage that generally fails, resulting in a decreased capacity. If the anchorage system could be improved, the ductility and capacity of the strand system would be increased.

This increased ductility is extremely useful in certain applications. One such application is rocking shear walls in seismic areas. The post-tensioning acts as a self-centering mechanism for the building. The strand flexes with the building, so the higher the ductility, the more durable the system. Generally, capacity is improved by elongation the wedges, which distributes the stress more evenly over the grip. Recently, there has also been experimentation with changing the angle of the wedge and increasing the wedge crown size.

It has recently been noticed that by adjusting the geometry of a wedge in a post tensioned anchorage system, the strain limit of the strand can be greatly increase. This discovery has led to new geometries being developed and tested to attain a more durable design. To test these different geometries, each wedge type must be manufactured and destructively tested. This type of trial testing is expensive due to the destructive nature of the tests and the cost of manufacturing a small number of wedges with unique geometries. With today's technology it may be more practical to conduct computer simulations of the tests. This requires the construction of a numerical model that accurately represents the post tension anchorage's

internal mechanisms. An additional benefit of having a finite element model is that different aspects can be examined that are not observable in a destructive test. Things such as how the stress develops and the stress distribution at failure can be observed within a model. There has been very limited research in the area of finite element modeling of the anchors, and no research that has examined the effect of anchorage geometry using a finite element model. This study will construct two four piece models and compare their outputs to real destructive testing. The goal of conducting such comparisons is to assess if numerical modeling is a feasible option for future wedge geometry development.

1.2 Objectives

In accordance with the research needed in this area, the primary objectives of this report are as follows:

(1) To acquire test data and evaluate the performance for three wedge shapes through the accepted destructive testing method.

(2) To construct finite element models of two of the wedge shapes and assess if a finite element model is a feasible way to analyze wedges.

(3) To recommend adjustments for future models and determine if it is feasible to test different wedge geometries using an analytical model.

1.3 Scope and Approach

This study presents three different criteria for wedge comparison: (1) failure stress-strain relationship of the strand, (2) wedge displacement, and (3) anchor strain. These criteria will be used to compare the experimental tests to each other and to compare the experimental tests to the analytical results. There will also be three wedge types experimentally tested, (1) Standard, (2)

Modified, and (3) Modified Long. Only the two standard length wedges will be modeled and analytically assessed to determine if numerical modeling is a feasible method of comparison.

1.4 Organization of Thesis

Following this chapter, the reader will find background information that is useful for understanding the basis for this study. Chapter 3 contains a literature review which discusses previous studies that pertain to post tensioning anchorages and the modeling of such systems. Chapter 4 describes the testing equipment and procedure used in this study. The experimental results are reduced and compared in Chapter 5. Finally, the building of the two models is explained and a comparison between the models themselves and their respective experimental counterparts is carried out in Chapter 6. The study then concludes with a summary, which includes final remarks and recommendations for future projects.

Chapter 2: Background

2.1 Post Tension Anchorages

Post tension anchorages play an increasingly large part in modern civil engineering. The original concept of a post tensioning structures was introduced in the late 1800's but was not utilized until 1951, in the construction of the Walnut Lane Bridge in Philadelphia (Dinges 2009). The technique began to resurface in the late 1980's as the post tensioning method was rapidly refined and advanced. With the introduction of new high performance concrete and improved materials and procedures, the post tensioning process became a more practical option for use in structures (D. Marceau 2004). The system can now be utilized in multiple different structural applications including bridge decks, floor slabs, and shear walls. The system of post tensioning can also be used in new structures or in rehabilitation projects. As the post tensioning method is more frequently used in the industry it is imperative to expand the understanding of the mechanisms within a post tensioning system, specifically the un-bonded post tension strand's anchor mechanism. This understanding will lead to better application of post tensioning systems and to more advanced configurations.

The mechanism of an un-bonded post tension strand is a rather simple system to understand on a theoretical level. There are two types of systems that essentially have the same type of anchoring mechanism but different longitudinal characteristics. The first method requires running a strand through a cavity left in a concrete mass. The second method requires the strand to be greased and concealed in a plastic sheathing. The concrete mass is then poured around the sheathed strand. Regardless of the longitudinal characteristics, the strand is then anchored at either end of the concrete mass using steel anchors and wedges. There is no transfer of loads between the concrete mass and the strand along the length of the strands, all the load is

transferred at the anchor heads. The strand is tensioned using hydraulic jacks. The tensioning of the strand imparts a force on the concrete mass that puts the concrete into a compressed stress state. This can be seen in figure 2.1. Since concrete is always stronger in compression, this procedure greatly increases the capacity of the concrete mass. The applied service forces must first overcome the compression caused by the post tensioning before it can impart a tension stress on the concrete and create a failure. The issue with this design is that the anchorage system of the strand must withstand all of the initial tensioning force plus any additional tension cause by the applied loads, which can be substantial.

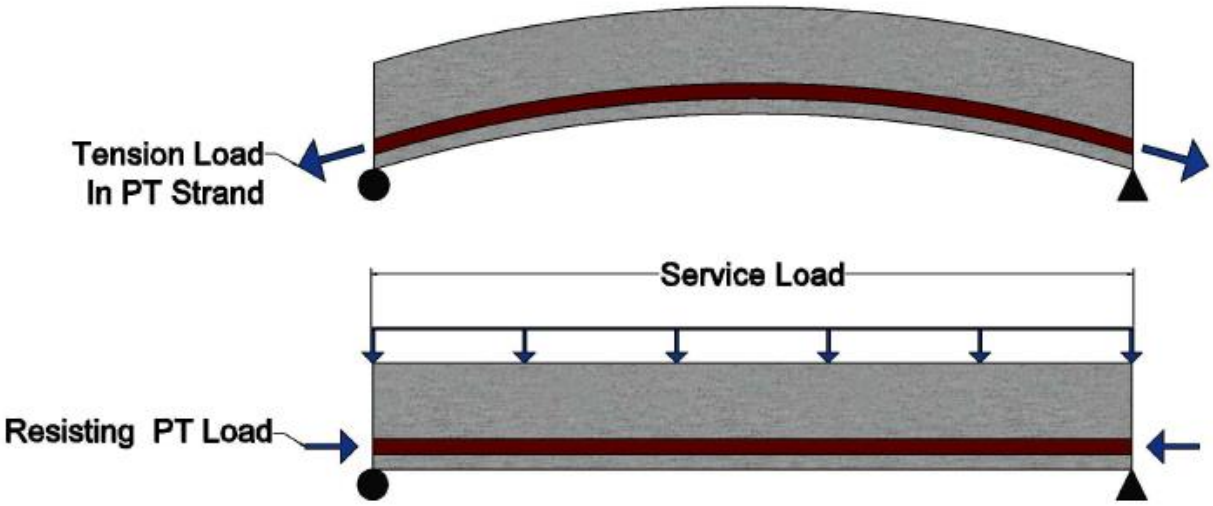

Figure 2.1: Post Tensioned strand Mechanism

The anchorage that must withstand this tension force is generally comprised of three main components. There is the anchor which is attached to the concrete mass through the second component, a bearing plate. The bearing plate evenly distributes the load over an area on the concrete mass. This diffuses stress concentrations around the anchor that would cause the concrete to crush. For some monostrand systems, the anchor and bearing plate are combined into one component. This component is referred to as a cast anchorage. These anchorages are not

utilized in this study but they are prevalent in the industry. Arguably the most critical component of the anchor mechanism is the wedge. The wedge grips the strand and transfers the tension force to the anchor which in-turn transfers to the bearing plate and concrete mass. The wedge grips the strand by utilizing small teeth that dig into the strand. The outside of the wedge is sloped so as the wedge is pulled down into the anchor, the teeth are forced into the strand and create a stronger gripping force.

There are many different styles of anchors and wedges for many different applications and load ranges. Some wedges are divided into thirds while others are divided in into halves (Figure 2.2a). Some anchors have a forged base plate, while others are a simple cylinder. There are also multi-strand anchorages and single strand anchorages (Figure 2.2a&b). The type of wedge and anchor set up that is utilized depends on the application of the system.

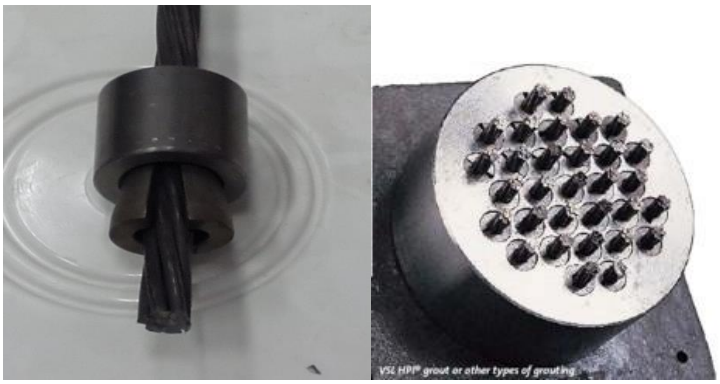

a b

Figure 2.2: Different Anchorages

An issue of standard testing and uniform results arise from these multiple configurations. It is expensive and time consuming to carry out destructive tests of all the different configurations, so it is proposed that defining a procedure for finite element modeling may be a solution. This model would allow the repetitive testing of an anchor under different conditions

and greatly expedite the research procedure. It would also allow for the model to be tested in other geometries and wedge configurations.

2.2 Wedge Principles

A key aspect of this study pertains to the geometry of the wedges being tested and modeled. Recently there has been the development of new modified wedges. (Patent No. US 7765752 B2) These wedges were developed by Norris O. Hays and Randy Draginis and are present in the testing population for this study. The wedges utilize two main principles: the principle of gap control and the principle of angle differential. Both of these principles and the prior research pertaining to them will be discussed at length in the Chapter 3; however a brief background on the mechanics involved is required.

The principle of gap control refers to the gap that is present between the two wedges within an anchor. This gap allows the wedges to move closer together as they are drawn down into the anchor. This allows the teeth of the wedge to more deeply grip the strand as higher loads are imparted. This additional space for movement also ensures that the wedges will not come into contact and prevent themselves from gripping the strand causing a pull out failure. This seems in theory to be a reasonable model; however, in practice it does not hold true. As the wedges are pushed deeper into the strand, stress concentrations begin to develop around the deformations caused by the teeth of the wedges. The research presented in Chapter 3 shows that the strand's strength can be fully developed within the length of the wedge with a reduced penetration of the teeth, which results in lower stress concentrations and higher failure strength for the system. This reduction of penetration is achieved by using a wedge that has a larger crown. The wedges come into contact with each other as the load on the system is increased, which prevents the teeth from penetrating further. At the time that the wedges engage each other,

the strand is sufficiently gripped to prevent a pull out failure. This larger crown width is one feature of the modified wedge.

The principle of angle differential pertains to the method the wedge engages the strand. The standard practice is to design wedges that have the same angle as the anchors with which they are being used. This creates a system where all the teeth of the wedge engage the strand at the same time. This means that there is more area that the stress can be transferred over. This should cut down on stress concentration, which it does, but it also introduces a new stress that is internal to the wedge. As higher strains are reached, the strand wants to be able to elongate, such is the definition of strain. If the wedge has fully engaged the strand there is no room for the portion of the strand in the wedge to elongate. This causes a tension force that is isolated to the wedge and can cause cracking.

The modified wedge has an angle that differs from that of the anchors. This angle differential prevents all of the teeth from simultaneously engaging the wedge. At the beginning of the loading sequence, only the teeth at the top of the wedge are engaged with the strand. As higher loads are reached, the wedges slowly deform and bend with-in the anchor. This deformation allows for the strand with-in the anchor to elongate as it is gripped. This prevents the internal stresses from building up in the wedges and causing failure.

2.3 Finite Element Modeling

The development of a finite element model is desirable because once the interactions within the anchorage system are understood, the geometry of the system can be altered to simulate different cases and determine an optimal wedge/anchorage configuration. Once a desired result is obtained, the geometry can be produced and tested in the lab. This will save time and materials by reducing the need to produce multiple geometries. If the lab results coincide

with the predicted results, it can be assumed that the model was a success and that the geometry at hand is the most durable. The system can then be put into field use. This method would save countless resources, materials, and man hours.

Finite element modeling is a practice that has been gaining ground as computers become more powerful. It allows a designer to run multiple iterations of a model without destroying any physical materials. The designer can also vary or hold constant different variables that allow for almost an infinite amount of different tests to be run from one base model. Furthermore, valuable internal information such as internal strain distributions, stress concentrations, or percentage of the yielded volume can be obtained from a given model. These aspects cannot be observed from laboratory testing (J. Bastien 2007). The reason for this is because there is no way to see what is occurring within the anchor in a physical test. In a finite element model, the anchor can be cut in half and an internal view is accessible. There is a clear benefit to developing these types of models, but it is not always an easy task. There can be multiple parts to a model, such as a tri-wedge anchor system, and it must be ensured that the parts interact in the model in the same way as they would in the real world.

The process of generating a model begins in the laboratory with destructive testing. These tests give initial conditions that can be defined within a model to ensure the model represents the real physical behavior. For a wedge, anchor, and strand model some limits that are needed are wedge seating, stress in the anchor, and ultimate strength of the tendon. Once these parameters are obtained, a computer model of each component is generated and meshed. The mesh allows the stress distribution to be calculated over the component. When the model is assembled, the interactions between components must be defined. It is this that causes most of the difficulty in generating an accurate model for a post-tension anchorage.

There has been little research conducted on the interaction of the components of a wedge-anchor system. The research that has been done will be covered in Chapter 3 and contribute to the ultimate goal of developing a working model. The important aspect to understand is that there are three interactions to be concerned with; the anchor and plate, wedges and anchor, and wedges and strand. These are the three interactions along the load path as load is transferred from the strand to the concrete mass and therefore it is imperative that they are represented correctly (D. Marceau 2003).

Once these interactions have been defined, the model can be loaded and compared to the range of data obtained through experimental testing in the lab. If the model produces the same results as the laboratory test than it is acceptable and can be modified to test other conditions. This is the ultimate goal of creating the finite element model.

Chapter 3: Literature Review

There is limited documented research focused on the behavior of un-bonded post tension anchorages. There has been even less effort made in the process of developing a finite element model that accurately represents the mechanisms within an anchor. This literature review will describe the previous research which was used to inform and develop the current research program as well as provide the theoretical background for a finite element model of an un-bonded post tension strand. All the following information has been published and is considered scientifically sound.

3.1 Strand Anchorage Testing

The most comprehensive study available was conducted at the University of Notre Dame in Indiana. It was titled *Behavior and Design of Unbonded Post-Tensioning Strand/Anchorage Systems for Seismic Application.* (Walsh and Kurama 2009). The motivation for such testing was the sudden failure of a single strand with-in a tendon in a post tensioned shear wall in an earthquake area. This single failure substantially reduced the capacity of the strand and its damping properties. In the study multiple different configurations of mono-strand anchorages were tested. The different variables that were altered were strand diameter, anchor type, anchor physical properties, number of wedge pieces, and the presence of a binding ring around the wedges. Different loading configurations were also evaluated. The configurations that were tested are load rate, eccentricity of anchor heads, cyclic loading, and initial stressing of the strand (Walsh and Kurama 2009). The objective of the study was to evaluate which set up yielded the greatest ductility. Ductility is a critical aspect to the damping properties of a strand in this application. The study also wished to test the validity of the industry testing requirements and ensure that they were sufficient.

This study is considered to be the most inclusive and modern study to date. The experimental program and observation processes that will be used in the following testing method are based off of Walsh and Kurama's procedure. There was only one study conducted prior to Walsh and Kurama that was focused on the behavior of post-tensioned anchorages. It was a study conducted by Schechter and Boecker in 1971. The data from that 1971 study may be outdated given: the likelihood that material manufacturing and usage have changed in the past four decades, the anchor components tested are not common today, the "dynamic" testing was done at much lower stress levels than are pertinent today, and multi-strand anchorages were used (Walsh and Kurama 2009). It was these factors and the fracture of strands at the wedge within the anchor that motivated the investigation of the anchor mechanism.

The results developed during the testing of Walsh and Kurama will be compared to the results developed during this study to ensure that the procedure was followed correctly and that the base values for the computer model are accurate. The same free length fracture test that Walsh and Kurama used was conducted on the .5 inch diameter strand that is present in this study. The material properties are independent of the anchor so the free length stress strain curves that were acquired by Walsh and Kurama 2009 (Figure 3.1) should resemble the curves obtained by this study. The results will vary slightly given that the strand is not identical, however the curves will be similar.

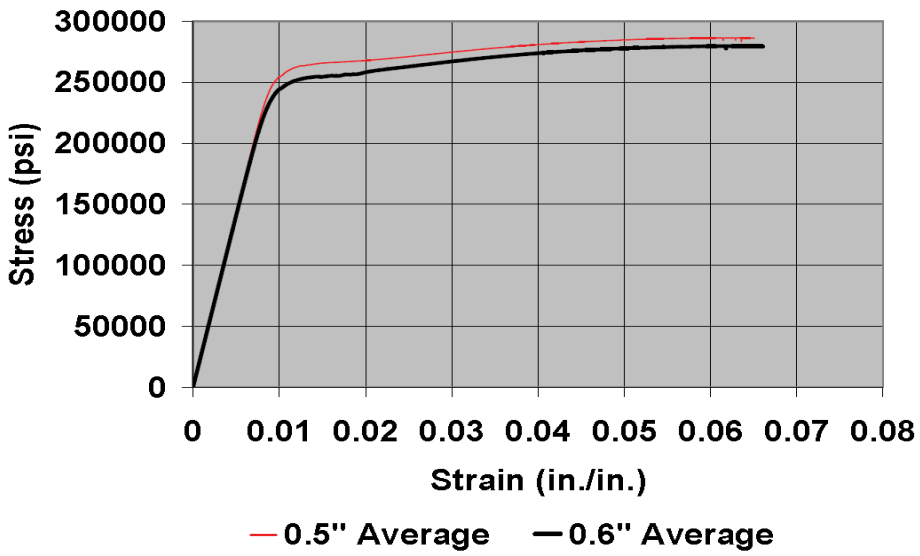

Figure 3.1: Average Stress Strain Curve for 0.5 and 0.6 Strands (Walsh and Kurama 2009)

Walsh and Kurama did use anchor barrels and wedges similar to those present in this study, however they were milled by a different company and may differ slightly in geometry. Therefore there may be discrepancies between the results.

Walsh and Kurama did not evaluate the effect of modified wedge geometry on the performance of the anchorage system, as the study at hand has done, but rather focused on the comparison of different systems to each other and to the accepted standard at the time. Their results were generalized into three different bulleted points:

(1) A strand strain design limit of 0.01 in/in should be used for structures in seismic areas, since premature strand wire fractures can limit the lateral strength, stiffness, ductility, and self-centering capability of unbounded post-tensioned structures.

(2) The current ICC-ES loading procedure for observing post yield behavior does not allow the strand to enter into the post yielded state. A higher limit should be applied to the fifty cycle test.

(3)The post-yield cyclic loading of a strand, such as the impact of a seismic event, have the largest contribution to a lowering of average fracture strains within the anchor system. In summary their study concluded that the current standard was not adequate for classifying the performance of post tension strands. They recommended that the standards be revised and that more testing conducted to reduce the standard deviation of strand properties. The final recommendation of the study was that more research should be put into understanding the failure mechanism inside the anchorage and wedge system. Ideally the model developed by this studywill yield some understanding of that mechanism.

The testing procedure that will be followed is defined in Acceptance Criteria for Post-tensioning Anchorages and Couplers of Prestressed Concrete (ICC-ES 2007). The specific procedure is outlined in Chapter 4. The main aspect that will be drawn from ICC-ES 2007 is the displacement rate that should be maintained during the loading procedure, which is 0.197 to 0.887 inches per minute for a 42 inch long strand. Additionally this specification denoted a pre-load not in excess of 1000 lbs. The specification called for a 36 in extensometer to be used to record the strain experienced by the strand. However, previous research has demonstrated that in the case of unbonded post tension strands, extensometer gage length does not appreciably affect the strain measurements (Walsh and Kurama 2009). For this reason, a uniaxial strain gage will be place on one individual wire with-in the strand. Once the anchor has fully engaged the strand, the single wire accurately represents the strain in the entire strand.

3.2 Modified Wedges

K.Q. Walsh and Y.C. Kurama along with the aid of two others conducted a later study that focused on the impact of modified wedges on the ultimate capacity of a post tension anchorage system. The report was titled, *Effects of Anchor Wedge Dimensional Parameters on*

Post-Tensioning Strand Performance (Walsh and Kurama 2013). This study focused solely on the principles of wedge angle differential and gap control through increased crown thickness. Both of these modifications to wedges have been patented by Norris O. Hayes and Randy Daginis (Patent No. US 7765752 B2). Since two different variations of modified wedges are present in this study, it is important to understand the differences they have from the standard wedge.

3.2.1 Taper Angle Differential

The first principle that Walsh and Kurama investigated was the "Wedge Taper Angle Differential" (Walsh and Kurama 2013). In the current practice of manufacturing wedges, it is typical that the outside angle matches that of the inside angle of the receiving anchor. The current accepted standard angle for these wedges and anchors is 7 +/-0.5 degrees; however it is practice to not allow the angle to deviate more than .33 of a degree from the standard 7 (Patent No. US 7765752 B2). This congruency of angles forces the wedge to pinch the strand at the tapered end of the wedge. Walsh and Kurama suggest that increasing the angle from 7 to 8 degrees would substantially reduce this stress concentration. Over exaggerating this angle will have adverse effects. A comparison of visual evidence represented by imprints on post tested anchors can be seen below: (Figure 3.2)

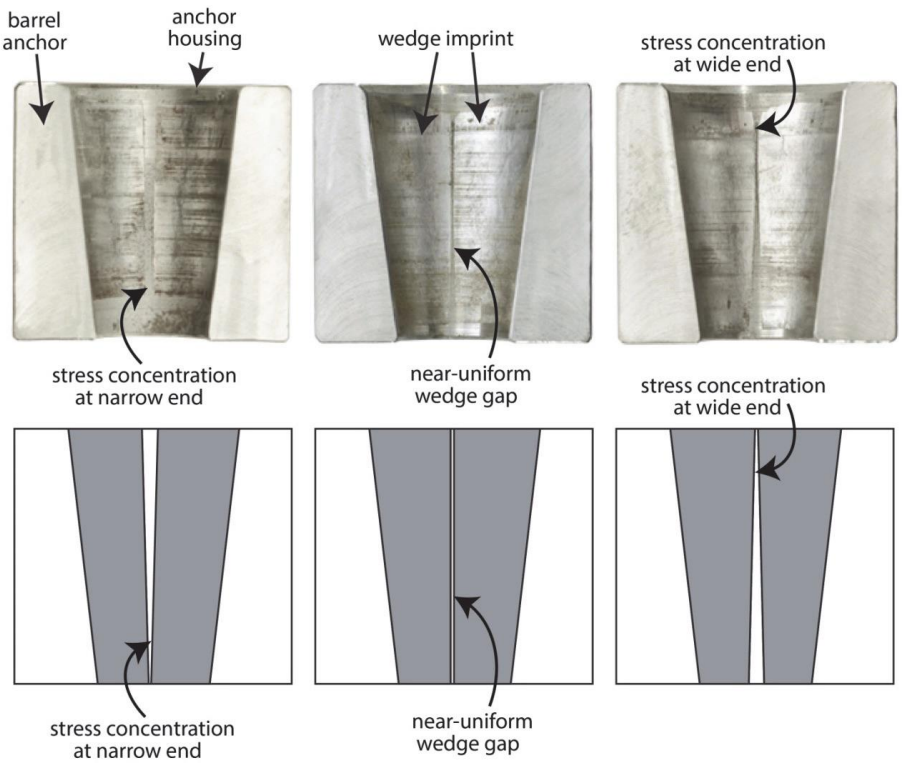

a) standard taper b) optimal high taper c) over taper

Figure 3.2: Visual Evidence of Wedge Alignment (Walsh and Kurama 2013)

The gap in the imprints show where most of the pressure is being transferred from the wedge to the anchor. With the standard and over tapered edges it is obvious that there are stress concentrations building up at the bottom and top of the wedges, respectively. However when the optimal taper wedge is inspected it can be observed that the imprint lines are nearly parallel the entire length of the anchor. This is evidence of a more uniform stress distribution compared to the other two tapers (Walsh and Kurama 2013).

Walsh and Kurama summarized their findings on modified wedges in five bullet points outlined below:

1) Increasing the wedge taper angle by roughly 1 degree and increasing the crown thickness can significantly improve the ultimate performance of the strand-anchorage

system by increasing the strand ultimate strains at failure and potentially reducing the variance in ultimate strains.

2) Visual evidence suggests that there is an improved distribution of stress transfer within the anchor zone when using modified wedges as compared to standard wedges.

3) Outer wire slippage should be avoided and multiple wire fractures should be sought for improved performance within the effective ranges of the recommended geometries and quality control tolerances.

4) As an important consideration, increasing either the wedge taper angle or crown thickness too far outside of the effective ranges can lead to reduced ultimate strains and increased variability. Therefore, quality control measures should be specified when producing such wedges.

5) It is suggested that two piece wedges may be more desirable than three piece wedges for the sake of eased gap control.

Daniel Abramson also observed these phenomena in his study titled *Comprehensive Evaluation of Multistrand Post-Tensioning Anchorages Systems for Seismic Resilient Rocking Wall Structures* (Abramson 2013). Abramson was studying different configurations of wedges and anchors that would improve the durability of multi-strand post tensioning systems within shear walls. Abramson attributed the stress concentration to the fact that when the anchor engages the strand uniformly, there is no room for elongation within the wedge. This means that strain is concentrated at the nose of the wedge since strain elongation is halted there. With the increase of the angle from 7 to 8 degrees, the wedge is able to grip the strand sequentially from the back to the nose (tapered end) as the load increases. This changes the way the teeth engage the strand and allows for the strand to elongate within the anchor as more load is added until

failure. (Abramson 2013) This means that the elongation is distributed over the wedge rather than concentrated at the nose. This distributes the stress more evenly. (Figure 3.3)

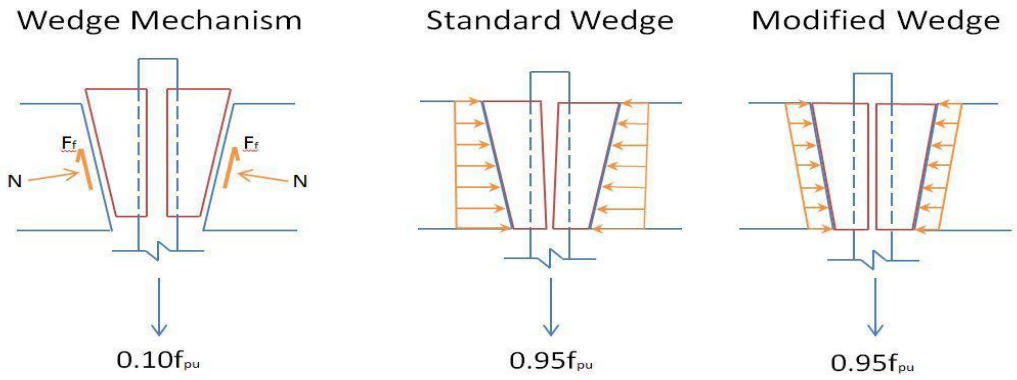

Figure 3.3: Force Mechanism and Stress Distribution (Abramson 2013)

Abramson also observed evidence of the disadvantageous effects of simultaneous gripping when the tested wedges were examined. As seen in Figure 3.4, there were different crack patterns on the physical wedges. The standard wedges, Figure 3.4a, had a straight line tension crack that cut through the wedge. This signified that there was an internal tension force within the wedge. When this crack occurs, the wedge loses the gripping capability of the top segment of the wedge. This will reduce the capacity of the anchor. When viewing the modified wedge, Figure 3.4b, spider web cracking is observed. This indicates a flexural deformation of the wedge. As higher loads were reached the wedge deformed to fully engage the strand. This means that the gripping capacity increased as the load demand increased (Abramson 2013).

a) Standard Wedge

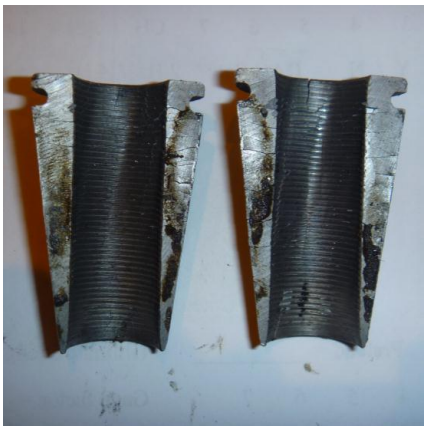

b) Modified Wedge

Figure 3.4: Comparison of Wedge Cracking (Abramson, 2013).

3.2.2 Gap Control

The principle of gap control has the same effects as taper control. The method is mentioned by both Walsh and Kurama 2013 and Abramson 2013. The generally accepted wedge, the standard wedge, is designed to remain in a near "free floating" position inside the anchor housing cavity. The reason for this is to prevent the wedges from coming into contact even when the strand is fully loaded. (Walsh and Kurama 2013) If the wedges came into contact they would be prevented from sinking down into the anchor and fully gripping the strand. This would leave the system with the potential for a pull-out failure.

Alternatively, Hayes and Draginis have designed a wedge with a larger crown (US Pat. No. 20090205273A1). This larger crown actually allows the wedge pieces to come into contact. The wedges are designed to ensure that the contact occurs after the strand is fully engaged by the wedge. This contact prevents the wedge from over penetrating the strand and inducing extra stress concentrations into the strand. Additionally, the contact means that the entire perimeter of the strand is engaged by the wedge, helping to dissipate the stresses being transferred over the wedge (Abramson 2013). Similar to the wedge taper angle differential, the crown thickness has a

range of suitable values. For a 0.5 inch strand the crown thickness is about 0.488 (Walsh and Kurama 2013). If the crown is thicker than this value, a pull out failure becomes a concern.

3.3 Finite Element Modeling

3.3.1 Wedge Anchor Studies

For the finite element modeling of the wedge and anchor system, there has not been a study conducted on the scale of the Walsh and Kurama 2009 study. However there have been multiple small scale studies. (D. Marceau 2004, A. Chabert 2001, J. Bastien 2007, D. Marceau 2003). The main focus of these studies was gaining an understanding of the interaction characteristics between the different parts of the strand anchorage system. In most of these studies, Coulomb's friction theory was applied to the surfaces of the wedge and anchor and the anchor and the plate. The interaction between the strand and the wedge was modeled multiple ways.

The earliest study and modeling of the anchor-wedge system is A. Chabert (2001). The paper specifically deals with an experimental and numerical study of a mono-strand wedge-anchor head mechanism (A. Chabert 2001). The study was conducted using mono-strand anchorages and three part wedges, which can be seen in Figure 3.5.

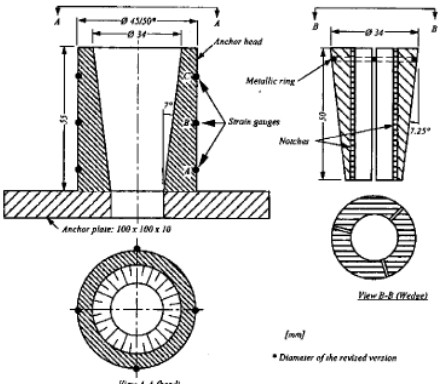

Figure 3.5: Anchor-Wedge Assembly (A. Chabert 2001)

The first part of the numerical study, a calibration procedure based on experimental results, leads to the determination of frictional coefficients acting at the diverse interfaces (wedge-anchor head interface and anchor head-plate interface). These coefficients were then placed into a model of a standard anchor mechanism and a modified anchor mechanism (A. Chabert 2001). The experimental tests were run on a universal testing machine. The concept of an equivalent wedge was introduced at this experimental stage. This equivalent wedge was a standard representation of a wedge and strand interaction at the time, especially for studies that were focused on the anchor stresses rather than the wedge mechanism, as this study was. According to A. Chabert 2001, Bastien (1992) has shown that, under loading, the strand and wedge act together and therefore their behavior can be accurately represented by a monolithic component presenting an outer conical shape similar to a wedge (A. Chabert 2001). This substitution eliminates the strand-wedge interaction and greatly simplifies the model and results. Therefore, there was no actual wedge and strand present in the experiment. The forces were imparted to the anchor by compression on the equivalent wedge rather than tension on a strand. Once the strains over the loading procedure were collected, a numerical model was developed.

An elastic-plastic material behavior pattern was applied to the anchor and the anchor plate. This material model was used because the main objective of the numerical study was to assess if there were any permanent (plastic) strains developed within the anchor. Assigning simple elastic properties to the components would not allow for such deformation. Since the focus of the study was not the wedge and because the wedge acts mainly as stress imposer, the equivalent wedge that was used in the experimental procedure was modeled as a perfectly elastic material. This assumption is justified by the very hard surface of the wedge due to heat treatment (A. Chabert 2001).

Since an equivalent wedge was used, the strand and wedge interaction was eliminated from the entire scope of this project. However, the frictional coefficients used for the surface interactions were extremely useful for the current study. It was found that the frictional coefficient could be ranged from 0.10 to 0.12 for the interaction between the equivalent wedge and the anchor head (A. Chabert 2001). The coefficient was varied from 0.08 to 0.10 and it was observed that this caused a 70% decrease in axial and circumferential strains. However, it was also found that the design prestressing load could not be reached for certain coefficients. After all of these aspects were taken into consideration, a frictional coefficient of 0.11 was used for the wedge-anchor interaction (A. Chabert 2001).

A rigid plate was used during the experimental procedure and therefore, normal steel friction coefficients were used between the anchor and steel bearing plate. These coefficients varied from 0.20 to 0.30 and appeared to have a negligible influence on the development of strains, stresses and wedge slippage. According to these results the frictional coefficient between the anchor head and the standard anchor plate could be taken as 0.25 (A. Chabert 2001). The comparison of the numerical models using different coefficients of friction between the wedge and anchor can be seen in Figure 3.6.

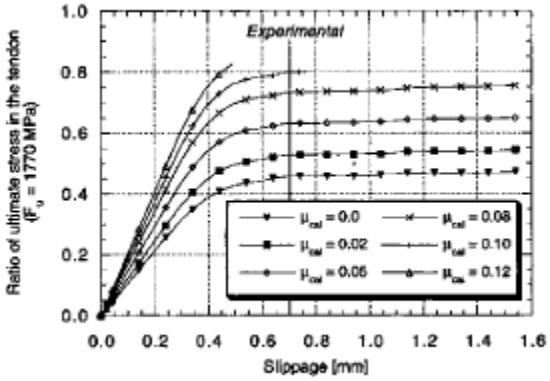

Fig. 4 Estimation of μ_{cal}: Slippage of the wedge

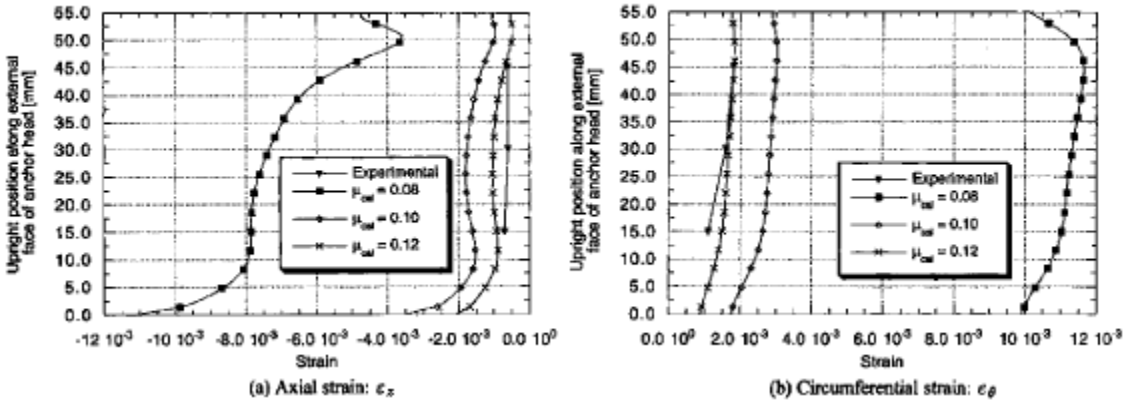

Figure 3.6: Comparison of Numerical Models to Experimental (A. Chabert 2001).

Another study that focused mainly on the anchor stresses was *Use of FEA for Design of Posttensioning Anchor Head* (J. Bastien 2007). This study focused on a multi-strand anchorage and the stresses and strains it experiences. The study followed similar procedures to A. Chabert (2001), an experimental stage and then numerical modeling, and was meant to be a semi-continuation of the previously mentioned study. This being said, there were substantial differences, the most notable being the use of actual tendons in the experimental stage. This means that a tension force was imparted to the anchor head, rather than a compression force as with the equivalent wedge. This is important to mention because it means that the strand-wedge

interaction was accounted for in the experimental procedure. The test set up can be seen in Figure 3.7.

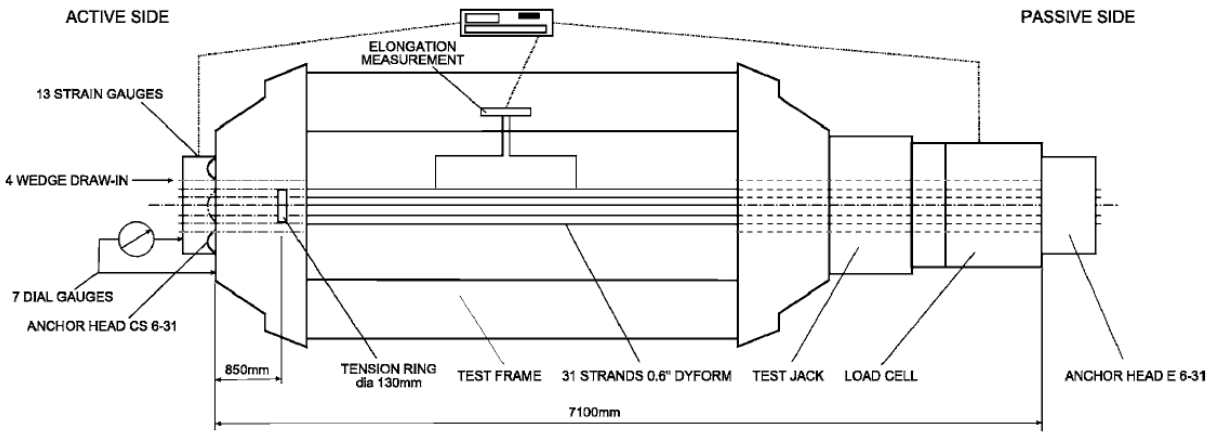

Figure 3.7: Test Set-up (J. Bastien 2007)

The numerical model took into account three types of nonlinearity: large strain; plasticity; and contact between some interfaces (J. Bastien 2007). There were also assumptions made that could have added discrepancy between the experimental tests and the numerical model. First, the wedge-strand gripping action was considered to be such that the two components (wedge and tendon) may be assumed to act in a monolithic way. It is here that the equivalent wedge that was utilized by A. Chabert (2001) is introduced, but only in the numerical model. The equivalent cone was assumed to have purely elastic behavior because of the hard nature of the wedge and the elastic response of the strand during testing (J. Bastien 2007). This was an acceptable simplification because the testing procedure ensured that the strand never left the elastic region of its stress-strain curve. Additionally, when the numerical model was loaded, it utilized a compressive force on the equivalent wedges, under the assumption that all 31 tendons were axially and simultaneously stressed at the same loading level. This simplification differs greatly

from the experimental model, which takes into account the loading reaction of the strand and the interaction of the wedge and strand.

As mentioned, the interaction of the wedge and strand was again replaced by an equivalent wedge model. The remaining two interactions were modeled as Coulomb friction relationships. The coefficients used, based on past experience in anchorage devices analysis, were 0.05 and 0.10 for the anchor to wedge interaction and the head to anchor plate interaction, respectively. These coefficients are much lower that the values used by A. Chabert (2001). Despite the use of lower friction coefficients, the results obtained from the numerical model match well with the experimental results as seen in Figure 3.8. The explanation for this could lie in the fact that the multi-strand anchor may allow for a wider range of coefficients due to the multiple anchor holes. Since there are more interaction surfaces, there is more variability. The explanation also may come from the fact that multiple generalizations were used that caused the numerical model to differ from the experimental model.

Table 1. Wedges Relative Slippage (mm)

	W4	W5
Experiment	1.35	1.6
Numerical model	1.46	1.48

Table 2. Anchor Head Bottom Surface Radial Deformation (μm/m)

Radial deformation	Location		
	A	B	C
Experiment	1,480	1,570	9,160
Numerical model	1,050–2,790	1,330–1,660	8,840–22,600

Figure 3.8: Comparison of Experimental and Numerical Observations (J. Bastien 2007)

3.3.2 Wedge Tendon Studies

There are two particular studies that specifically focus on gaining an understanding of the wedge and strand interaction: *Constitutive Law for Wedge-tendon Gripping Interface in Anchorage Device* (D. Marceau 2003) and *Numerical Study of Mono-strand Anchorage Mechanism Under Service Load* (D. Marceau 2004). These may prove to be the most useful studies in trying to understand how to model the transfer of load from an elastic-plastic strand to

an elastic wedge. The first study mentioned focused on specifically developing equations to define the interaction between the teeth of the wedge and the strand and comparing that relationship to experimental tests. The later study focused on modeling the relationship in a full model and comparing it to experimental tests. Both of these studies will aid in the understanding of the gripping mechanism within the wedge.

In developing the interaction for the wedge gripping interface, the wedge and anchor were looked at as a whole. In order to perform a reliable finite element analysis, the following requirements, among others, must be met: adequate application of elasto-plastic materials with a large strain approach, adequate modeling of the interfaces between the wedge and anchor and the anchor and plate, and most importantly, adequate modeling of the wedge and strand interaction (D. Marceau 2003). This interaction becomes extremely difficult to model because of the triangular teeth that bite into the strand to grip it and maintain the strand in place while load is applied to the strand. By adding this interaction into the model, more refined and accurate results can be expected compared to using the equivalent wedge mentioned in the previous studies. Having a wedge strand interaction defined becomes extremely important when looking at stresses developed in the anchor mechanism as a whole.

The experimental testing was done using a mono-strand cylindrical anchor. This anchor was loaded with a strand and then stressed to roughly 80% of the strand's ultimate load. This is the standard ETAG (Engineering & Technical Assessment Group) recommendation. The strands were never brought to full failure during this study. The strains throughout the anchor were recorded along with the displacement of the wedge relative to the anchor. Observation of permanent deformity of the anchors suggests that they experience inelastic behavior. The wedge

is assumed to remain in an elastic state due to its hardening, while the strand also operates in an elastic state due to the controlled loading (D. Marceau 2003).

For the strand wedge interface some assumptions were made by Marceau. The first assumption was that longitudinal displacement between the strand and wedge is minor if it occurs. Additionally in the tangential direction, the standard Coulomb friction law is applied. These simplifications allow the radial relationship can be described as a hyperbolic law described as follows: (D. Marceau 2003)

$$t_r = \frac{n g_u}{g} \tag{3.1}$$

Where n represents the stiffness of the wedge in the radial direction and g represents the actual distance between the wedge and the tendon:

$$g = g_0 - g_u \tag{3.2}$$

$$g_u = -n_* * [u_*^1(X_*^1, t) - u_*^2(\Psi_0(\xi), t)] \tag{3.3}$$

Where g_0 defines the fictitious gap between the wedge and the tendon. The terms u represent displacement fields within the model. g_0 is associated with the depth of the teeth within a wedge. The n and g_0 are considered the unknowns and must be solved for to fit a given model.

A range approach was used in order determine the unknown coefficients. This iterative approach required the testing of multiple combinations of unknown coefficients. After the unknowns were determined, the system was said to "learn" how to determine the coefficients. It was at this point that experimental data was introduced and the model was tested. The analysis showed that the tangential friction coefficient between the wedge and strand was not significant and therefore it was held at 0.3 as was the coefficient between the anchor and base plate (D. Marceau 2003). The following ranges were also established for the unknown parameters:

$$1000 \leq n \leq 5000 = 3000$$

$$.01 \leq g_0 \leq 1.5 = 1.5$$

$$.02 \leq \mu \leq .15 = .09$$

These ranges were shown to give reasonable results for the given model and testing procedure. It was noted, however, that if a different wedge, anchor material or geometry were used that these coefficients should be reevaluated.

The *Numerical Study of Mono-strand Anchorage Mechanism under Service Load,* (D. Marceau 2004), utilizes the model previously discussed where the wedge strand is modeled as an interaction rather than an equivalent wedge. The testing procedure that was used in the experimental test set-up was identical to the one in the previous study. Therefore, all the same constants and variables were applied to the numerical model. Given the previous research a friction coefficient of 0.09 was established as the applicable value for the wedge anchor interaction. A frictional coefficient of 0.30 was utilized for the relationship between the strand and the wedge.

The equivalent wedge model was compared to the tendon-wedge interaction model and substantial differences were found. Penetration of the wedge into the strand was much higher with the two component model. This was due to the high stiffness in the radial and tangential directions associated with the equivalent wedge. The experimental results for penetration matched the two component model. The two component model also showed a higher percent yield of the anchor head at lower stresses than those observed with the equivalent wedge. These graphs are shown in Figure 3.9. This suggests that it may be hazardous to draw conclusions from an equivalent wedge model. It is for these reasons that the tendon, wedge, and anchor shall all be modeled as individual parts and the interactions developed in these two studies shall be used.

This study also investigated the effects of the misalignment of wedges and of lubricated wedges; however these aspects do not directly pertain to the study at hand.

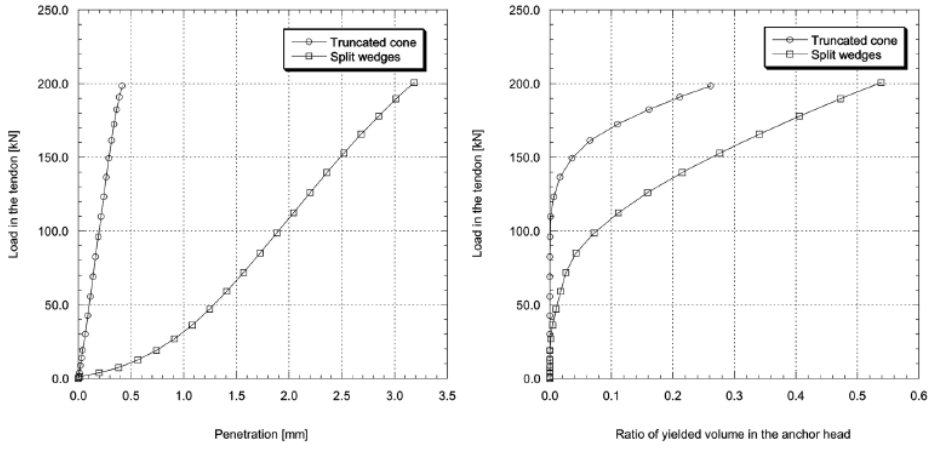

(a) Penetration of the gripping device into the cavity (b) Yielding of the anchorage

Figure 3.9: Equivalent Wedge (Truncated Cone) vs. Two Component Wedges

(D. Marceau 2004)

The four studies described demonstrate the refinements made to the modeling of monostrand post-tensioning anchorages. They laid the ground work for the study at hand and when the interactions along the load path of the anchor were first modeled, these studies provided the starting coefficients. Ideally, coefficients close to the ones already attained will yield the same results as observed in the laboratory and this study will act as a verification that the interactions already defined can be applied to different wedge geometries.

Chapter 4: Testing Procedure

Two different test procedures were utilized to acquire data relevant to the model being constructed and assessed. There were also only two main machines used in the testing process. The first machine was a Tinius Olsen Universal Testing Machine. This machine was used to conduct free-length fracture tests to assess the ultimate strength of the tendons. This data was used to assign material characteristics to the tendon. The second machine was a Test Star MTS 810 machine, which was used to assess the strength characteristics of the wedge-anchor system. These results, once gathered will be compared to the finite element model's output and ensure the model is preforming accurately. Both tests were heavily instrumented to ensure complete recording of the data. This section will cover the testing approach, equipment and methods that were used in order to load the specimens.

The procedures start with a preparation stage that was essential to ensuring that all the specimens were uniform and unbiased. The free length testing procedure and the MTS loading procedure will follow in their respective order. It is important to take note of the MTS loading procedure because it will be represented in the model and will have similar characteristics.

4.1 Preparation Stage

It was in this stage that the tendons were cut from their spool. There were 24 tendons cut from the spool using an abrasion saw. The lengths varied from 36 to 42 inches. Once all 24 tendons were cut, a strain gage was fastened to a single wire within the tendon (Figure 4.1(a)). The strands were assumed to behave in a monolithic way because of the twisted pattern in which the individual wires are arranged and the conclusions from previous studies. The strain recorded for one wire was assumed to be the strain in the tendon. Yates observed that after a certain load is applied and each wire is fully anchored, the subsequent strain increases are relatively linear

with near equivalent slopes. For this reason, Yates recommended that only strain readings corresponding to stresses higher than 50 ksi be considered for the preparation of a linear calibration curve (Yates 1988). However, through extensive instrumentation and testing, Acosta later concluded that when all strain gages are installed at one particular cross-section and at an equal distance of at least 24 in. from the anchorage ends, the gages measure similar values of strain even at low stress levels (Acosta 1991). The procedure for attaching the strain gages is described in Appendix A *Application of Strain Gages*. *S*train gages were also applied to half (12) of the anchors. There was a strain gage attached to the top edge and bottom edge of each anchor to allow a strain differential to be observed (Figure 4.1(b)).

a) Gage on Strand b) Gages on Anchor

Figure 4.1: Example Strain Gage Location

4.2 Free Length Fracture Testing

The free length test was the first test carried out. This test proved to be the most challenging to conduct because of the required result of obtaining a free length fracture. A free length fracture occurs when the strand fails in its free length, or the length between the two grips. Traditional strand failures occur where the wedges grip the strand and there is a stress concentration. This stress concentration causes one of the individual wires within a strand to fail. Failure of the strand at the grips prevents the strand from reaching its full strength capacity.

When the strand fails within the free length, all of the wires within the strand fail at the same point and at the same time which can be observed in Figure 4.2. This is usually a very violent and sudden failure. In order to correctly model the system, the ultimate strength properties of the strand need to be known. The test also provides a reference point for determining the reduction in the capacity of the strand that occurs when traditional wedges are used.

Figure 4.2: Example of a Free Length Fracture

4.2.1 Testing Machine

The machine that was utilized in the free length tests was a Tinius Olsen Universal Testing Machine with a capacity of 100 kips. This machine was extremely old and needed to be calibrated and retrofitted to be compatible with the newer data acquisition systems and for safety. The machine had a cross head that moved in an upward direction to impart a tension force on the specimen. A sketch of the entire test set up can be seen in Figure 4.3.

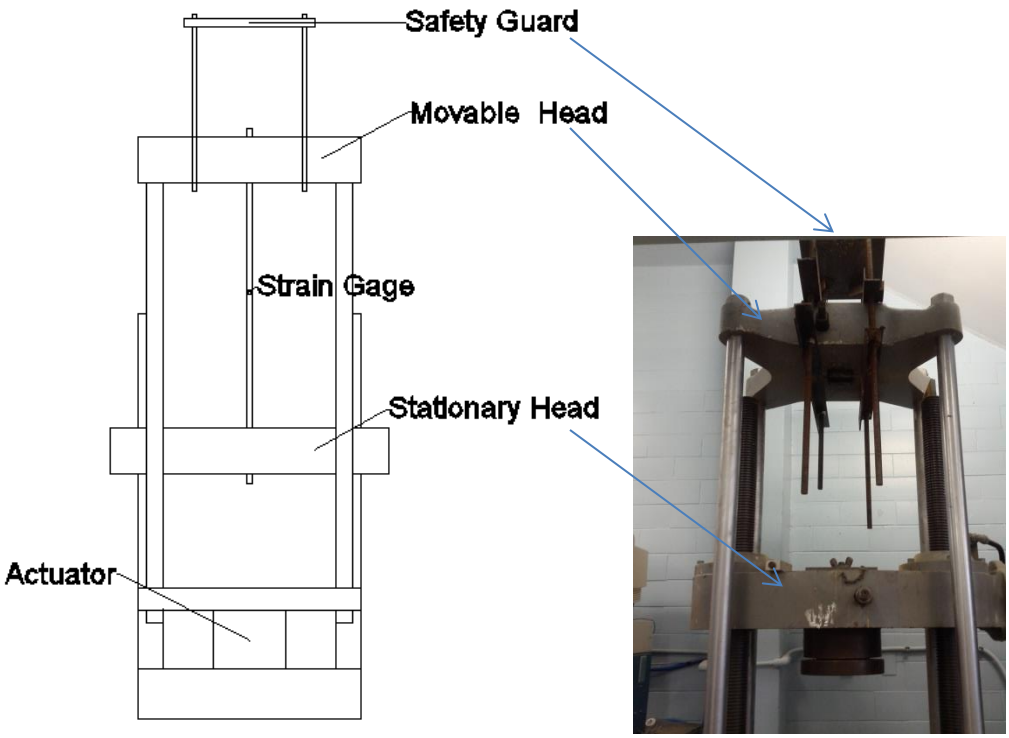

Figure 4.3: Sketch of Free Length Set-Up

The plate that is present at the top of the machine is part of the retrofit added for increased safety during the test. Depending upon the failure mode, the entire strand will fail so violently that the grips and half of the strand will shoot out of the top of the machine. This was witnessed multiple times during the testing procedure. The plate, while not keeping the grips and strands in the machine, prevents damage to the ceiling.

Additionally, there are no potentiometers present to measure displacement in the test setup. This is also because of the violent nature of the failures. To prevent the expensive cost of replacing multiple potentiometers, they were excluded from the test setup. The displacement of any component was not a critical aspect of these tests. What was critical was obtaining the stress strain curve of the strand up to failure of the section. A strain gage was applied to the strand at mid-height to record the strain in the strand.

4.2.2 Grips

The grips used in the free length test warrant special explanation. A trial and error approach was used to achieve the most efficient grip set up. The dimensions and geometry of the free-length grips were based off of the grips used by Walsh and Kumara for their free-length fracture tests. The grips that were in the Tinius Olsen were not sufficient to generate enough friction to achieve a free length fracture. To solve this problem, custom grips were milled for this test. They can be seen in Figure 4.4.

Figure 4.4: Custom Grips for Free Length Tests

The grips were roughly eleven inches long and had channels that were milled to the depth of the strand radius plus 1/16th an inch. The grips were bolted at only one end and the remaining free end was inserted into the Tinus Olsen. The grips slowly became bowed after multiple impacts with the safety plate. Had the grips of the Tinus Olsen been the only point of contact with the custom grips, the bowing would not have allowed the strand to be efficiently grasped. However, by bolting together one end of the grips and putting the other end into the grips of the Tinus Olsen, the bow was essentially eliminated and the grips could effectively allow a free-length fracture to be developed.

Once all of the equipment had been instrumented, the free length fracture testing portion began. The final procedure used in this section of testing was personally developed by the author

during previous studies that are currently unpublished using partial input from Walsh and Kurama (2009). The grips that were custom manufactured at Villanova University were filled with saturated sand that had passed through a #16 sieve. This sand was the main gripping mechanism throughout the test. The packed grips can be observed in Figure 4.5. The grips must be fully and evenly filled with sand in order to allow for an even load distribution.

Figure 4.5: Unfilled Grips vs. Filled Grips

After the grips were filled with #16 sand, the individual strand was worked into a grip by a rocking motion to ensure that the sand filled the voids between individual wires. The second grip was then placed on top of the strand and again rocked. These two grips were then bolted to the strand using the apparatus shown in Figure 4.6. This process was then repeated for the alternate end of the strand using two other grips. Finally the entire strand, with both grips bolted on was inserted into the Tinius Olsen Machine described in 4.2.1.

Using hand cranks on either head of the machine, the grips were tightened. These hand cranks were counterproductive because as one was tightened, the other would loosen. To resolve this situation, the heads were pulled apart as the cranks were tightened. It was ensured that no substantial load was imparted to the strand during this phase.

Figure 4.6: Bolted Custom Grips

4.2.3 Specimen

The specimens that were being tested were 0.5 inch diameter prestressing strands. All samples were cut from the same spool of ASTM A416 – Latest Low Relaxation 7 Wire Strand. The strand was rated as having an elastic modulus of 28.7 Mpsi and a cross sectional area of $0.1503in^2$. The lengths varied over the free length tests but all strands were between 36 and 42 inches. There was no special treatment applied to the strands and they were tested just as if they were being put into use in the field. A specimen in the test apparatus is shown in Figure 4.7. In this photo one can see the bolted grips and the strain gage.

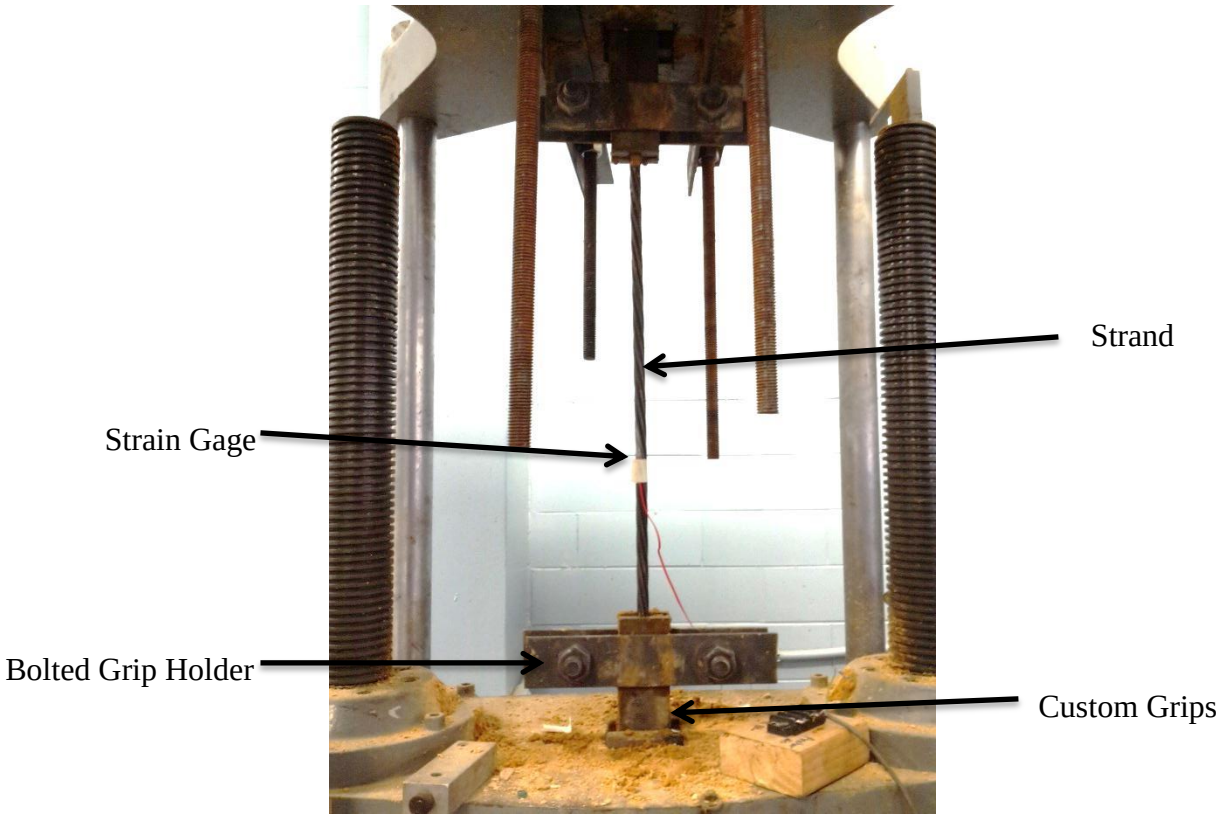

Figure 4.7: Specimen in Test Apparatus

4.2.4 Data Acquisition

As mentioned, the Tinus Olsen needed to be retrofitted to be compatible with the data acquisition system. The machine had previously been used with a data acquisition system by attaching a simple potentiometer to the needle of the dial gage on the Tinus Olsen machine. However, the output method had long been disconnected and rewiring was necessary to allow the potentiometer to connect to the data acquisition system.

In order to make these two systems compatible, an indirect method of collecting data was used. First, the potentiometer that was connected to the large dial on the Tinus Olsen was spliced into the data acquisition system. An excitation of 2 Volts was then applied across the circuit. A Honeywell Model 43 Load Cell with a range of 50 kips was also attached to the data acquisition system. A concrete cylinder was then placed on the load cell and both were placed within the

Tinus Olsen. The cylinder and load cell were then loaded respectively with in their elastic range. The load read by the load cell was then recorded along with the change in voltage over the potentiometer. A calibration factor was then back calculated using the following equation.

$$C_f = \frac{L - 0}{V - 0}$$

This formula was applied to each data point with in a test and then was averaged over the entire test. Since the cylinder was loaded within its elastic range the slope of the line directly correlated the load to the voltage. This was done for three separate tests and a calibration factor of -7500$\frac{lb}{volt}$ was obtained. This load factor was applied to the data recorded during the free length tests. A load cell could not be utilized in the free length tests because the tests were tension controlled, rather than compression controlled.

Once the load was calculated from the recorded voltage, stress was able to be calculated. The only other type of data that was needed from this test was the strain in the strand. This was recorded using an Omega strain gage with a gage length of 2 mm and a resistance of 120 Ω that was bonded to the strand. This gage simply read a change in resistance that corresponded to the elongation of the strand. Since the strain gage was standardly produced, it came with a calibration factor equal to 2.105 that was used in the data acquisition system to return a micro-strain value. See Appendix A *Application of Strain Gages* for strain gage application methods.

4.2.5 Loading

The loading method for the free length fracture test was unique for each strand due to the limitations of the testing machine. The Tinius Olsen has no electronic loading control or safety shields. It was for this reason and due to the violent failures, that after 20 kips was loaded onto the tendon, the area around the machine was evacuated. This means that the strand continued to be loaded automatically, without manual control, until failure. A hand crank was used to set the

speed of loading between 0 and 20 kips, however this load rate was monitored at the discretion of the tester, since the only available real time out-put was a load and not a strain rate. Despite these limitations, this machine had to be used as it was the only machine capable of being adapted to accept the custom made grips.

There were six specimens tested, with the goal of having three successful free length fractures. Five of the six specimens fractured within their free length, however only three specimens returned usable data. The other two free length fractured specimens were tested with a disconnected gage and thus returned a zero reading from the load potentiometer within the Tinius Olsen. These two trials were therefore thrown out of the study, and only the three successful tests were utilized.

4.3 Wedge Testing

The second portion of testing was done on a Test Star MTS 810 machine with a capacity of 110 kips. This testing was done to determine the effect of wedge geometry on the system performance, as well as to provide data for calibration of the finite element model described in Chapter 6. It was necessary to have real world results to compare to the model output in order to refine the model and validate its performance. Three different wedges were tested; however, only two will be included in the modeling phase of this thesis.

The anchor and wedge testing was more standardized than the free length fracture testing. This was because the equipment used was more advanced and because more precise data was needed from the tests. The Test Star MTS (Material Testing System) 810 machine was attached to a computer controller and a real time data acquisition system. The computer ran a preprogramed loading procedure that allowed the strand to be loaded at a constant rate. This

allowed for a more consistent loading procedure. This amount of control and precision is needed in order to have accurate results to compare to the finite element model.

4.3.1 Apparatus

A sketch of the test set up can be seen in Figures 4.8a and 4.8b. As can be seen in the figure, this set up is much more intricate than that of the free-length fracture test.

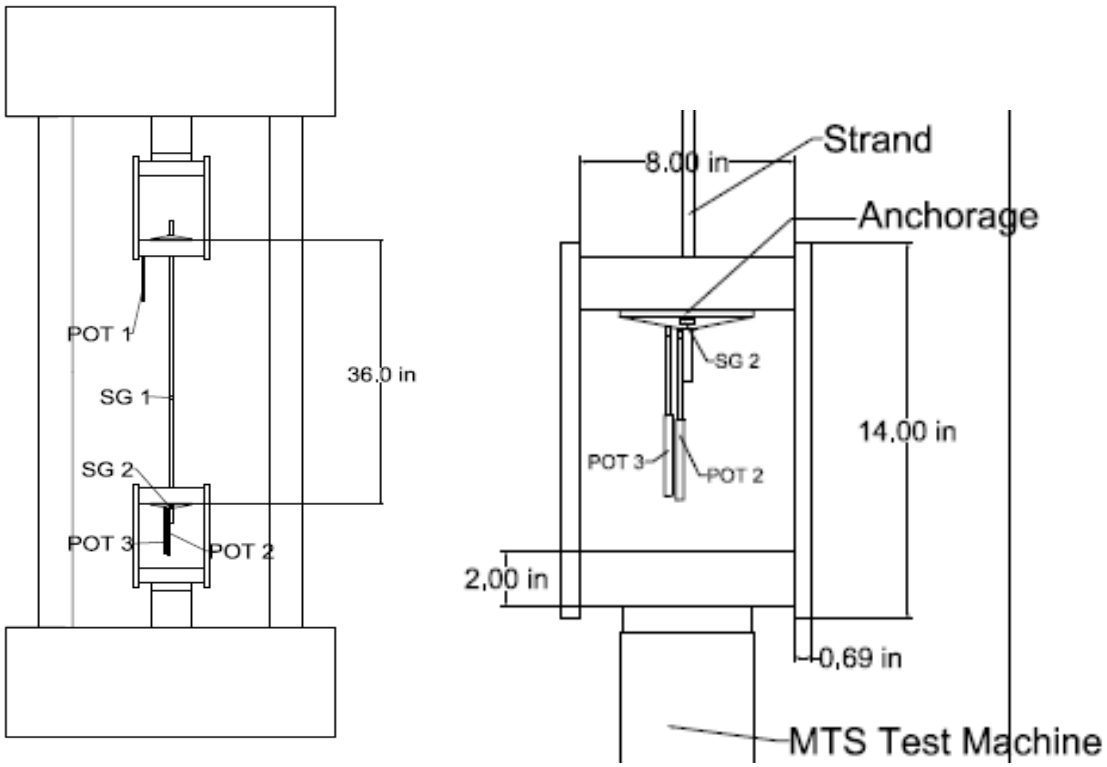

a) Full Scale MT b) Close up of Lower Grip

Figure 4.8: AutoCAD Sketch of MTS Machine

This test includes three potentiometers manufactured by P3 America that had a 2 inch stroke (POT 1, POT 2, POT 3), three Omega strain gages with 2 mm gage length and resistance of 120 Ω (SG 1, SG 2) (SG 2 consisted of two gages, one on the top of the anchor and one on the bottom of the anchor), and the load cell and displacement transducer embedded in the MTS loading frame. Again, special grips needed to be constructed for these tests, which can be seen in Figure 4.9(a). These grips were simply a steel box that was held together by five bolts at each

corner. There was a hole in the inside plate that the strand was placed through and then attached to its anchor. The anchor was the only gripping mechanism holding the strand in place. This new grip set-up ensured that the entire load was transferred through the wedge and the anchor mechanism (Figure 4.9).

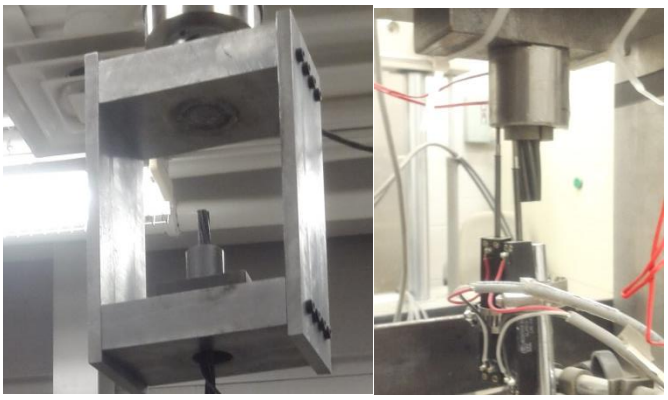

a) Top Anchor Set-up b)Bottom Anchor Set-up

Figure 4.9: Anchor Configurations

4.3.2 Machine

The Test Star MTS (Material Testing System) 810 machine is a very advanced piece of equipment and needed virtually no adjustments except the installation of the specialized grips, and the addition of a rotational restraint mechanism. The rotation restraint was provided by a steel cross beam that was fastened to the stationary supports of the Test Star MTS. This beam rested against the lower box grip and prevented any unwanted rotation. The data acquisition system was already linked to the machine and a controller PC was already linked to the machine.

4.3.3 Specimen

The prestressing strand that was used for the MTS tests was from the same spool as the strand used for the free length fracture test. The different specimens were cut all at the same time and the strain gauges were applied before either of the tests were run. This ensured that a uniform group of samples being evaluated tested. When placing the strand into the MTS loading

frame, care was taken to ensure that the distance between the anchors was 36 inches. The length became imperative when determining the strain based on relative head displacement. The length was obtained by simply allowing extra strand to stick out past the end of the anchor. This technique is illustrated in Figure 4.10.

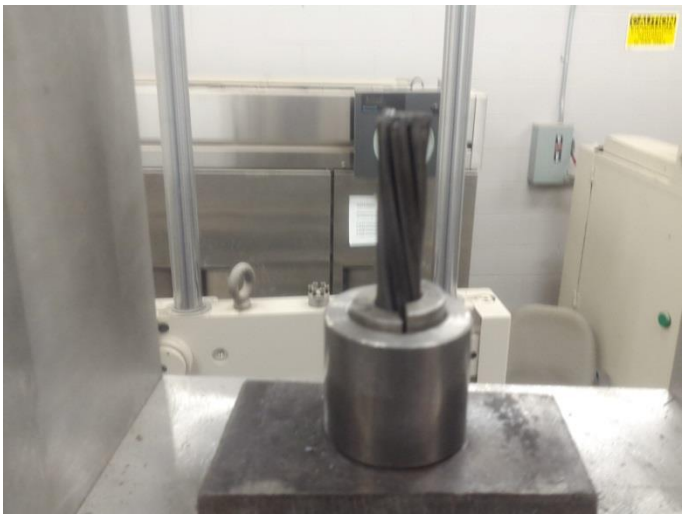

Figure 4.10: Extra Strand Extended Past Anchor

4.3.4 Procedure

The instrumented strand was first inserted into the two holes on the specialized grips. An un-instrumented anchor and two wedges were then used to grip the tendon. It was at this point that the head differential was adjusted to ensure that the distance between the two anchor positions was 36 inches. The other anchor and two wedges were then attached to the bottom of the stand using the seating procedure described below. POT 2 and POT 3 were positioned to measure the anchor displacement and the wedge displacement. Examples of this set up are shown in Figure 4.9(a)and 4.9(b)

Prior to the placement of POT 2 and POT 3 an anchor seating load was applied to the wedge-anchor mechanisms. The load was imparted using a small hydraulic hand jack, a load cell and a steel tube. A force of 900 lbs (0.9 kips) was imparted to both the top and the bottom

anchor-wedge configuration. This seating load was chosen based on the ICC-ES AC 303 test method requirements that state that a the applied preload may not exceed 1000 pounds on a monostrand system (ICC-ES AC 303). The procedure of seating the wedges into the anchor was implemented to ensure the wedges were applying an equal force over the entire circumference of the strand. This would additionally cut down on stress concentrations due to an uneven gripping of the strand. Finally this practice replicated the dead end seating procedure that is applied in the field and replicated it in a more repeatable way. The hydraulic jack set up can be seen in Figure 4.11.

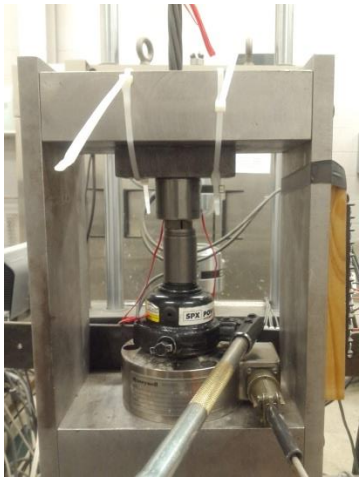

Figure 4.11: Hydraulic Jack Arrangement

After both anchor-wedge mechanisms were subjected to the seating load, they were loaded using a ramp load sequence. The ramp load sequence had been programed into the Test Star system as a displacement controlled ramp. The lower head of the MTS was lowered at a rate of 0.361 in/min. This displacement rate corresponds to a strain rate of 0.0113 in/in/min. The ICC-ES AC 303 test method requires that the loading rate be between 0.197 and 0.887 in/min for a 42 in specimen, which corresponds to a 0.00616 in/in/min and 0.0277 in/in/min strain rate, respectively, for a 32 inch specimen. Given the MTS machine that was utilized in this study, it

was not practical to test a 42 inch specimen. However, it was believed that the strain rate and displacement rate should still fall within the standards that are established.

Once the strand had reached a load of 35 kips, or approximately $0.875(F_u)$, the potentiometers were removed. It was at this point approximately that the strand began to enter its inelastic region. From this point forward the strain gage, internal displacement and load cell were the only data systems still recording information. The removal of the potentiometers was prompted by the possibility of a violent failure, which could destroy the potentiometers under the anchor or beside the strand. The potentiometer data was used to check that the internal displacement and strain gage were reading accurately. The data was also used to zero the strain and account for wedge settling in order to determine the true strain as discussed in Chapter 5: Analysis and Results. Once all the delicate instrumentation was cleared, the displacement controlled ramp was reengaged and the strand was brought to failure.

4.3.4 Anchors and Wedges

Figure 4.10 shows the anchors and wedges in their customary set up. As can be seen, for the testing done, two wedges were used per anchor. This set up was replicated at the alternate end of the strand to allow for failure at either end of the tendon. This method seemed to best represent the situation that would be encountered in the field.

In this study the same barrel anchor design was utilized for all tests, while three different types of wedges were used. All of the parts were produced by the same company, Hayes Industries, to ensure uniformity. A picture of each component can be seen in Figure 4.12 and wedge dimensions are shown in Table 4.1.

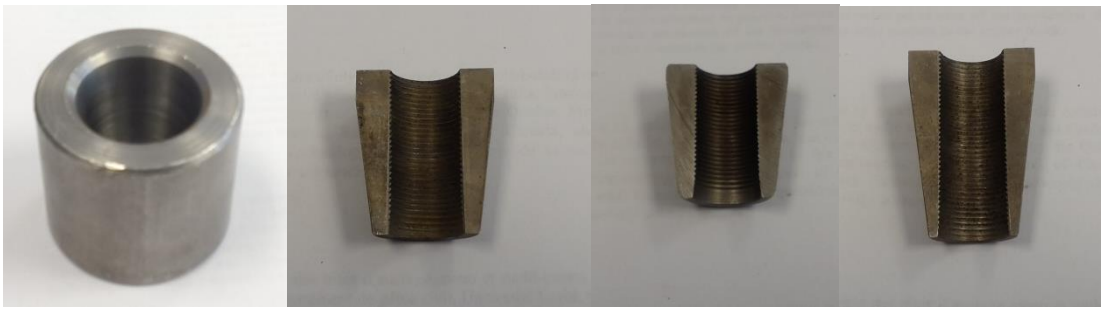

a) Standard Barrel Anchor b)Modified Wedge c)Standard Wedge d)Long wedge

Figure 4.12: Anchor and Three Different Wedges

Table 4. 1: Dimensions of Wedges

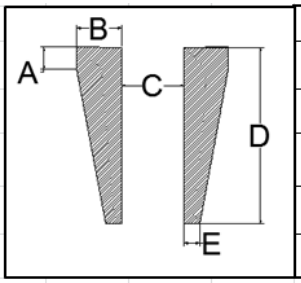

Dimension	Standard Short	Modified Short	Modified Long
A (in)	-	0.25	0.25
B (in)	0.27	0.26	0.26
C (in)	0.5	0.5	0.5
D (in)	1.16	1.2	1.5
E (in)	0.12	0.12	0.06

The barrel anchor is a standard anchor type that is consistently used in prestressing facilities and can be used in the field with the addition of a base plate to distribute the load over the mass concrete. Since specialty grips were used in the testing procedure, they were considered a substitute for an actual baseplate. The standard wedge is the wedge that is generally used in the field today. It has been a long-standing model and is generally accepted for most applications. The other two types of wedges used in this study are still in the development stage. The modified short wedge has similar size compared to the standard wedge but alters the geometry slightly (See Section 3.2). It is hoped that this wedge more evenly distributes the forces over the gripped length of the tendon, thus cutting down on the buildup of stress concentrations that lead to an individual strand failing. This same theory is behind the design of the long wedge. This wedge takes the geometric aspects of the modified short wedge and applies them over a longer gripping

length. It is common knowledge based on simple mechanics that the longer the gripping length of a strand, the more evenly distributed the gripping force, and the more likely a multiple wire failure is to occur at a higher strain and stress compared to a standard wedge.

4.3.5 Testing Configurations and Variables

There were only three main independent variables within this study: a standard wedge, modified short wedge, and a modified long wedge. These wedges were briefly described in Section 4.3.4; however, being that these are the main variables in this study, it is important to take a closer look at each wedge and assess why they warranted being tested. This section will give a more in-depth look at each wedge and its mechanism before the results are discussed in Chapter 5. Each of the following wedges were used in conjunction with the standard barrel anchor, as is common practice in the field. This eliminates any unintentional variability induced by a custom anchor.

The standard wedge, whose dimensions can be observed in Table 4.1, is considered the industry standard for a wedge. The wedge's angle of 7 degrees is designed to perfectly match the anchor's interior angle of 7 degrees. This, in theory allows for an even contact surface along the interior of the anchor. Additionally, these wedges were designed to have the wedge be relatively free floating, which means that even at failure, the wedges do not come in contact with one another. The reason for testing this wedge is to have a base line to compare to the modified short wedges. This will be regarded as the generally accepted control specimen.

The modified short wedge keeps the dimensions of the standard wedge relatively the same. The main two changes that are applied are an increase in the angle of the wedge and a thickened crown. The angle of the wedge is increased to 8 degrees, which causes a minor lever action to take place within the anchor when loaded. This lever creates a more evenly distributed

stress pattern as the load in the system approaches failure that in turn reduces the stress concentration at the thin edge of the wedge. The lever action also allows for the strand to elongate as higher loads and strains are reached. This allows the strand-wedge-anchor assembly to withstand much higher strains. The increase in crown thickness reduces or eliminates the gap between the wedges at failure, allowing for a more even stress distribution around the strand. This also increases the strain capacity of the strand.

The third and final wedge is a long modified short wedge. This wedge takes the geometric improvements of the modified short wedge and applies them over an increased length. The wedge has all of the same benefits of the modified short wedge mentioned above but they are distributed over a larger area on the strand. It was necessary to have 11 inch grips to achieve a free length fracture condition, so that would logically suggest that a longer wedge would allow for a capacity closer to that of the actual strand. This theory is supported by the basic concept of mechanics that a larger area allows for larger stress transfer and will reduce stress concentrations that lead to a non-free-length fracture.

4.2.6 Data Acquisition

As can be seen from Figure 4.8, there is significantly more instrumentation on the wedge testing setup than for the free length setup. This is because there is more refined data needed for the comparison of the finite element model to a real world test than is necessary for simply obtaining strand properties. There were a total of four different displacements that were measured during the testing of the three different wedges: relative grip displacement (POT 1), anchor displacement (POT 3), wedge displacement (POT 2), and finally relative head displacement (internal transducer).

POT 1 and the internal potentiometer were used mainly to verify that the strain gage was accurately reading the strain within the tendon. POT 3 and POT 2 were used to directly calculate the seating of the wedge into the anchor. This was a crucial aspect of the experiment because the wedge strand interaction law is dependent on this relative movement.

There were also three different strain gages present in the test: one on an individual wire of the strand and two on the anchor at the lower end that measured radial strain. In order to assess the stress distribution over the anchor, two strain gages were required. This way the stress gradient obtained from the anchor from the finite element model can be better compared to the actual anchor. Finally, there was an internal load cell that measured the load imparted to the strand.

Chapter 5: Analysis and Results

The following chapter will discuss the acquired raw data and how the data was analyzed in order to return useful values. All data was obtained using the instrumentation discussed in Chapter 4 and the analysis procedures explained in this chapter. The primary objectives of this chapter are to obtain the elastic-plastic curve of the tested strand, and the stress-strain curves associated with the strand and anchor during the anchor and wedge testing. These are the main two parameters that will be used in the building of the model and in the comparison of the model to the actual experimental tests. Additionally, displacements at select locations and strains along the anchorage were recorded in order to have additional parameters to compare to the model.

5.1 Free Length Fracture

The first tests that were run pertained to the free length fracture strength of the strand. As mentioned in Section 4.2, a scaling factor was needed for the conversion of potentiometer voltage to load. To obtain this factor a concrete cylinder was loaded and unloaded three times while voltage and load were recorded. The scale factor between the voltage and load was found and this became the calibration factor. The values obtained are shown in Table 5.1. Note that the sign change is due to a reversal of wires. The free length scaling graphs can also be seen in Appendix B.1.

Table 5.1: Scaling Factors for Free Length Test

Trials	Values (lb./volt)
Scale Factor #1	75502
Scale Factor #2	-75803
Scale Factor #3	-74658
Average	-75321

The value that was used in the actual tests was -75000 lb/volt. This value was justified because there is electrical noise throughout the tests and a simple round number is easier to handle. It should be noted that the difference between these the highest and lowest value of these three tests is 1.5%, which indicates there may be small errors present in the measured values. These numbers also roughly match the value previously recorded as the scaling factor. This value of -72000, was used in previous tests that utilized this machine.

Once the scaling factor was obtained, the testing of the strands could begin. Each strand was loaded until failure. The strain within the strand and voltage were the only two values recorded at a rate of 5 samples per second. The voltage was reduced to a load reading using the scale factor and Equation 5.1 which returned a force in pounds. This force in pounds was then divided by the cross sectional area to determine the normal stress in the strand (Equation 5.2).

$$V \times -75000 \frac{lb}{V} = lb \tag{5.1}$$

$$lb/_{.1503\ in^2} = \sigma\ (psi) \tag{5.2}$$

The stress-strain curves for each of these tests were then plotted on a single graph to allow for comparison. This plot ensured that each test was run correctly and that there were no extreme outliers in the data sets. To generate an average stress strain curve, the stresses for predefined strains were pulled from each test. The predefined strain interval was 1000 micro strain and ranged from 0 to 63000 micro strain, which was the highest strain achieved by two of the three strands. The three stress values at each strain interval were then averaged to return the average free length stress at a given strain. This table of values can be observed in Appendix B.2. Once the average stress-strain curve was obtained, it was plotted along with the three individual stress strain curves. This was an easy visual check to ensure the averages fell along the same trend as

the actual tests. The graph can be viewed in Figure 5.1. The average values will be used to calculate the input properties for the strand in the model phase.

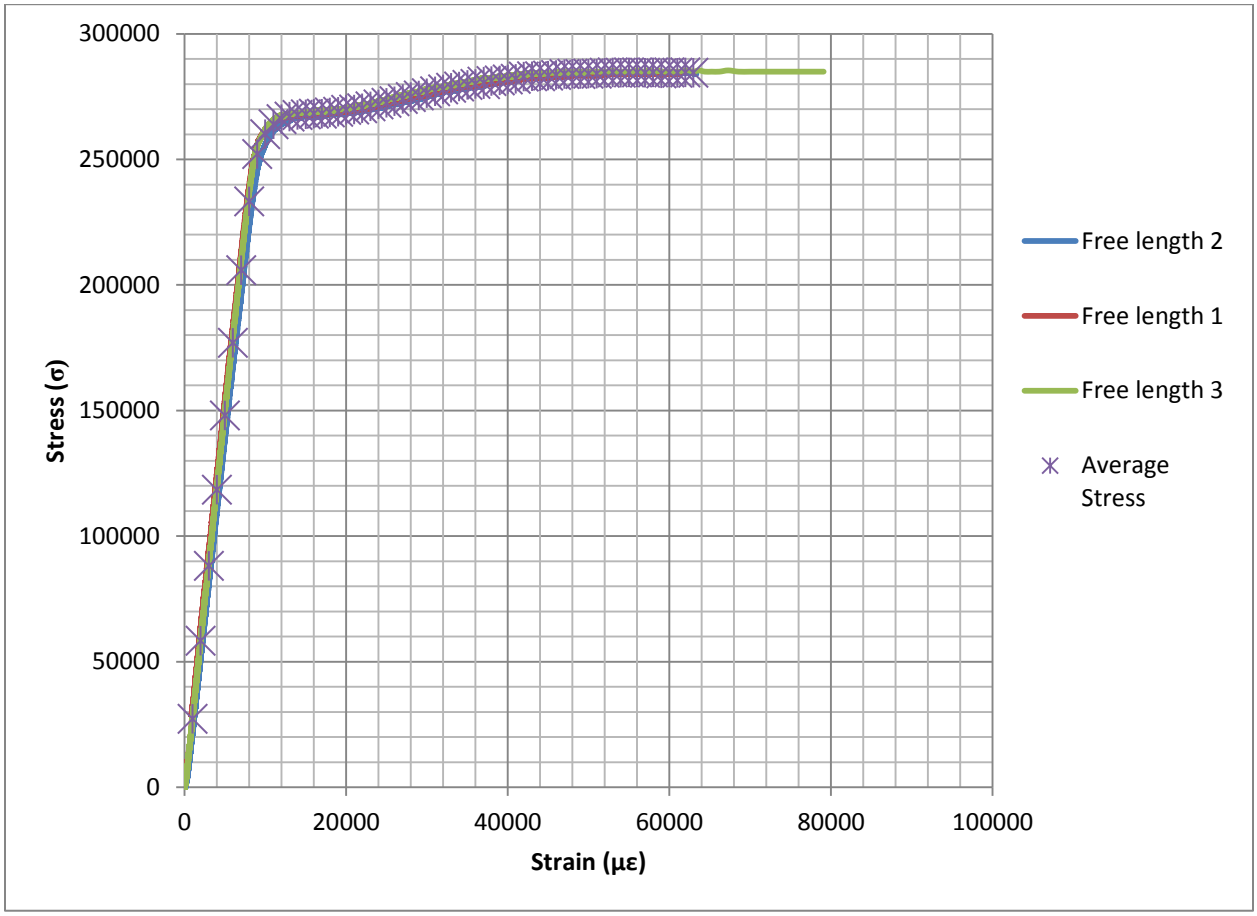

Figure 5.1: Free Length Stress Strain Curves

Table 5.2: Free length Failure Points

Trial Name	Strain (με)	Failure Stress (σ)
Free Length 1	61204	283932
Free Length 2	63337	283932
Free Length 3	79090	284930
Average Free Length	67877	284431

5.2 Anchorage System Testing

The remaining results were all obtained from the testing done on the MTS machine. These results include the three main criteria used to calibrate the finite element model. First, the general stress-strain curve will be discussed. The curve represents the strength capacity and behavior of the entire system. It will be a key criterion in the comparison of the different wedges. The anchor strains will also be evaluated and discussed. By looking at the strain gradient throughout the anchor, different inferences can be made about how the wedge is interacting with the anchor. The final result that will be discussed is the displacement value associated with how far the wedge penetrates into the anchor.

5.2.1 Stress-Strain Curve

The load carried by the strand was recorded directly using the load cell integrated into the MTS frame. This load was converted to stress using Equation 5.2. The strain capacity of the strand was more complicated to calculate than the stress. The strain in the strand was calculated three different ways: adjusted relative grip displacement, adjusted frame displacement, and gage strain. The adjusted relative grip and adjusted frame strains were then used to produce a final strain for the strand. The anchor and wedge displacements were also recorded and utilized in the reduction of the raw displacements in calculating strain.

The relative grip displacement was measured by POT 1 in Figure 4.8. This potentiometer returned a displacement in inches (Δ_g). The distance that the wedge sunk into the anchor (Δ_w), recorded by POT 2, was then subtracted from this number and divided by the strand length (which was 36 inches for all samples) to provide micro strain (equation 5.3):

$$\frac{\Delta_g - 2(\Delta_w)}{36 * 10^6} = \mu\varepsilon_{rg} \qquad 5.3$$

The justification for subtracting two of the wedge displacements is that the amount of wedge sinking into both anchors would add apparent elongation when the strand was not elongating, but rather just seating. The value produced ($\mu\varepsilon_{rg}$) was also regarded as the relative grip strain and the final strain ($\mu\varepsilon_{fin}$) until the strand reached the inelastic phase at which point the potentiometers were removed and this no longer was a viable way to calculate strain.

From this point forward the frame strain was used as the final strain. This value originated from the displacement recorded within the MTS machine via its own internal potentiometer (Δ_f). The MTS machine could not take into account the deformation that occurred in the box grips or the wedges sinking into the anchors. For the portion of the test where the potentiometers will still in place, the data from POT 1, POT 2, and POT 3 could be used directly to calculate strain. However, once the potentiometers were removed, equations were derived to determine the movement of the anchor and wedge at a given load. Inherent in this calculation is the assumption that the box and wedge continue to behave linearly. This assumption is justified by the data shown in Figure 5.2. The graph represents the elongation of the box grip combined with the shortening of the anchor itself. This is a generally linear pattern with a slight curve. For such a small value and in order to make the calculations more practical, it is safe to assume the displacement follows the average slope of the line below for each test. This assumption is again confirmed by figures in Appendix B, which shows a comparison of all the different stress-strain curves calculated for a given wedge. All the calculated strains match well with the gage strain which suggests the assumptions are accurate.

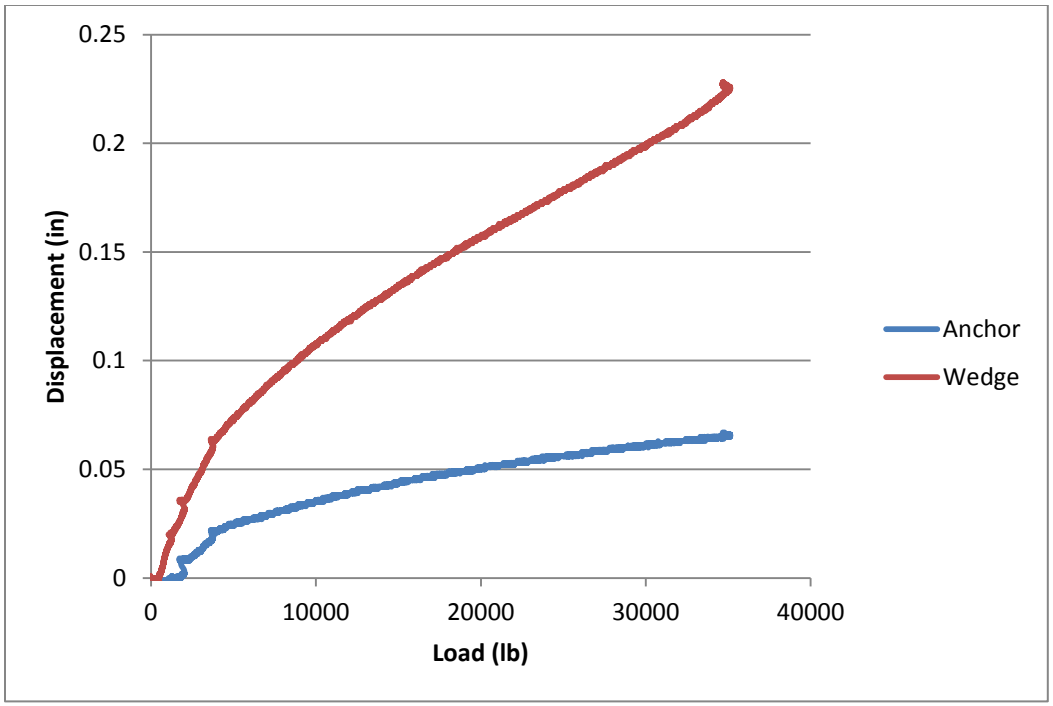

Figure 5.2: Anchor/Box Displacement

First an equation of a straight line was derived from the known anchor displacement recorded by POT 3 over the elastic range of the strand. This displacement represented the elongation of the box grips. Two points were used to derive the necessary parameters: slope (m) and intercept (b).

$$m = \frac{y_1 - y_2}{x_1 - x_2} \quad 5.4$$

$$b = x_1 - \frac{y_1}{m} \quad 5.5$$

This slope was then multiplied by the load (P) at any given point to give the assumed grip elongation. This was multiplied by two (to account for the top and bottom grips) and subtracted from the frame displacement to give the adjusted frame displacement (Δ_{f*}):

$$\Delta_{f*} = \Delta_f - 2 * m_a * P \quad 5.6$$

The wedge displacement was then multiplied by two and subtracted from the adjusted frame displacement which was divided by the length to give the micro strain;

$$\mu\varepsilon_f = \frac{\Delta_{f*} - 2(\Delta_w)}{36*10^6} \quad 5.7$$

This value became the final strain when the strand reached its inelastic state. At this transition, when the potentiometers were removed the frame strain was adjusted to coincide with the relative head displacement to ensure the final strain was a continuous smooth curve. First the slope of the line corresponding to the wedge displacement was found using Equation 5.4. Then the difference between the strain calculated from the potentiometers and the strain calculated from the frame was determined (0_{fac}). All of these values are taken at the last step that the potentiometers were present.

$$0_{fac} = \frac{\Delta_{f*} - 2*\frac{P}{m_w}}{36*10^6} - \mu\varepsilon_{rg} \quad 5.8$$

This zero factor was subtracted from the strains calculated at all future points from the adjusted frame displacement.

$$\mu\varepsilon_{fin} = \frac{\Delta_{f*} - 2*\frac{P}{m_w}}{36*10^6} - 0_{fac} \quad 5.9$$

This gave the value that was used as final strain after the potentiometers were removed. The strain output by the strain gage was simply zeroed, as all the final values were using the following procedure. No other adjustment was made.

In order to zero all the final quantities the intercept and slope of the elastic portions of the curves were found using the procedure shown by equation 5.4 and equation 5.5, using two random points along the elastic portion of the curve. This intercept was then subtracted from the strain found at each time interval for the respective methods of finding strain.

$$\mu\varepsilon_0 = \mu\varepsilon_x - b_x \quad 5.10$$

These final zeroed values, specifically the final and gage strains, were used to compare different strands and anchor configurations.

A comparison of the stress strain curves that were developed for each wedge type can be seen in Figure 5.3(a,b,c). The failure points for each test are also shown in Table 5.3(a,b,c,) and a comparison of failure points is shown in Figure 5.4 (a,b,c) which correspond to failure stress, failure gage strain, and failure final strain, respectively. The values of gage and final strain will be slightly different due to some debonding of the gages that was observed on select trails of the modified and modified long wedges. The final strain and gage strain are shown for each wedge type. The stress-strain curve for each individual test can be observed in Appendix B. The graphs in Appendix B contain all three values of strain in order to ensure all the calculations fell within a reasonable range of each other.

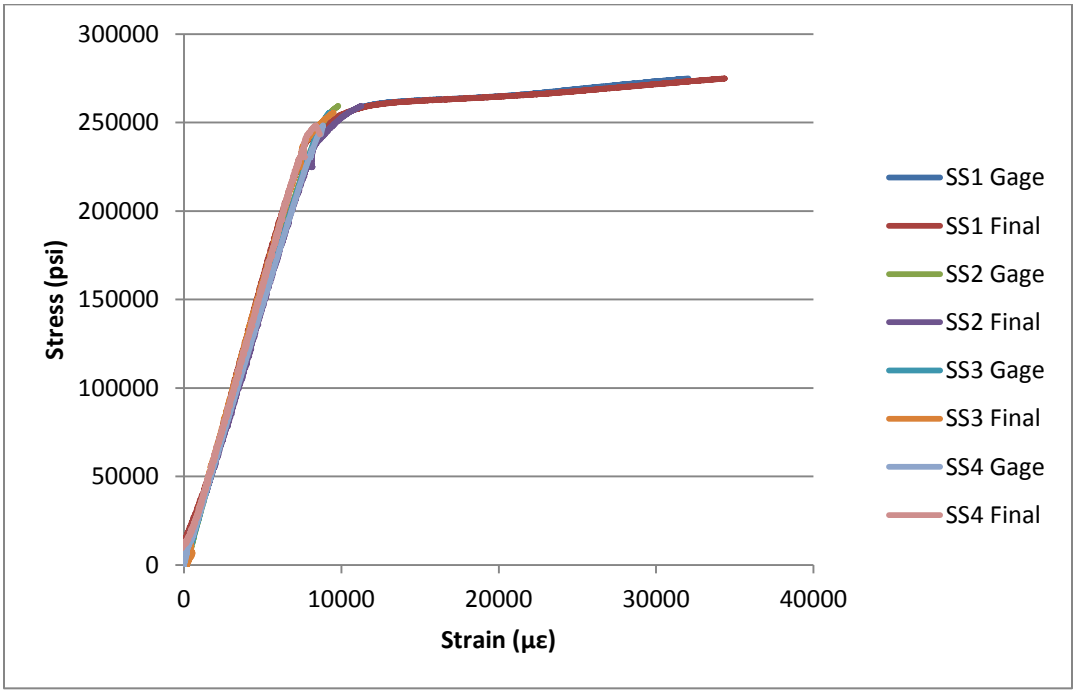

(a) Standard Short Wedge

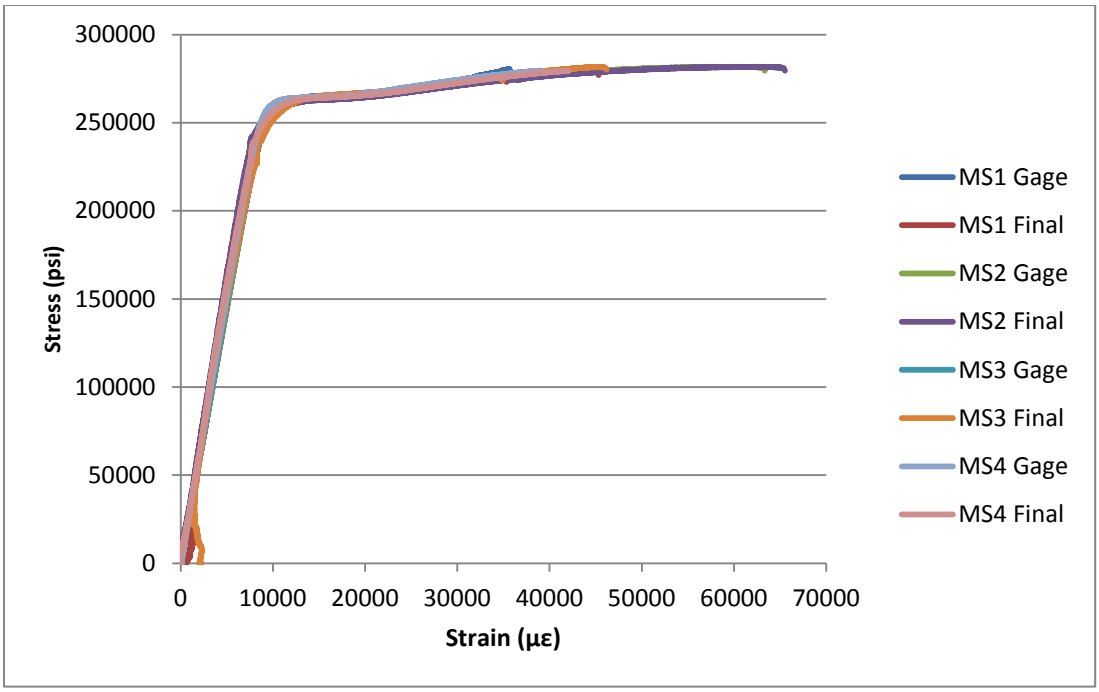

(b) Modified Short wedge

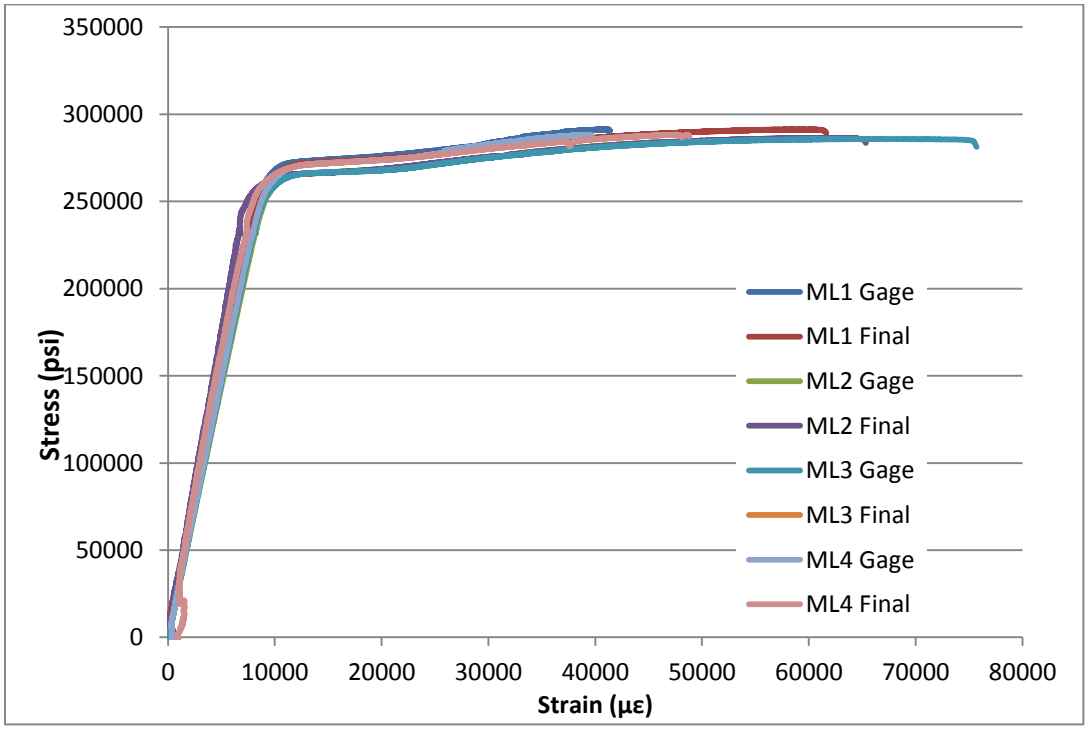

(c)Modified Long Wedge

Figure 5.3: Comparison of Individual Tests within Their Respective Samples

Table 5.3: Failure Points for Each Test

(a) Standard Short Wedges

	Stress (psi)	Gage Strain (με)	Final Strain (με)
#1	274874	32060	34323
#2	259340	9812	11189
#3	255624	9241	9591
#4	243257	8726	8781
Average	258274	14960	15971

(b) Modified Short Wedges

	Stress (psi)	Gage Strain (με)	Final Strain (με)
#1	277007	35511	45322
#2	279504	63332	65523
#3	280175	41119	46177
#4	279444	39104	42042
Average	279032	44767	49766

(c) Modified Long Wedges

	Stress (psi)	Gage Strain (με)	Final Strain (με)
#1	289008	41289	61643
#2	283525	45861	65335
#3	281271	75699	64476
#4	287302	39642	48820
Average	285277	50622	60068

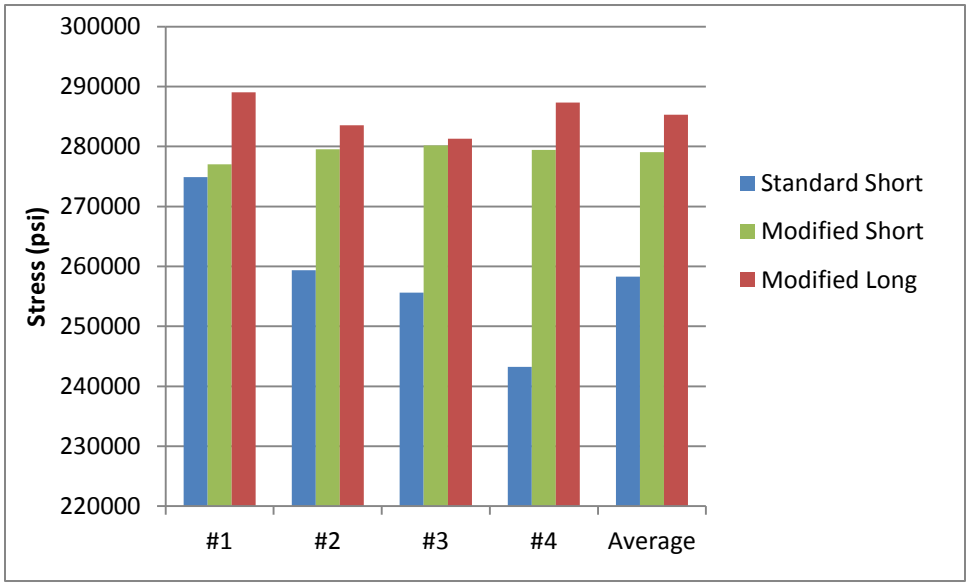

(a) Failure Stress

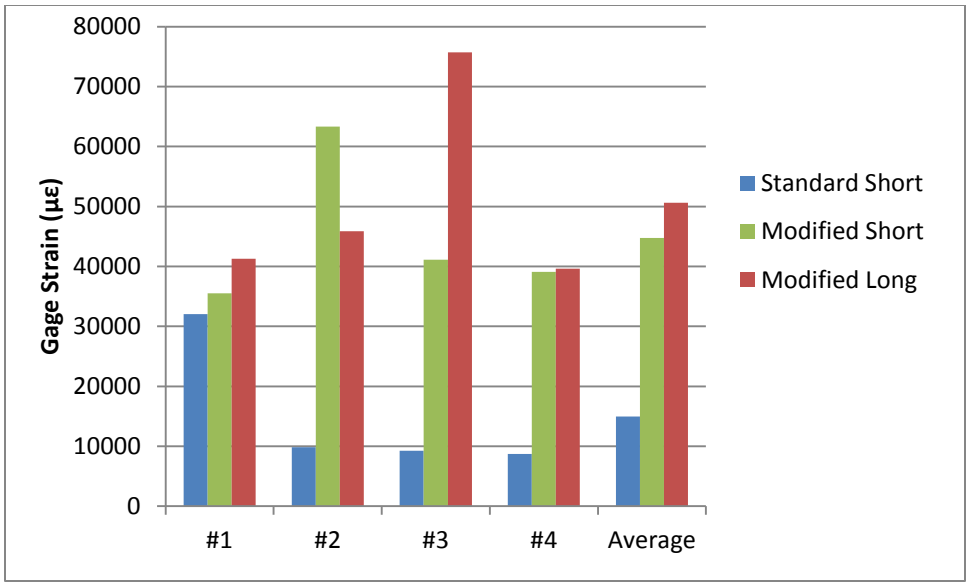

(b) Failure Gage Strain

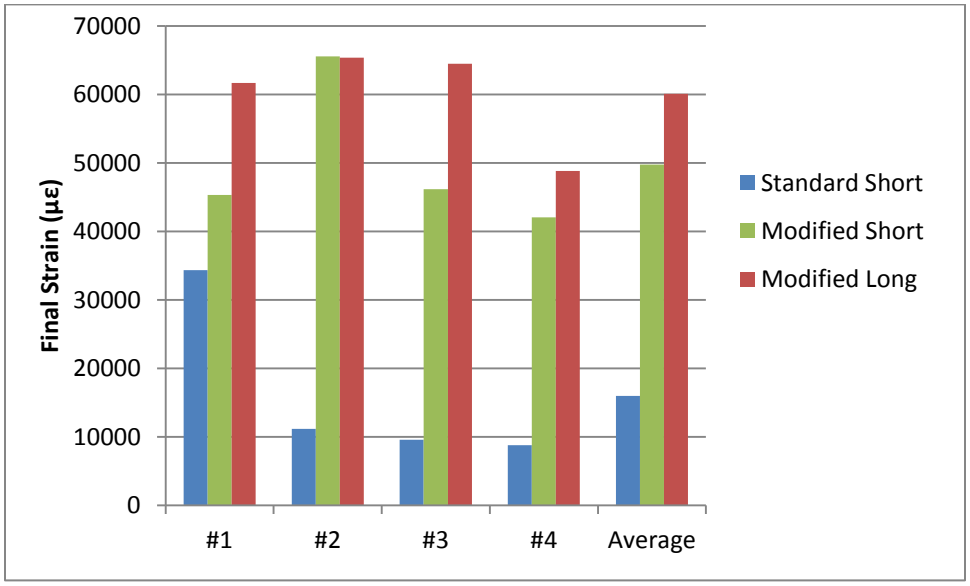

(c) Failure Final Strain

Figure 5.4: Comparison of Failure Points

The effectiveness of the modified short wedges is apparent when the above tables and graphs are compared. The stresses are relatively similar for the modified short and modified long geometries, while the stresses are slightly lower for the standard short wedges. The small differential between the stress values is due to the inelastic behavior of the strand. Once the

strand has reached the inelastic portion of the stress-strain curve, the rate of stress gain drops dramatically as the strand continues to elongate until failure. As can be seen in Figure 5.3(a), the majority of the standard short wedges caused a failure before the strand could enter into a full inelastic phase. This explains why the stresses are lower for the standard short wedges compared to the two modified geometries.

Additionally, the modified geometries allowed for significantly higher strains to develop in the strand, meaning that the strand could survive longer into its inelastic phase with the modified geometries. This is a positive aspect because the larger strain value means that there is more deformation before failure and therefore, while the strand cannot hold significantly more load, it can withstand higher displacements, which is a critical aspect in many post-tensioning applications. This deformation will translate into visible deflections in field cases and signal that the concrete mass is reaching a critical failure point. The standard wedges that fail at the peak of the elastic range would provide no such warning. Additionally, in a seismic rocking wall application, the larger elongation allows for an increased allowable displacement of the wall.

This additional elongation along with the redistribution of strains seen in the anchor comparisons supports the theory that there are stress concentrations that build up in the standard wedges which cause failures at lower displacements. By reducing these stress concentrations, as done by the modified geometries, the system is able to utilize more of the strand's potential elongation. This can significantly improve the performance of post tension strands in civil applications. Two of the four modified long wedges experienced a free length facture during the wedge testing. This means that the wedge allowed the full capacity of the strand to be developed.

5.2.2 Anchors

The anchors were instrumented with two strain gages, as discussed in Section 4.1. The orientation of the tests led to the outer most end of the anchor, the end where the wedge enters the anchor, to be denoted as the bottom of the anchor (Ex. SSB= standard short wedge, bottom strain gage). The inner strain gage, or the gage closest to where the post tension strand exits the anchor, is referred to as the top of the anchor. See Figure 5.5 for clarification. There was great variability observed in the strains produced in the anchor by the loading of the strand. The graphs of the bottom and top strain values for the standard short wedge can be observed in Figure 5.6 (a) and (b) respectively. These graphs along with the graphs for the other wedge types are reproduced in Appendix B. Each test of certain wedge geometry is superimposed on the same graph for better comparison of values.

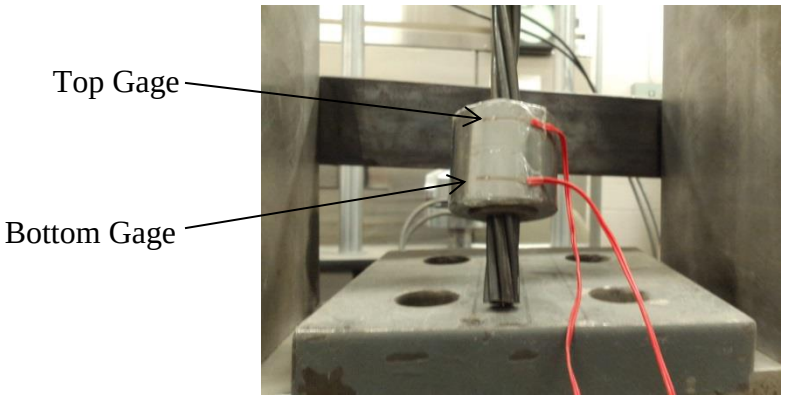

Figure 5.5: Clarification of Gage Notation

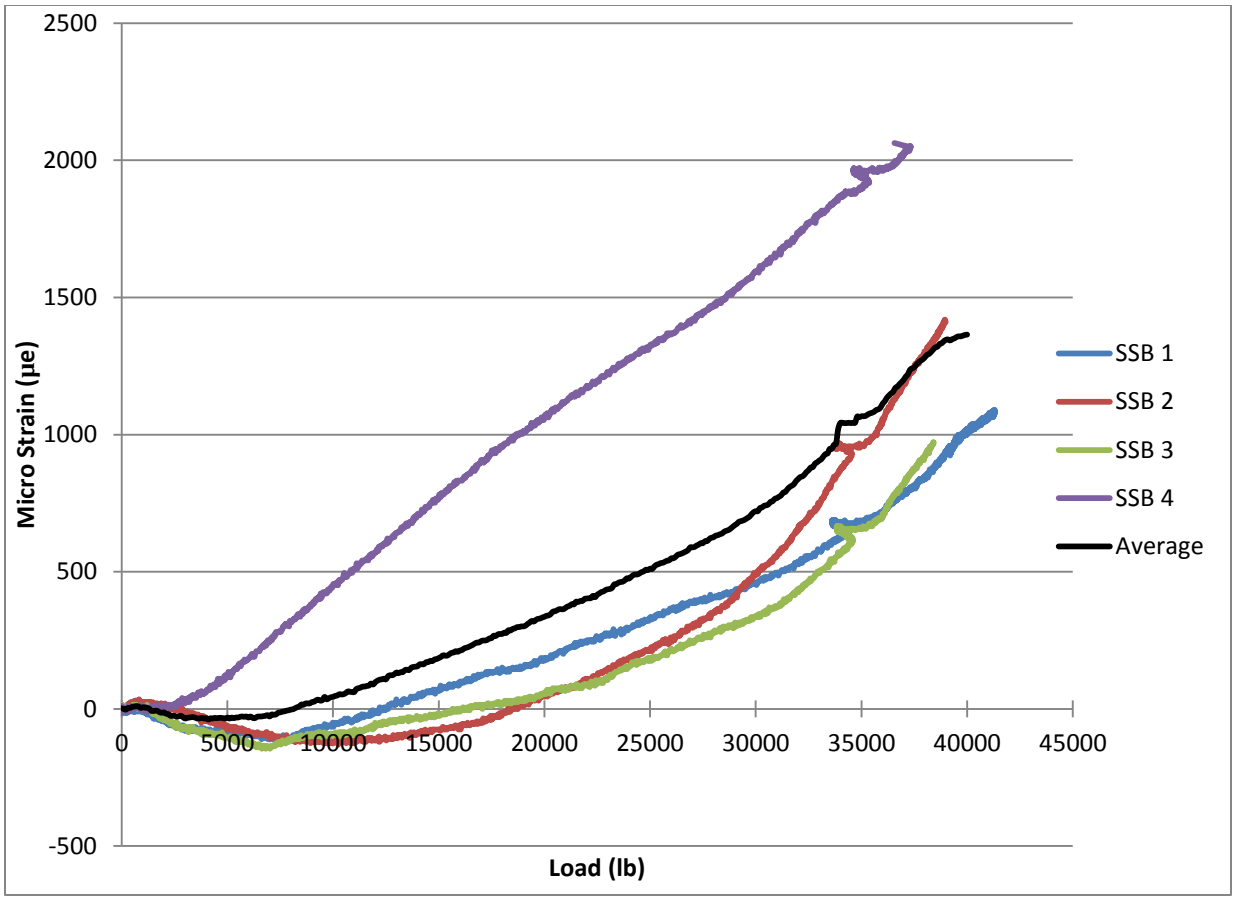

a) Standard Short Wedge Bottom

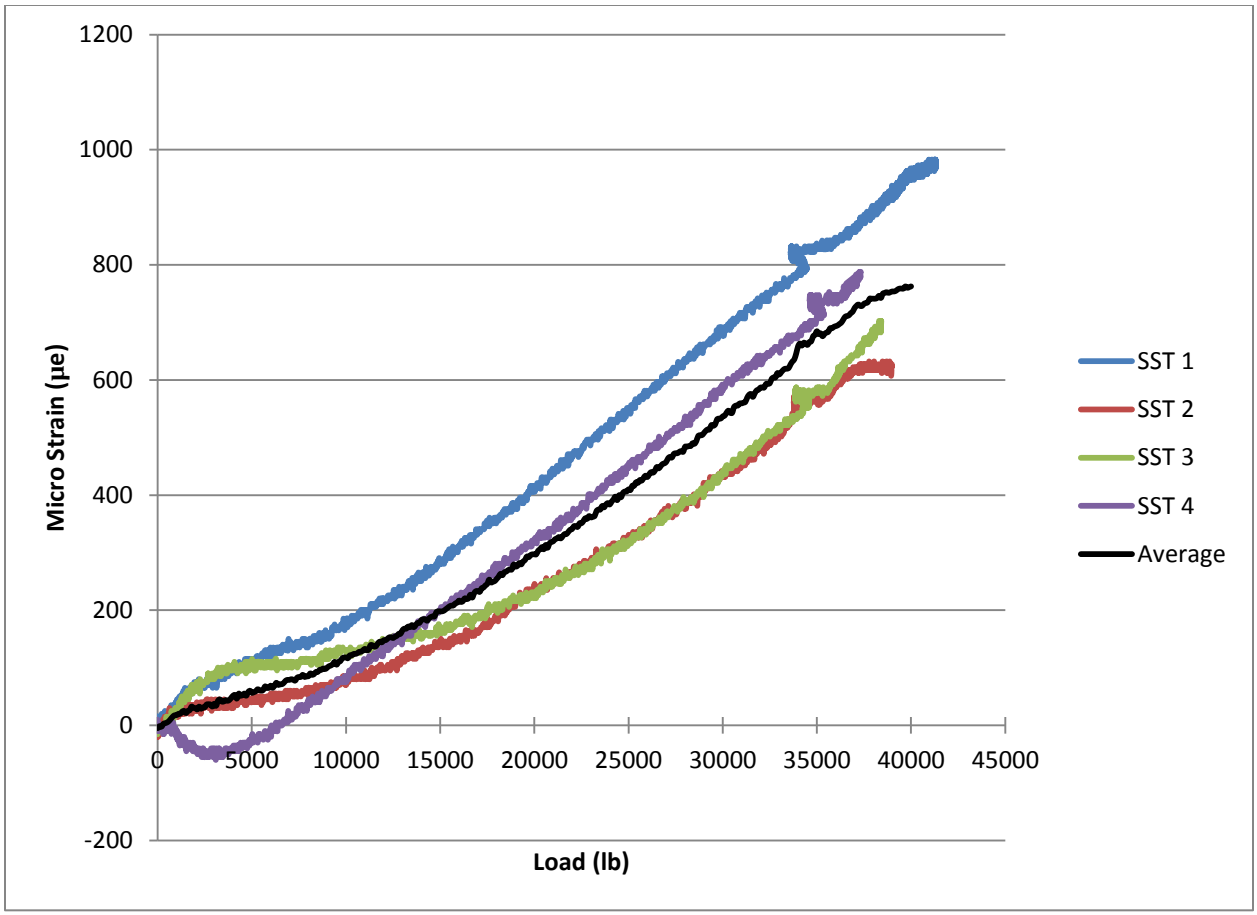

b) Standard Short Wedge Top

Figure 5.6: Strains Present in the Anchor

The above graphs show that, despite the variability, all the curves follow similar paths, except for specimen SSB 4 which experience much higher strain in the bottom gage than any of the other specimens. There are multiple explanations as to why the strain measurements are so varied. The first pertains to the seating load of roughly 900 lbs. This seating load was applied prior to data being recorded. This means that the anchor may have had a strain build up prior to loading. When the strand was loaded, the strain distribution shifted before becoming more stable. One possible cause of this redistribution would be the way the seating load was imparted to the system. The wedges were pushed into the anchor using a hydraulic jack. When the strand was loaded the wedges were pulled into the anchor. This transfer from a compression to tension force

could easily cause to the wedges to go through a rocking motion as they settle and become fully engaged.

Also important is the orientation and depth of the wedges. It was customary during testing that the strain gages were in line with one of the two wedges, meaning there was a direct line between the wedge, anchor and gage. This aspect of the experiment was not specifically monitored and if there had not been a direct line, the strains may vary. Additionally the orientation of the strand with-in the wedge may have affected the transfer of strains. Since the strand is a helix, there are different contact points between the strand and the wedge. Since these contact points can vary, different strain distributions may have been observed.

The most important result from this data is the comparison of strains in the anchors with different wedges. (All the wedge graphs are present in Appendix B) The strain that is measured at the top or bottom of the anchor is correlated to the amount of load being passed from the strand through the wedge at that location. The standard wedges had much higher strains at the top of their anchors at failure. This observation supports the theory that there is a stress build up at the nose of the wedges that causes the strand to fracture and fail. The modified short wedge reduced the top failure strain by roughly 130 micro strains, while the modified long wedges reduced the top failure strain by roughly 200 micro strains. While the modified short wedges substantially reduced the strain experienced at the nose of the wedge, it greatly increased the strain at the back of the wedge. This redistribution of strain is what the wedges were designed to do. The wider crown and adjusted angle allowed the strain to be distributed to the thicker part of the wedge and away from the nose where failure traditionally occurs. The increase in strain at the thicker part of the wedge indicates an increase in the load transfer to the strand at this location. This increase is also partially due to the fact that the anchor contains less material

towards the bottom of the anchor. This lack of material reduces the strain distribution in the anchor and thus returns a higher strain value. This creates a higher stress at the back of the wedge and a lower stress at the nose of the wedge, which increases the capacity of the system because the higher stress occurs at the location of lower overall stress in the strand. The average failure loads and strains are provided in Table 5.4 to allow simpler comparison.

Table 5.4: Failure Loads and Strains

	Failure Load (lb.)	Top Strain (με)	Bottom Strain (με)
Standard Short	38000	750	1330
Modified Short	41000	620	4990
Modified Long	42000	540	3850

5.3 Comparison Criterion

Besides proving that the modified geometries do increase the performance of the strand anchorage system, it is important to correlate the real world results to the computer-modeled results. There are three values that are of importance when conducting the comparison: stress-strain curve, wedge displacement and anchor strain. These parameters are ranked in order from most important to least. The goal of the model will be to accurately represent the interactions between the wedge and anchor as well as the wedge and tendon, to obtain a realistic representation of the system behavior. Additionally, it will be important to compare the modified and standard geometries to each other in order to see if the impact of the gap control and angle differential principles can be observed in the model.

The stress strain curve that will be used to represent the strand is shown in Figure 5.7. It is a free length fracture curve that has the failure points of each wedge test plotted. This graph

also helps emphasize the improved performance of the modified geometries. It is possible to observe that each wedge type is confined to a certain region along the free length stress strain curve. If it is possible to observe a failure within the model, the failure point will be compared to its respective wedge's failure point (modified short or standard short).

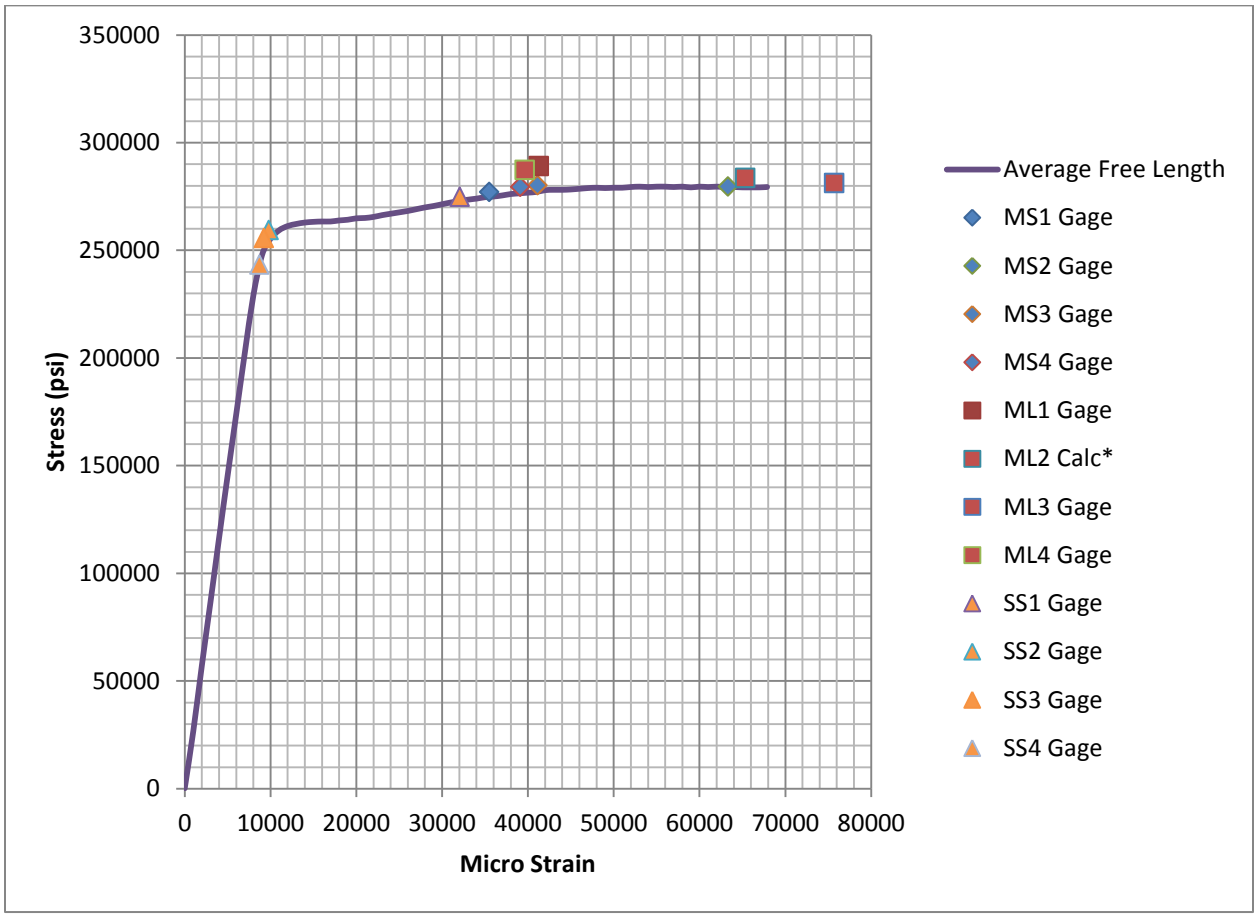

Figure 5.7: Failure Points of Wedges vs Average Free Length

The second comparison criterion is the amount of wedge displacement. This parameter will be one of the deciding factors on what friction coefficient is to be used between the anchor and the wedge. The average wedge displacements associated with the modified short wedge and the standard short wedge are shown in Figure 5.8(a) and (b) respectively. Ideally, the displacements should be relatively similar, but the stress-strain failure points are more essential to determining if the overall model was a success.

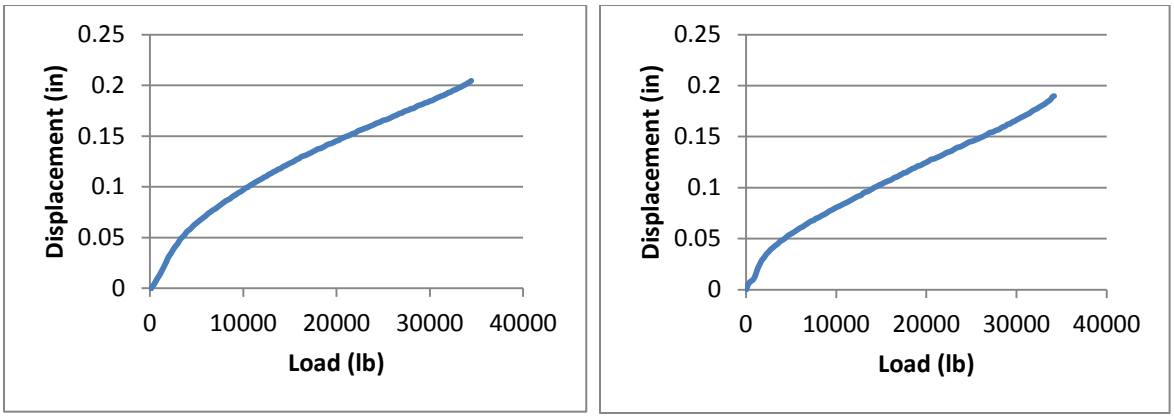

a) Modified short wedge b) Standard Wedge

Figure 5.8: Average Wedge Displacements

The third criterion that will aid the comparison between the modeled strand and the experimental strand will be the strain distribution within the anchor. The average strains in the top and bottom of the anchor, shown in Appendix B, will be compared to the strains measured in the model's anchor for the respective wedges. This comparison should determine if the anchor is modeled correctly and if there is an accurate transfer of strains between the strand and anchor. All of these parameters will be discussed more in depth in Chapter 6, where the model results are compared.

Chapter 6: Finite Element Modeling

The program that was chosen to run and construct the model of the anchor wedge mechanism was Abaqus CAE 6.13-3. This is a very powerful finite element modeling program. It is all encompassing, which means that the model is built, run and analyzed in one suite. The model was constructed and run in an explicit mode. This mode greatly differs from a standard mode. In the explicit mode multiple time steps are used and each sequential time step is based off of the previous one. This allows for deformations to influence how the system will react in the time steps following the deformation. A standard model would not have taken this deformation into account and simply restarted analysis at the beginning of the next time step.

The first step was building each piece. The geometry of all the individual parts had to be created within the program. All the pieces then needed to be assembled in the model space and boundary conditions needed to be applied. Then an independent variable needed to be selected. Different iterations were then run with different values for the independent variable. From these iterations various types of data were extracted. The raw data was then reduced in Excel so it could be compared to the data acquired from the experimental tests. All of this is used to determine if it is feasible to model post tension wedges in a finite element program. In order for the model to be considered feasible the failure stresses and strains would need to match the experimental values and the modified short wedges would need to fail at higher strains than the standard wedges. The wedge seating and anchor strain will serve as secondary comparison criteria.

6.1 Construction of the Model

The first step of creating the model was the geometric construction and assignment of material properties of the individual parts. These inputs served as the base point for the model.

The strains and stresses observed ultimately depend on the definition of the material properties. It is also important to note that Abaqus has no unit functions. This is to say that all units must be uniform throughout all inputs and the output will coincide with the input units. For this study all units were pounds, inches and seconds. The modified short wedge's gap control and angle differential properties all stemmed from the difference in the geometry between the standard and modified short wedge. If a difference between the modified and standard wedge mechanisms was to be observed the geometries had to reflect these mechanisms. Additionally, if the material properties were different from those that were used in the experimental part of the study, the conversion between strain and stress would be incorrect.

The limits place on the model represented the actions or constraints that were placed on the experimental model. These consisted of a fixed constraint, an applied load, and a displacement. These limits correspond to actions observed in the experimental procedure; reaction at the support, seating load, and displacement load, respectively. These limits are what allow forces to develop with in the model and eventually lead to the stresses and strains being developed.

The interactions between components are the most variable part of the model. It is necessary to define how certain surfaces will interact. Without these interactions, the faces of parts will simply move through each other within the model. Interactions are specifically important for this model because of the extremely dynamic relationship between the strand, wedge and anchor. The interaction between these surfaces is what causes the gripping action of the strand, which ultimately causes the failure of the strand.

6.1.1 Geometry and Materials

The first part created was the strand. This was assumed to be one solid cylinder. The part was drawn as a circle with a radius of 0.25 inches and a length of 20 inches. This length was chosen to ensure that an even stress and strain distribution would be able to build up within the strand. Additionally, the twenty inches allowed there to be extra strand above the grip which prevented a pull out failure. The cross-sectional sketch of the strand can be seen in Figure 6.1. This strand was used for both the modified trials and the standard trials.

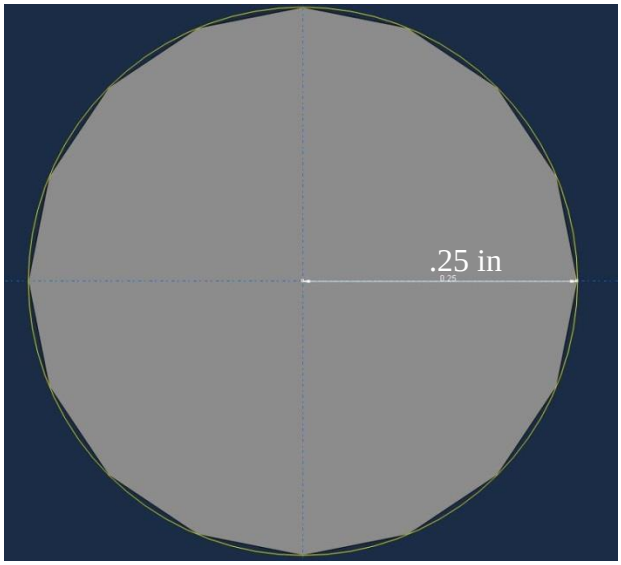

Figure 6.1: Cross-section of Strand

The strand's material properties were by far the most important material properties within the entire model. The strand properties would determine when a failure occurred while the model was running. If these properties were inaccurate, the stress-strain curve observed in the model would not match that observed in the experimental tests. A particularly difficult aspect of this stress-strain input was that a plastic region was required to fully represent the strand behavior. This requires the stress-strain curve obtained from the free length tests, described in Section 5.1,

needed to be adjusted to true plastic stresses and strains in order to be entered into the material model of Abaqus.

The first step to obtaining the true stress and true plastic strain was calculation of the elastic modulus. This was simply done by finding the slope of the elastic region of the free length curve. It was found to have a value of 28.64 x 10^6 psi. The remaining plastic values were then run through the following calculations. A table of the resulting values can be observed in Appendix C. The following equations originate from LS-DYNA Support.

True Stress

$$\sigma_o * (1 + \varepsilon_o) = \sigma_T \quad 6.1$$

True Strain

$$\ln(1 + \varepsilon_o) = \varepsilon_T \quad 6.2$$

True Plastic Strain

$$\varepsilon_T - \left(\frac{\sigma_T}{E}\right) = \varepsilon_{TP} \quad 6.3$$

Ultimately, three different types of material characteristics were assigned to the strand: density, elasticity, and plasticity. The density value used was 0.28 lb/in^2. The elasticity property required the elastic modulus which was entered as 28.63 x 10^6 psi and a Poisson's ratio which was entered as 0.3. Finally, the plasticity values were entered in the form of a table containing the true stress and true plastic strain as discussed above.

For the anchors and wedges the initial geometry was obtained from shop drawings obtained from Hayes Industries, the company that manufactures the wedges and anchors used in this study. However, some dimensions needed to be manually calculated from the given dimensions since the drawings were not complete. Additionally, there was no shop drawing for the standard wedge provided. Due to these challenges, it was decided that the model's geometry

would be based off the dimensions of the samples that were available from the population that was tested.

These extra untested samples were measured using a digital caliper and the dimensions were entered into the model. Once these initial dimensions were entered, it was ensured that the standard wedge's angle was approximately 7 degrees. The modified short wedges angle ultimately was calculated to be lower than the expected 8 degrees indicated on the shop drawings. The dimensions within the modified short wedge were slightly adjusted in order ensure the critical angle was met. This adjustment pertained to the 0.26 inch vertical dimension which was increased from 0.25 inch. The anchor dimensions were also checked to ensure it had the critical 7 degree angle. The section drawings can be observed in Figure 6.2(a) through (c).

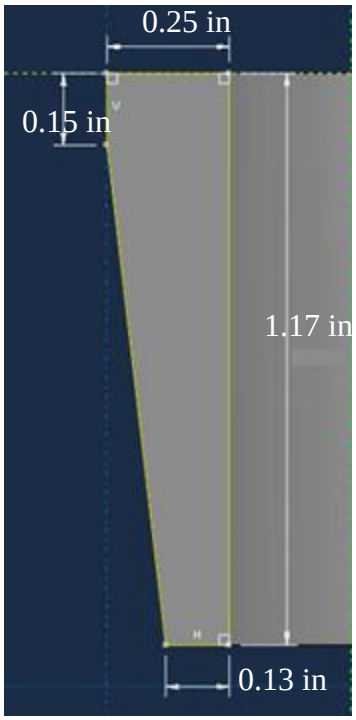

a)Standard Wedge

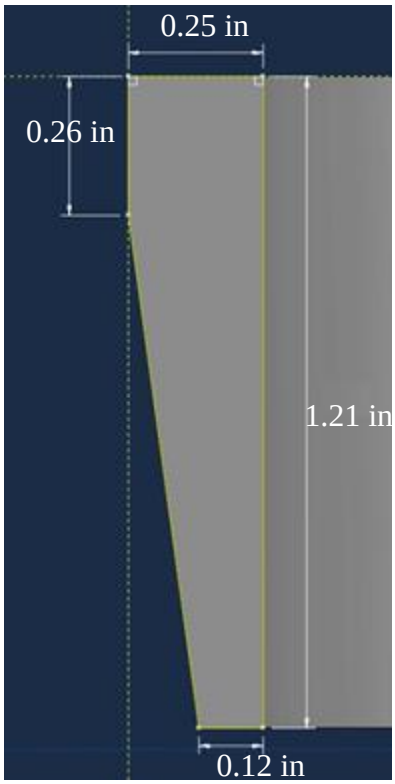

b)Modified short wedge

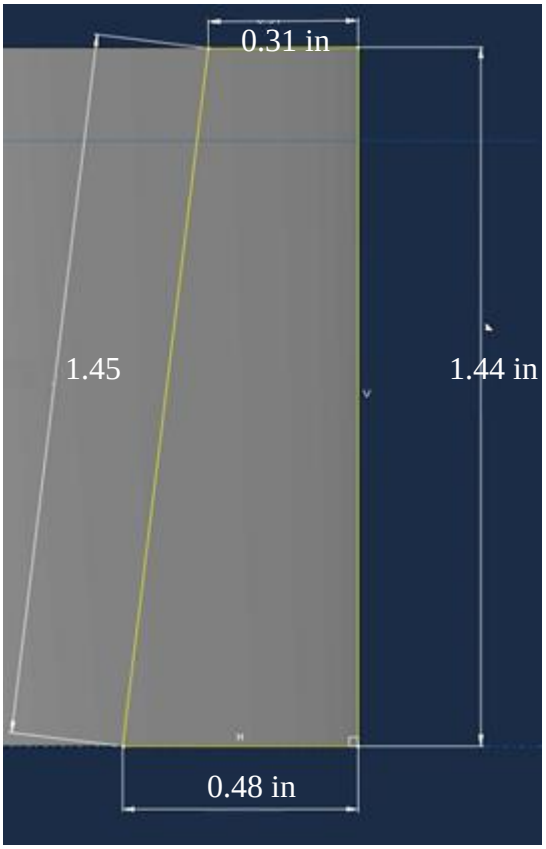

c)Anchor

Figure 6.2: Cross Sectional Sketches

To create a three dimensional object from these sketches, they needed to be revoled in space. The anchor sketch was revolved by 360 degrees to create a solid object. The wedges, due to their different crown widths needed to be revolved about a specific axis. The two distinct paths can be observed below in Figure 6.3. The standard wedge's arc had a height of 0.46 in, while the modified short wedge had a height of 0.49 in. They both had a uniform width of 1 in. This difference ultimately gave the modified short wedge a larger crown width.

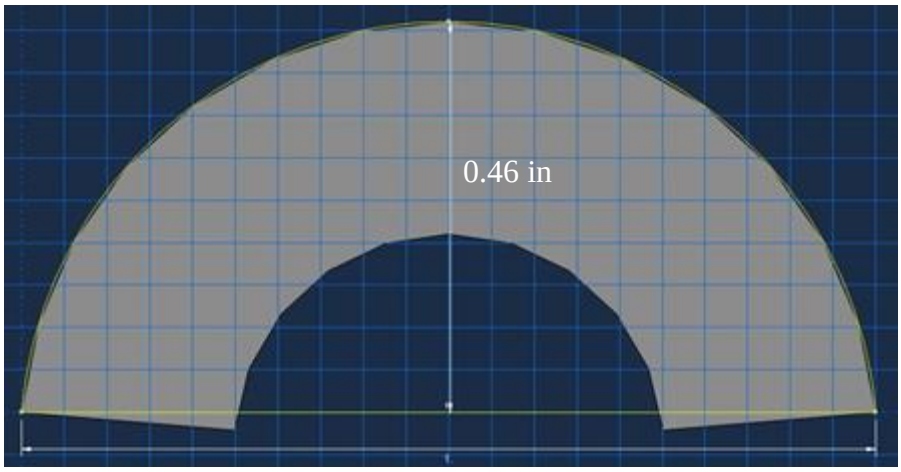

a) Standard Wedge

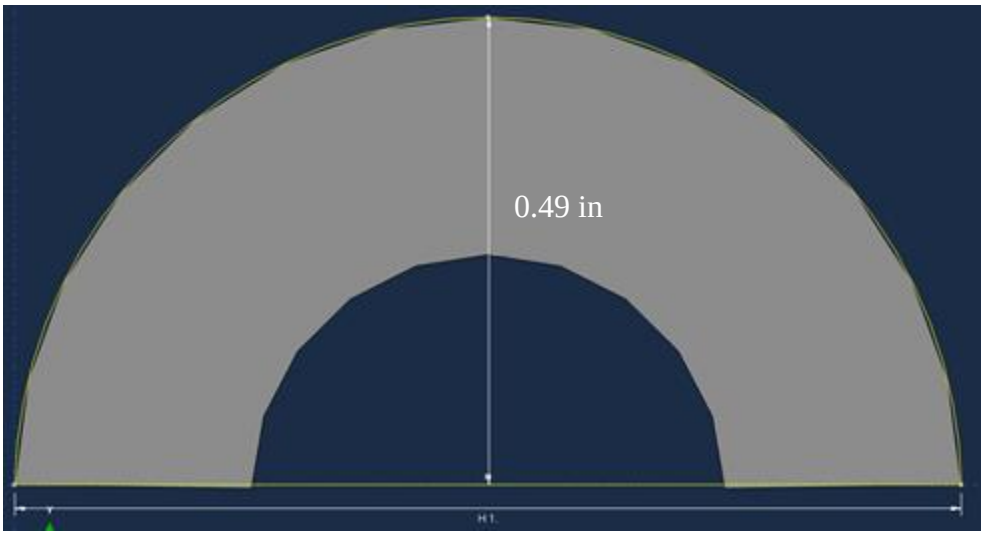

b) Modified short wedge

Figure 6.3: Sweep Paths for Wedge Revolution

Once the wedges were a three dimensional solid, they were copied to provide two wedges as needed for the model.

The material properties for the wedges were much easier to obtain relative to the strand and anchor. The wedges were hardened and therefore assumed to remain elastic throughout the test. For this reason only density and elastic properties were required. The density was set to

0.284 lb/in^2. The elastic modulus was given a value of 29 x10^6 psi and a Poisson's ratio of 0.35 was used.

The anchor steel proved slightly more difficult to enter. Since strain needed to be measured on the anchors, and permanent deformation could be observed in the experimental tests, a plastic aspect needed to be included in the anchor properties. A sample of anchor steel was not able to be obtained for testing so research had to be conducted to obtain the material properties. Multiple studies (Lean and Agile Precision Manufacturing Systems, ME843, and Mechanical Characterization of Pre-Fatigued Free-Cutting Steels under Dynamic Tension), were compiled that had done material testing on the type of steel used to create the anchor. The stress-strain curves that each study provided were averaged together and then run through the same calculations that were used to obtain the true stress and true plastic strain of the strand. The charts used and their sources can be observed in Appendix C, along with the true stress and true plastic strain table. The elastic modulus that was calculated was 28.89 x10^6 psi and a Poisson's ratio of 0.35 was also used. The same density as the wedge was assumed, and the value was set to 0.284 lb/in^2.

After all the geometric and material properties were assigned to each part, the model was assembled. This process consisted of moving the individual parts into their respective positions to replicate the experimental set up. The final assembly can be seen in Figure 6.4.

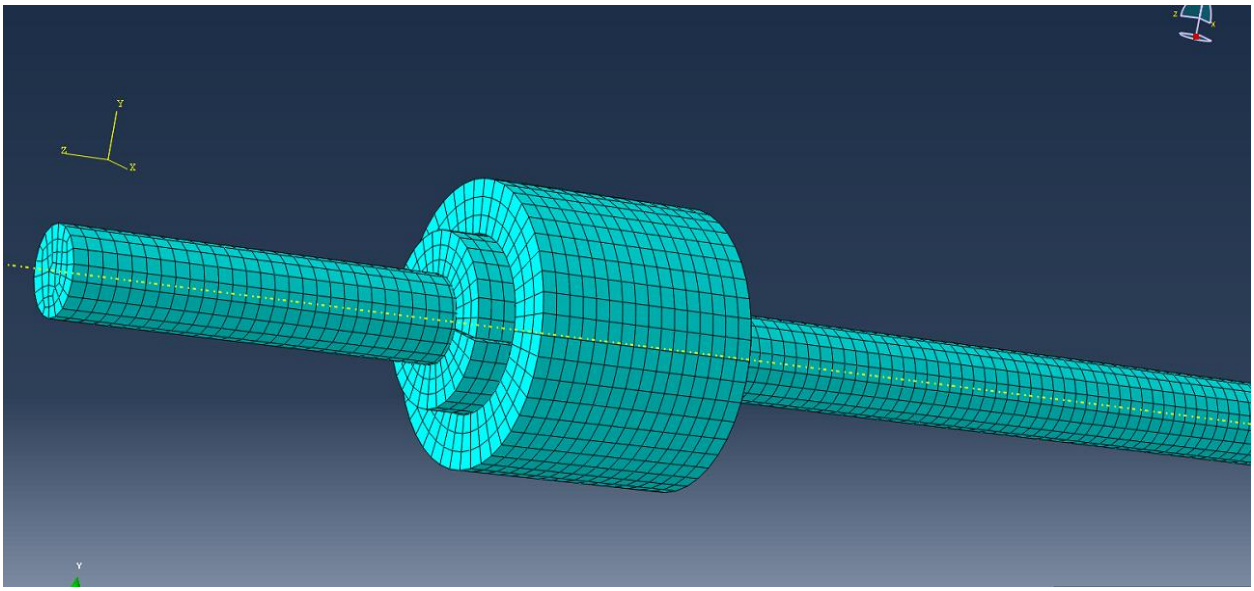

Figure 6.4: Full Assembly of All Parts

Once each part was positioned, each was individually assigned a mesh. The approximate seeding size can be observed in Table 6.1. Creating a mesh divides each part into analytical elements. Once the test is complete, data from any one of the elements can be obtained. If a model has a high number of elements, the data is usually more precise. However, the model will take much longer to run at extremely high element counts. The type of element used was a linear stress hexahedral element. The global seed sizes given in Table 6.1 represent the base size for the mesh.

Table 6.1: Seeding Global Size

Part	App. Global Size
Anchor	0.09
Modified Short	0.08
Standard Short	0.08
Strand	0.09

6.1.2 Boundary Conditions

Once all the parts were assembled and meshed, the next step was to impose the limits and determine at which step they began and ended. The first limit imposed was the fixed base of the anchor. This limit held the bottom of the anchor fixed from any translation or rotation in all directions. In reality, this was not fixed in the experimental set-up. The plate below the anchor was fixed. However, modeling the base plate proved to be an extremely complex task and during the experimental tests, no movement of the anchor was observed. This led to the simplification that the bottom of the anchor could be considered the fixed point for the model. This boundary condition was applied at the Abaqus default step named "initial". This ensured that the limit would propagate through all the following steps.

The second limit applied required the creation of a user defined step. This step was referred to as the loading step. It was during this step that the pre-load was applied. No data was recorded during this step, just as no data was recorded during the pre-loading in the experimental tests. A load of 1000 lb was applied over the top of the two wedges. This load ensured that the wedges were in contact with the anchor and strand before the displacement was applied, prevented the strand from simply slipping through the wedges. This load was applied only during the loading step and was removed for the following final step.

The final step was another user defined step denoted as "Step-1(displacement)". This step consisted of the displacement limit which was applied to the bottom of the strand. It was not within the ability of the user to define a rate based displacement, as was done in the experimental procedure. Instead a certain displacement of magnitude -2 in. was defined. Abaqus then enacted this displacement over the length of the step which was equal to one unit. Since this model was run in Abaqus' explicit mode, the program will calculate the displacement, strain, and stress at

multiple time steps determined by Abaqus based on the rate of deformation. This allows these conditions to be viewed as a progression of data, very similar to the data obtained during the testing.

During assignment of limits, multiple sets were created within the model. These sets are simply groups of either nodes or geometries. Having these sets defined allows for the extraction of data from a certain range of elements. It also allows for an easier process of assigning boundary conditions. There are multiple sets throughout the model and not every one will be discussed. The main sets used for data acquisition will be defined in the model results section. However, most of these sets and the required output requests were assigned at this point, before the interactions were defined.

6.1.3 Interactions

What proved to be the most challenging aspect of the model was defining the interactions. Selection of interaction models that produced reasonable results involved multiple iterations. Eventually, it was concluded that the interactions were dependent upon two aspects: mesh size and interaction properties. The mesh sizes stated in Table 6.1 are the final sizes that were used. However, during earlier iterations a larger mesh was used, in order to speed up the calculation times as to allow for more iterations to be run per day. It was observed that in order to have two surfaces interact in the correct way, the meshes must be small enough for multiple contact points. This way, the interaction property can recognize the contact surfaces.

For the interaction properties, four distinct types of interactions were defined: wedge-tendon displacement, wedge-tendon loading, wedge-wedge, and wedge-anchor. (Note the strand is referred to as a tendon as this was the terminology used in Abaqus) Wedge-tendon displacement was assigned to be active during Step-1 (displacement). This interaction defined

how each inner wedge surface interacted with the strand surface. It was necessary to define two types of properties to this one interaction, tangential and normal. The normal direction interaction was simply defined as a hard contact interaction. This prevented the strand from physically passing into the wedge. Essentially, it caused the model to replicate a normal force when the two parts pushed against each other. The tangential interaction property was defined as a rough interaction. This means that the two surfaces were held together with virtually no slippage along the faces once contact was initiated. This interaction is justified by the fact that the wedges have buttress style teeth that engage the strand once it comes into contact with the wedge. These teeth were not modeled within the geometry of the wedge, so it was necessary to represent their contribution to the system through the interaction properties. It is important to note that in early iterations of this model, this tangential property was modeled with a coefficient of friction. However this coefficient allowed for relative slippage between the strand and wedge that was not observed in the experimental trials. Therefore it was deemed more accurate to apply a rough condition.

The next interaction assessed was the wedge-tendon loading. The interaction was applied during the seating load, when the preload was applied. This interaction was applied to the same surfaces as the wedge-tendon displacement interaction. It even had the same normal interaction property. The difference was in the wedge-tendon tangential property. This interaction property was modeled as a frictionless interaction, rather than a rough interaction. This is because the wedges' buttresses were created with a sloped face on one side. This allowed the tendon to slide in one direction while being held in the opposite direction. (Figure 6.5) This allowed the wedges to slide along the tendon during the loading stage, until they were in contact with the anchor and

strand. Then, when the displacement step took over the wedges gripped the tendon with a relative displacement of zero.

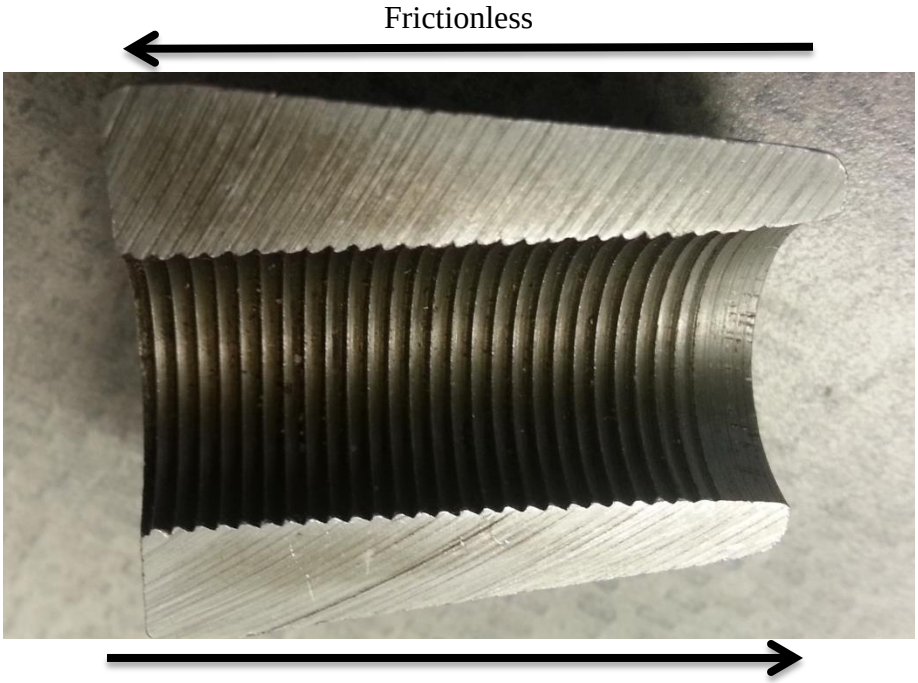

Figure 6.5: Detail of Buttresses

The simplest interaction within the model was the surface contact for when the wedges came into contact with each other. This is the wedge-wedge interaction. It was modeled as a normal hard contact interaction. This interaction was applied to all the faces with in the model, although it was initially designed for only wedges. The interaction ensured that all the solid parts within the model acted as solids and that no parts were allowed to meld into each another.

The final interaction that was assigned was the wedge-anchor interaction. This interaction had two distinct properties as the wedge-tendon interaction did. A normal component, modeled as a hard contact, was applied in the normal direction. A penalty friction interaction was defined in the tangential direction. This type of tangential interaction allowed a coefficient of friction to be assigned to the interacting surfaces. This coefficient of friction became the independent

variable in model iterations. As stated before, the previous studies suggested an acceptable range would be from 0.11 to 0.30. The range explored in this study went from 0 to 0.70. The coefficients of friction tested were: 0.0, 0.01, 0.11, 0.20, 0.30, 0.50, 0.60, and 0.70.

After all of these parameters were entered into the model, it was copied, and the standard wedges were swapped for the modified short wedges. Multiple copies of each model were created and each was assigned a specific friction coefficient. The models were then run and data was extracted from the predetermined sets. The process outlined above is the final simplified procedure of building the model. There were multiple iterations run that failed for various reasons. These debugging procedures were not directly recorded because an immediate solution was not always clear and often led to more issues than solutions. The above represents the most accurate description of a procedure to regenerate the model discussed in future sections. The input files for a base standard model and a base modified model are provided in Appendix D.

6.2 Data and Results

As mentioned previously, there were three different parameters that were investigated in the model: stress-strain failure points, wedge displacement, and anchor strain. The stress strain data was extracted from a single node on the tendon denoted as a set titled StrandN. This single node accurately represents the results that would be obtained from a strain gage placed on the strand. It was ensured that the node was not in the presence of a region that experienced localized deformation. The wedge displacement was taken as an average of all of the data returned over the surface of one of the wedges. This set was titled WedgeDisplacement. The load data was calculated using the sum of the reaction forces that were present at the fixed face of the anchor. The set was titled BottomofAnchor. A sum rather than an average was required because the output returned the force that each individual element contributed. Finally, the anchor strains

were obtained from a single node near the center of the anchor. This node was in a set titled AnchorN. By utilizing a single node, rather than two nodes to correspond to the two strain gages, the gauges could be used as boundary limits. From observing the recorded data for the experimental tests, it was assumed that the data from the analytical model will be very variable. Boundary conditions were a more effective way to quantify the strains experienced.

Once the data was extracted from Abaqus, it was put into Excel where it was reduced. One reduction consisted of trimming the data to remove data points that were recorded after a failure. As will be seen in the data images in Appendix E, extreme necking occurred within the model. During the necking, the stress was reduced dramatically. It was this point of extreme necking that was considered a failure. The sudden loss of capacity can be observed in Figure 6.6.

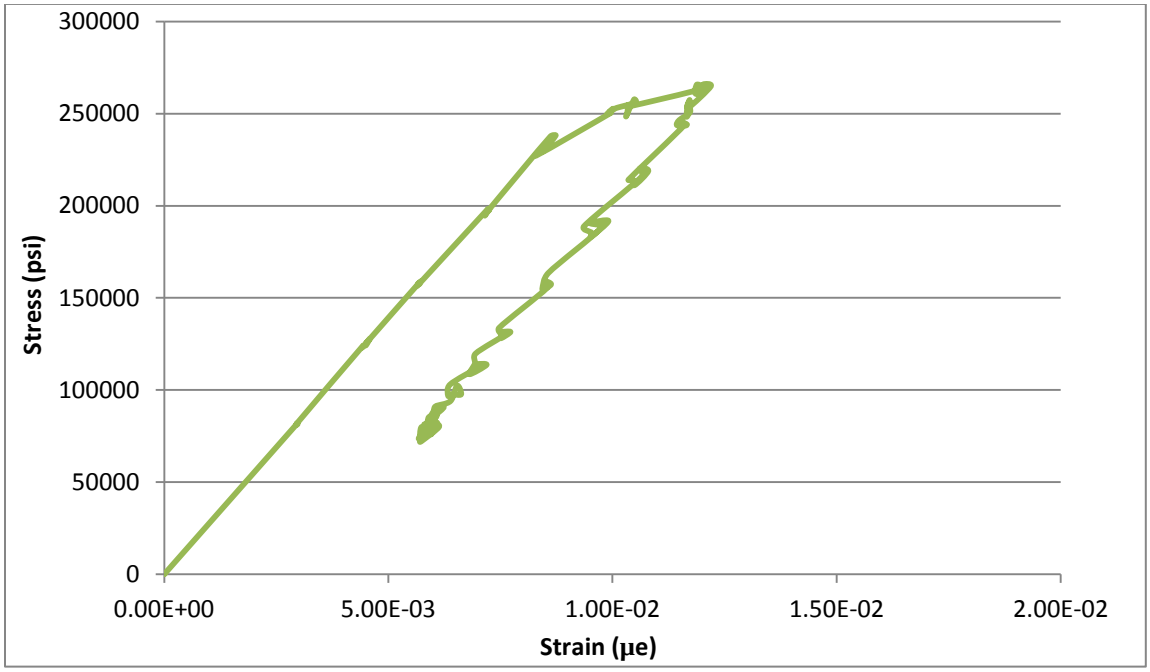

Figure 6.6: Example of Raw Stress Strain Chart

The other simple reduction was the multiplication of strains by 10^6 in order to have a micro strain value. These adjustments allowed the data to be compared to the experimental data.

6.2.1 Standard Wedges

The first model that was analyzed was the standard wedge model. This model returned very promising results for all the friction coefficients tested. A plot of all the stress strain curves for each coefficient can be observed in Figure 6.7. All the plots follow the same elastic modulus and have failure points around the stress strain coordinates that were observed in the experimental tests.

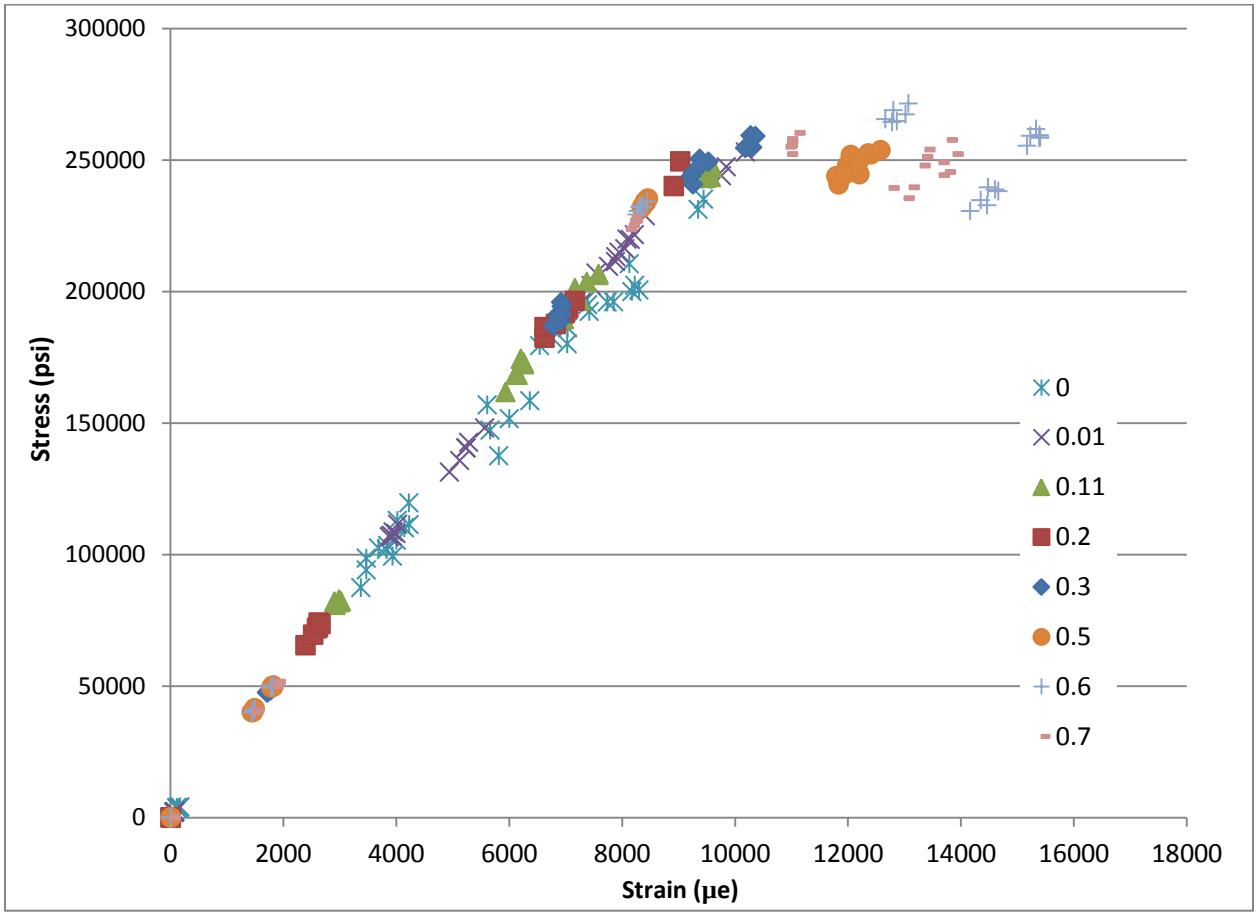

Figure 6.7: Standard Short Stress Strain Curves

It is important to notice that as the friction coefficients increase to higher values the plastic part of the curve becomes more prominent. This is also illustrated by Table 6.2. This phenomenon is believed to be a representation of the gap control principle being enacted by friction rather than by wedge contact. This theory of gap control by friction is also supported by the wedge

displacement which is discussed in the upcoming paragraphs. The wedge did not experience as much displacement at high friction coefficients as it did at lower coefficients. This means that the wedge was being held back from over penetrating into the strand. This is the same mechanism that is enacted by gap control. This phenomenon motivated the testing of higher unrealistic friction coefficients to see if the gap control mechanism could be replicated with higher friction values.

After each stress-strain curve was plotted, the failure points were extracted and organized into a table. These were then compared to the average failure point for the standard wedge presented in Table 5.3(a). There was one outlier in the standard short experimental trials. For this reason an adjusted average value is used when calculating the percent difference between the model and experimental trials. This adjusted average excludes the anomaly of the extremely high strain reached. The comparisons can be observed in Figure 6.8 and Table 6.2.

Table 6.2: Standard Short Comparison

	Stress (psi)	Avg Stress (psi)	% Difference	Strain (με)	Avg Strain (με)	% Difference
0.00	235031	252740	7	9444.95	9259.52	2
0.01	253014	252740	0	10185.7	9259.52	9
0.11	247163	252740	2	9603.38	9259.52	4
0.20	249473	252740	1	9027.96	9259.52	3
0.30	259017	252740	2	10364.2	9259.52	11
0.50	253751	252740	0	12579.9	9259.52	26
0.60	258562	252740	2	15409.2	9259.52	40
0.70	252236	252740	0	13868.5	9259.52	33

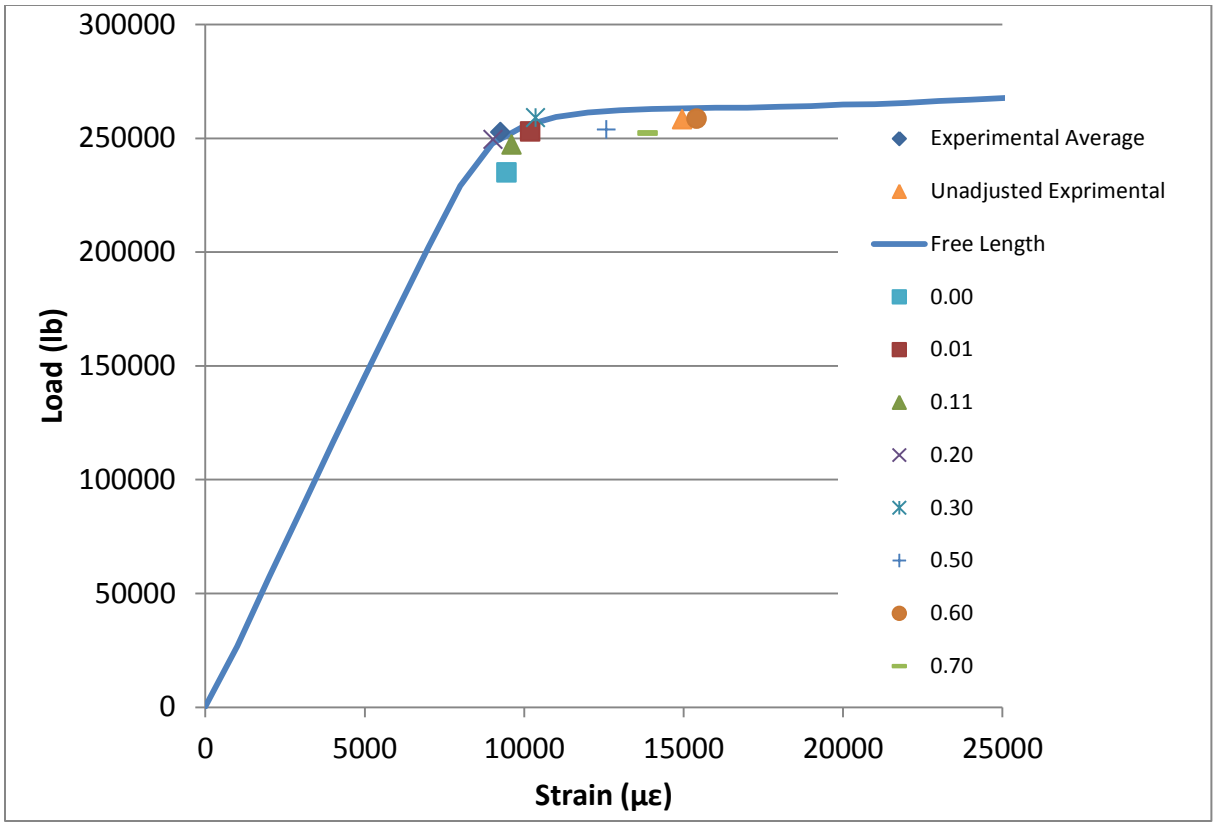

Figure 6.8: Standard Short Comparison

As can be observed in the above table and graph, the different coefficients of friction cause a failure just as the strand is entering its inelastic phase. This correlates extremely well with the experimental tests.

The second criterion that was examined was the wedge displacement. The comparison of wedge displacement proved difficult because of differences in loading rates and the absence of teeth on the wedge model. The model was loaded at a more rapid rate, which leads to a delayed seating effect. This is clearly visible in Figure 6.9. Additionally, the absence of the buttresses being modeled meant that the wedge was unable to penetrate into the strand which might have increased the wedge displacement. Finally, issues with the mesh interacting may have caused the delayed displacement. If the mesh had been in contact at multiple places, it may have taken a higher load to initiate motion. This would also explain why the modified geometry experienced a

more uniform displacement, because there were fewer points in contact. The load at which the wedge seating data was cut off corresponds to the same time point that the stress-strain curve determined there was a failure. Ultimately, it was decided to compare the final displacements of the analytical trials to the last known displacement of the experimental trials. Since the potentiometers were removed just as the strand reached its inelastic phase, it can be assumed that any elongation was picked up by the strain experienced by the strand. Table 6.3 and Figure 6.9 show a comparison of these points.

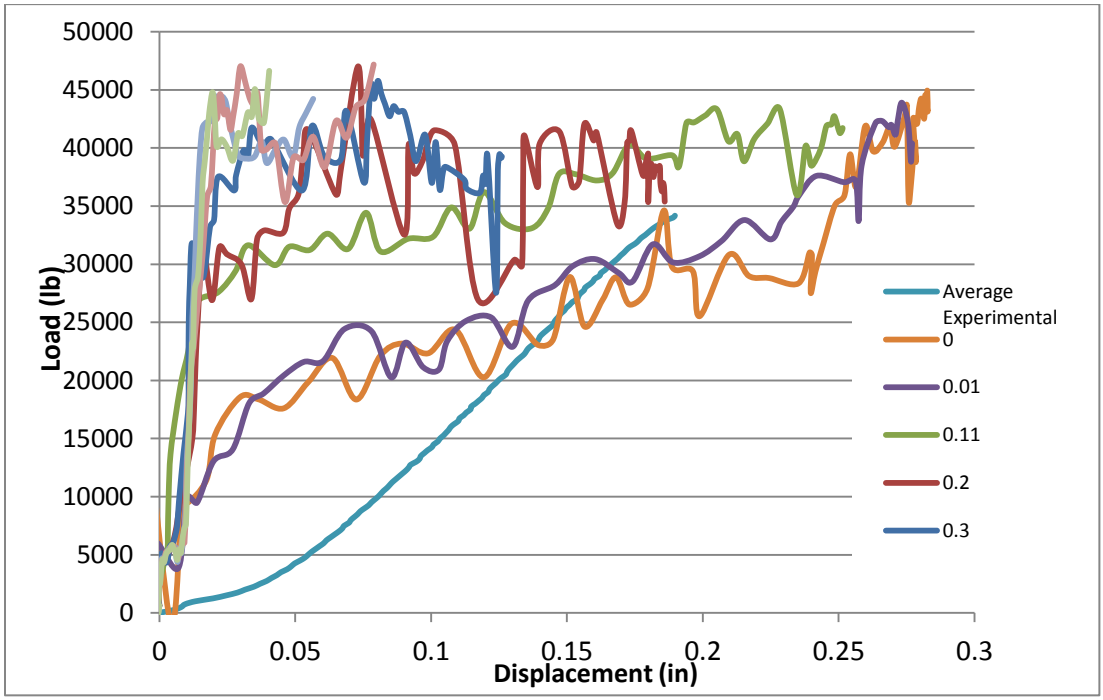

Figure 6.9: Standard Wedge Comparison

Table 6.3: Standard Wedge Comparison

Trial	Abaqus Displacement	Experimental Displacement	% Difference
0.00	0.2827702	0.18975	33
0.01	0.2770453	0.18975	32
0.11	0.2514694	0.18975	25
0.20	0.1859801	0.18975	2
0.30	0.1260717	0.18975	34
0.50	0.0566272	0.18975	70
0.60	0.0788825	0.18975	58
0.70	0.0404295	0.18975	79

The third and final comparison criterion was the strain in the anchor. A point in the middle of the anchor was used to obtain the strain data. This point was selected based on the theory that the curve should fall between the top and bottom average anchor strains. This was not the case as can be seen in Figure 6.10.

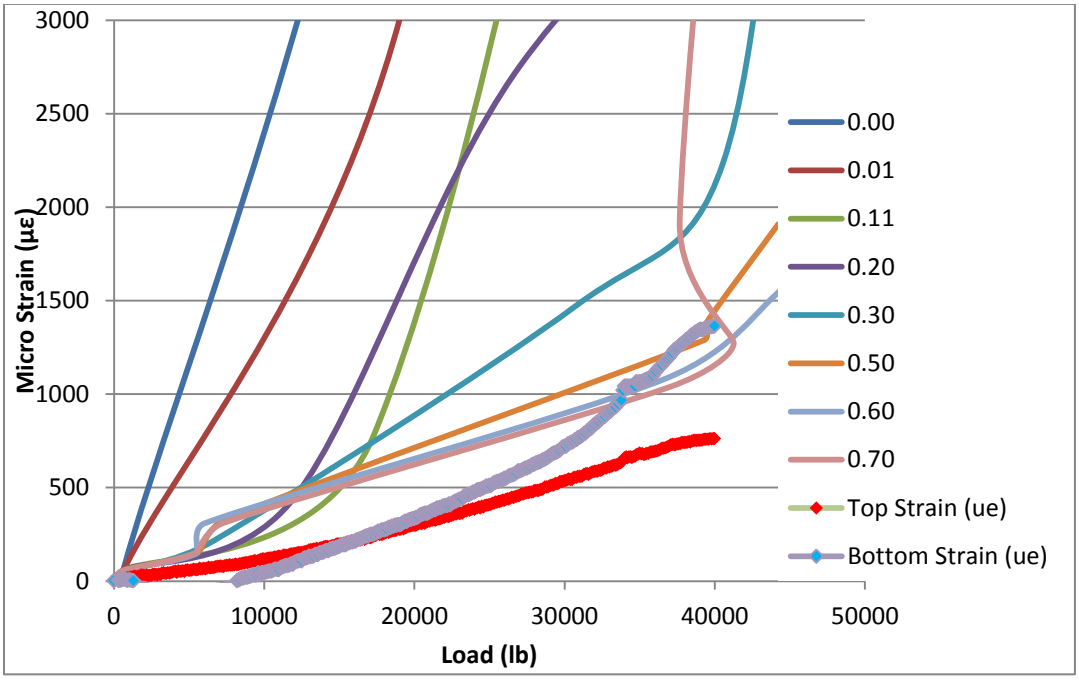

Figure 6.10: Standard Anchor Strain Comparison

The graph shows that the strains did not correlate well between the experimental data and the analytical data. This can be attributed to an error in the anchor material properties, since all of the other criterions seemed to be relatively accurate. The anchor material was input as a plastic material, as mentioned in Section 6.1.1. There were no actual lab tests carried out on the material and this may have led to inaccurate material properties being used.

The above data suggests that the most accurate frictional coefficient to use in the model is somewhere between 0.2 and 0.3. These frictional coefficients constantly return results that resemble those observed in the experimental trials. Additionally, when viewing the failed analytical models, which are present in Appendix E, the failure occurs at the nose of the wedge. This is expected because the nose of the wedge is where the stress concentrations form which prevent the strand from reaching its inelastic phase. The reason that the higher friction coefficients allowed for higher strains is due to the fact the wedge did not penetrate into the anchor as far as it did in the experimental trials. This prevented the pinching of the wedge, producing a similar effect to the enlarged crown for the modified short wedges. Thus using too high of a frictional coefficient will cause the return of inaccurate results and will represent a mechanism that is not present with standard wedges.

The above data suggests that an analytical model could be used to model the mechanism of a standard wedge. The data for the stress-strain failure points correlate very accurately. If the anchor properties are refined, the strain in the anchors will become more realistic. This could be achieved by carrying out material tests of the steel used to construct the anchor. Samples would have to be directly obtained from the manufacturer.

6.2.2 Modified short wedge

The modified short wedge model was assessed after the standard model had been reduced. The results from the analytical model were reduced and evaluated in a similar process as the standard wedge. First, the stress-strain data was extracted and graphed on a combined graph. The data for the modified short wedges returned much more variable data than the standard wedges. There were some substantial differences in the failure points for different coefficients of friction. This can be seen in Figure 6.11, which shows the analytical stress-strain curves.

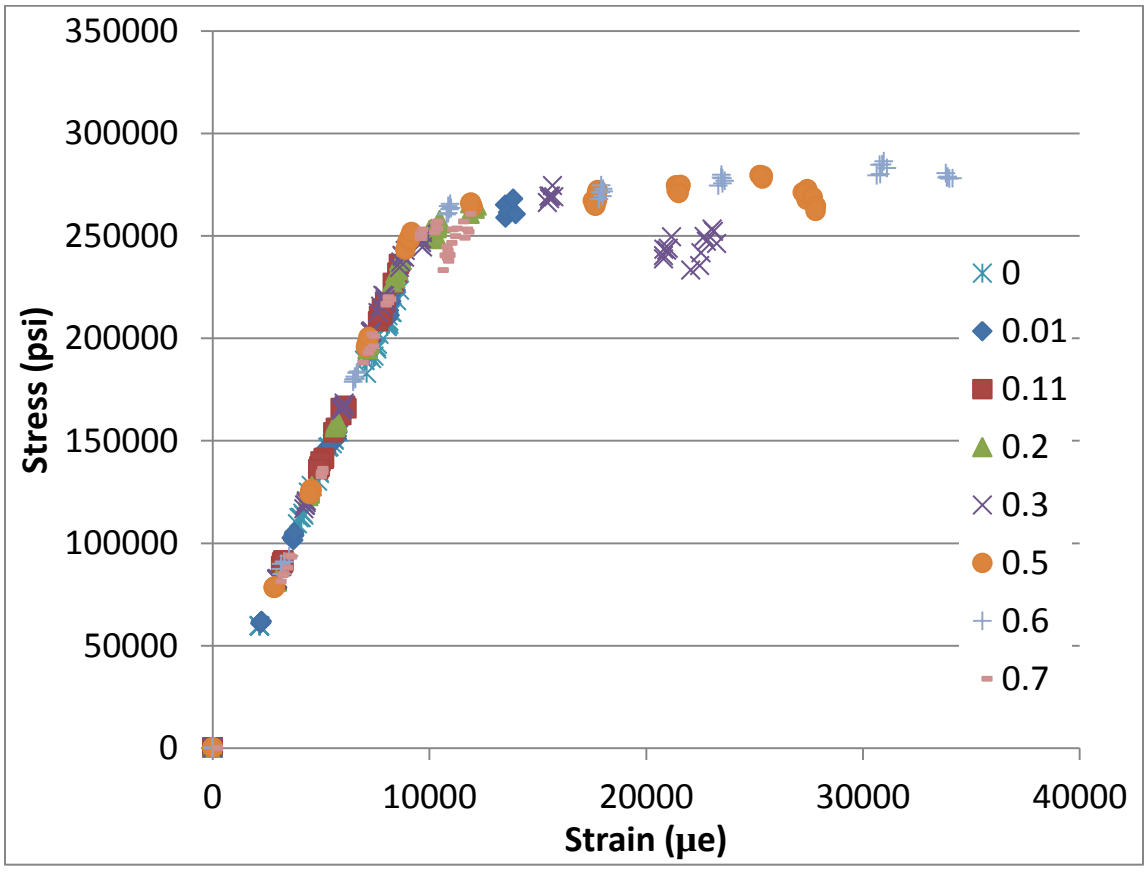

Figure 6.11: Modified Stress Strain Comparison

There are a few coefficients that allow the strand to reach high strains. However, eventually the coefficients start to counteract the wedge mechanisms. The coefficients of 0.3, 0.5, and 0.6 all

allow for higher strains, but the other coefficients seem to limit the strand to a strength just above the elastic portion of the graph.

Overall, the strains from the analytical model came out much lower than the strains observed in the experimental trials. This can be seen in Figure 6.12 and Table 6.4.

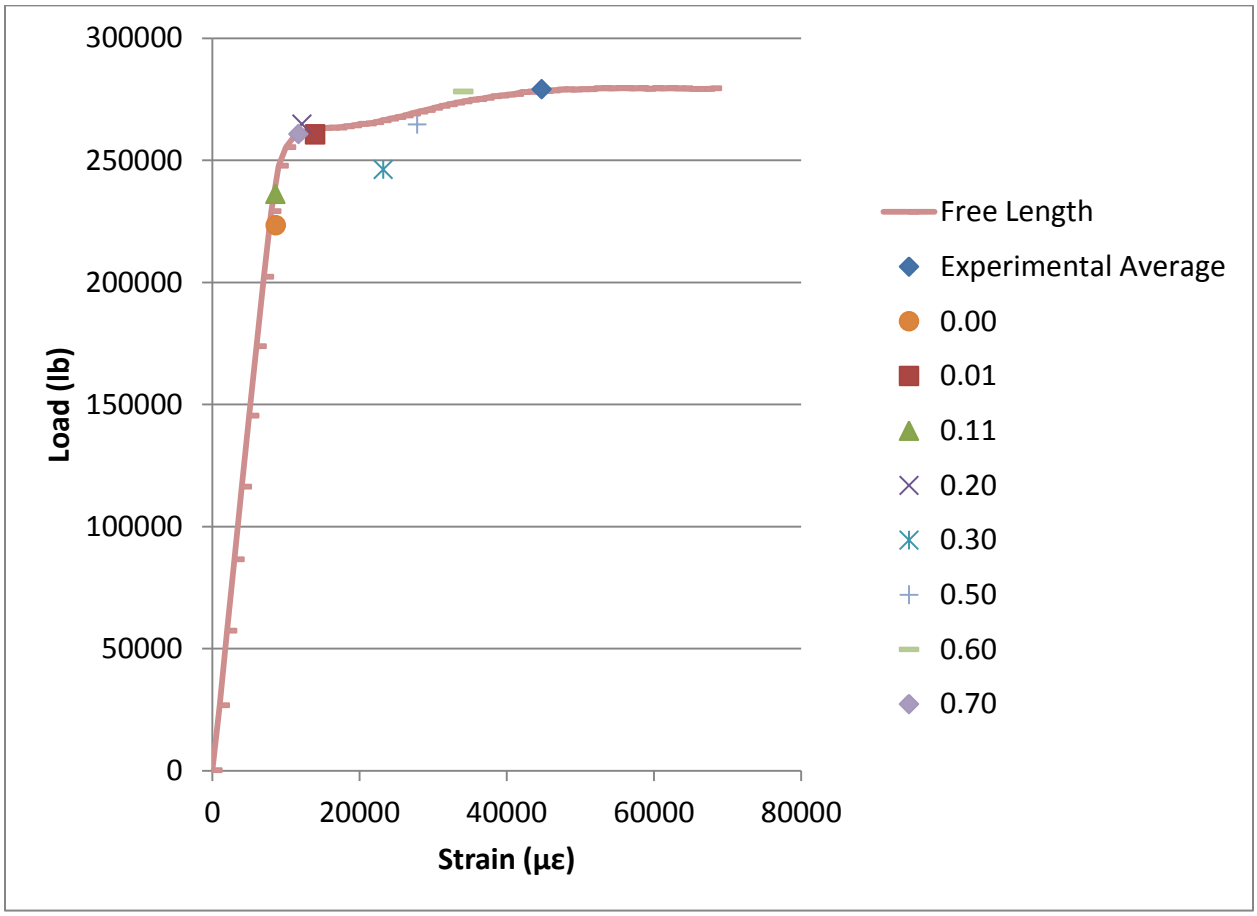

Figure 6.12: Modified Comparison of Stress Strain Failures

Table 6.4: Modified Comparison of Stress Strain Failures

	Stress (psi)	Avg Stress (psi)	% Difference	Strain (με)	Avg Strain (με)	% Difference
0.00	223397	279032	20	8627.89	44766.50	81
0.01	260519	279032	7	13981.1	44766.50	69
0.11	236259	279032	15	8604.76	44766.50	81
0.20	264836	279032	5	12193.2	44766.50	73
0.30	246218	279032	12	23258.5	44766.50	48
0.50	264632	279032	5	27839.3	44766.50	38
0.60	278130	279032	0	34132.8	44766.50	24
0.70	260666	279032	7	11696.2	44766.50	74

As can be observed, there is a significant percent error between the analytical failure points and the experimental average failure points. The reason for this is the sensitivity of the gap control. This theory is supported by the fact that as the friction coefficients rise in value, the strains achieved are higher, up to a coefficient of friction of 0.6. The observation of this phenomenon is what drove the use of unrealistic coefficients such as 0.5, 0.6, and 0.7. This was also observed with the standard wedges. The reason that this corroborates a failure in the gap control mechanism is because the higher friction coefficients prevent the wedges from fully penetrating into the strand, the same action that is prevented by gap control. The angle differential mechanism appears to increase the capacity because at realistic friction coefficients, such as 0.3, are returning strain values that propagate into the inelastic region, unlike those of the standard wedge. This justification will be explored more in-depth when the two models are compared in Section 6.3.

The modified short wedge displacement matched the experimental results much more accurately than the standard wedges. It was useful to compare the wedge displacement to see if the same frictional coefficients that returned accurate results in the standard wedge trial did so for the modified short wedges. A table of the compared values can be observed in Table 6.5, while a graphical representation can be seen in Figure 6.13.

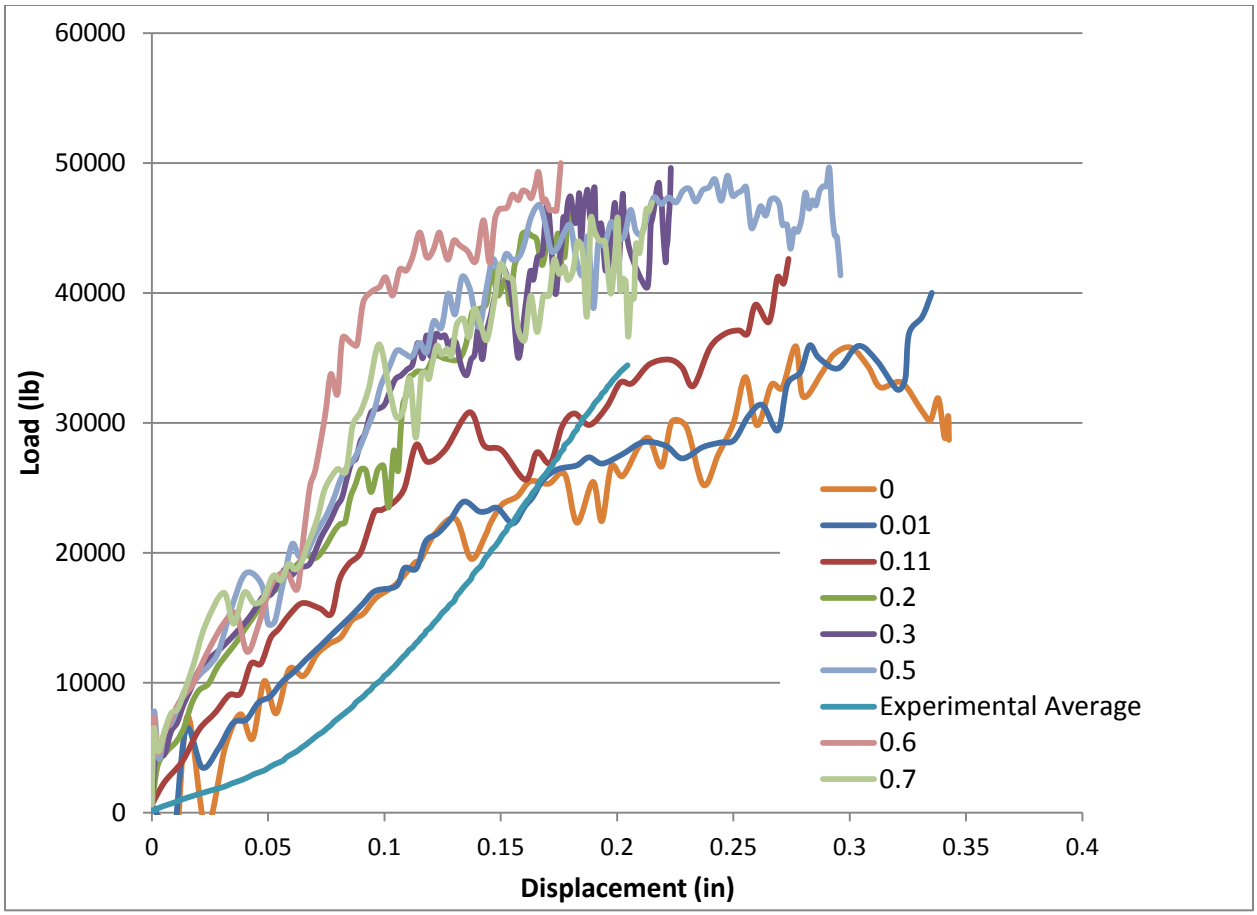

Figure 6.13: Modified short wedge Displacement

Table 6.5: Modified short wedge Displacement

Trial	Abaqus Displacement	Experimental Displacement	% Difference
0.00	0.3426632	0.2045	40
0.01	0.3353119	0.2045	39
0.11	0.2737056	0.2045	25
0.20	0.1856894	0.2045	9
0.30	0.2231028	0.2045	8
0.50	0.2960358	0.2045	31
0.60	0.1757785	0.2045	14
0.70	0.2150714	0.2045	5

Just as in the standard trials, the coefficients of 0.2 and 0.3 seem to return the most accurate wedge displacement values. These results continue to support the literature on analytical modeling, which suggests the use of 0.3 as a frictional coefficient.

The third and final criterion was the strain observed within the anchor. This graph can be observed in Figure 6.14.

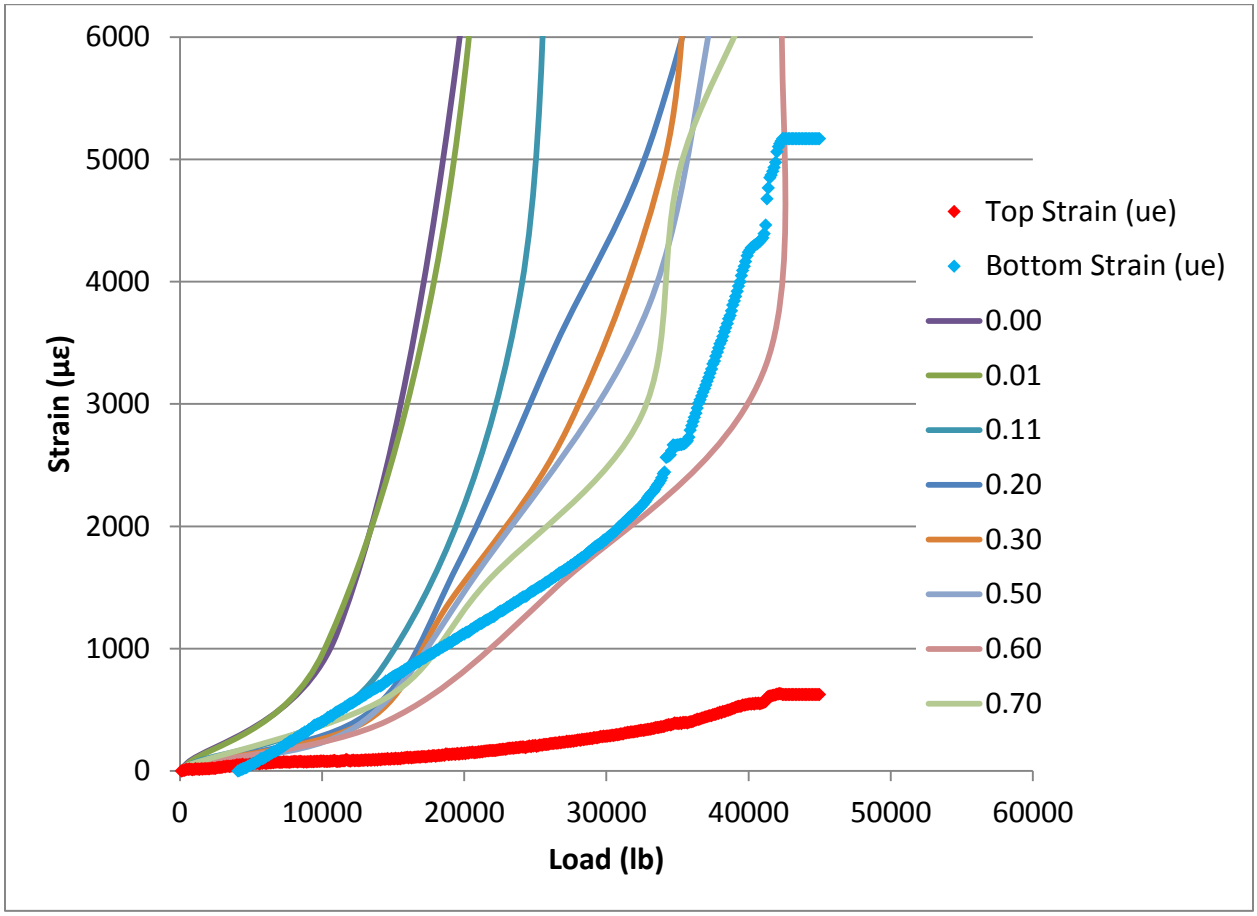

Figure 6.14: Modified Anchor Comparison

Since the anchor properties that were used in this model are identical to those used in the standard model it is safe to assume that the same error needs refining; the anchor properties. If, in material testing, the anchor material is found to have a higher elastic modulus than what is present in this model, less strain would be observed. This may bring the values within the boundary of the top and bottom strain gages.

All of these graphs indicate that the modified model may be a practical way to model the modified short wedge mechanism; however it does need to be refined. The gap control mechanism does not seem to be acacuratly represented in the model. This indicates that the

geometric parameters of the modified short wedges should be refined. It needs to be ensured that the wedges come into contact substantially before the failure of the strand as occurred during the experimental testing of the modified short wedge system. The inelastic strain values indicate that the angle differential can be accurately represented. This is also shown by the failure images that are present in Appendix E and the single picture in Figure 6.15. These pictures show stress concentrations along the back of the wedges initially. The stress then propagates forward through the wedges. This is exactly how the angle differential mechanism was designed to work, rather than have the entire wedge engage the strand as the standard wedge does.

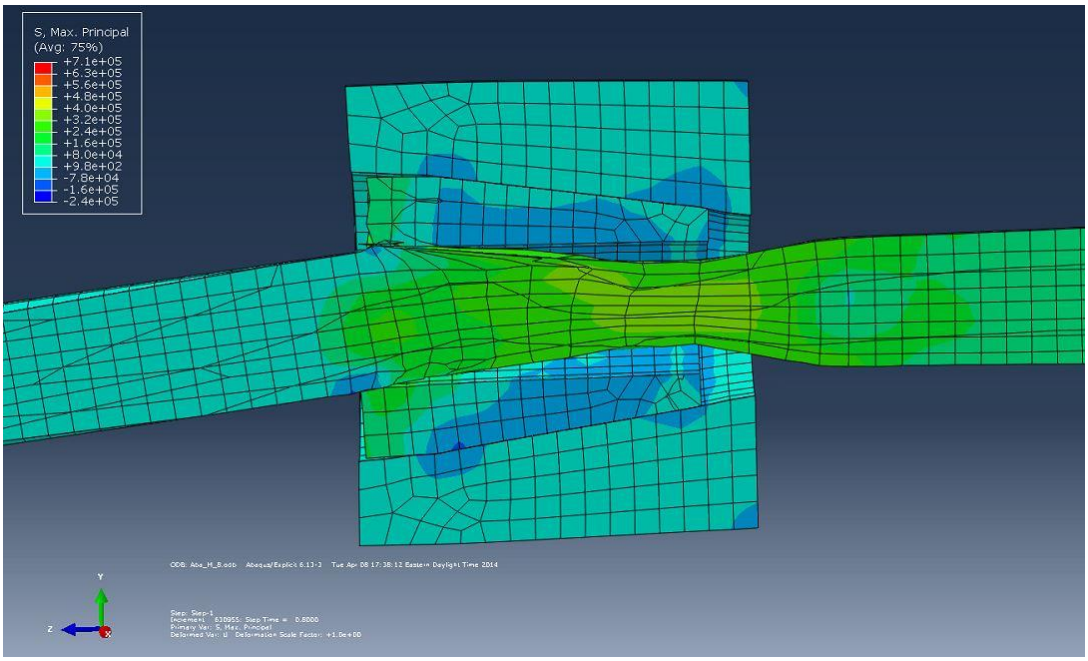

Figure 6.15: Modified short wedge Failure

6.3 Comparison of Models

In order to fully assess the feasibility of using a finite model to represent the mechanisms that occur within a wedge, the modified short wedge model and the standard wedge model must be compared to each other. If a difference between the two models is detectable it will support the theory that the modified model simply needs to be refined in order to align with the

experimental data. This is a plausible theory since the standard data correlates to the experimental data well.

The main comparison will be between the stress-strain failure points. This is the most crucial aspect of the modified short wedge because the modified short wedge was designed to increase the strain capacity of the anchorage system. If the model was not able to detect a significant difference between the strain limits of the two wedges, then the model would not be capturing the effect of the modified geometry observed in the testing. This comparison of strain values can be seen in Figure 6.16.

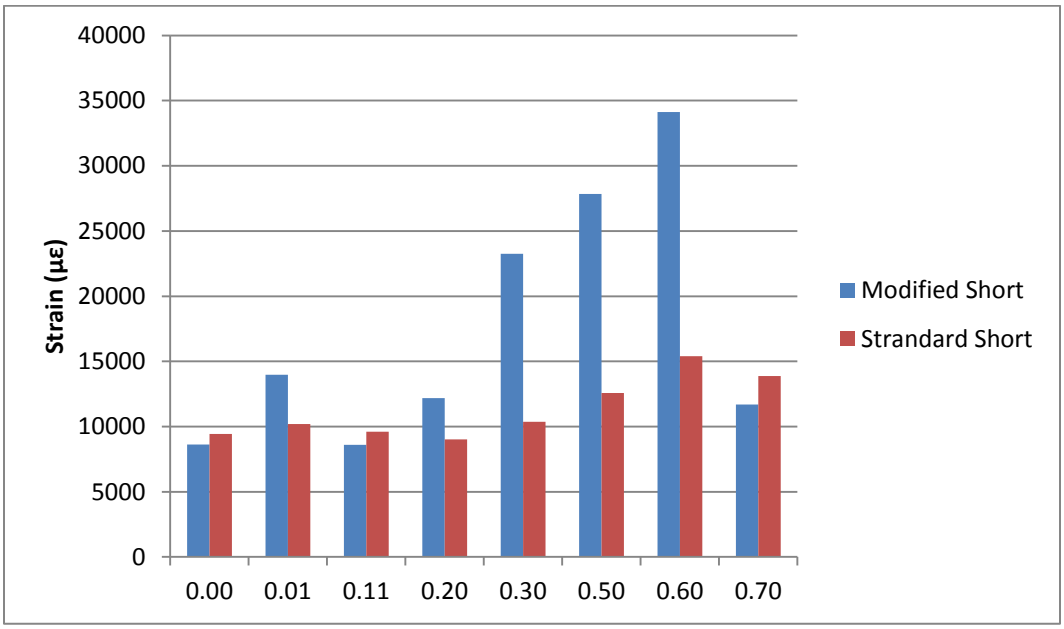

Figure 6.16: Strain Comparison between Trials

According to the evaluation of the individual models and how they compare to the experimental results, it was determined that 0.3 is the most realistic coefficient of friction to be used for the interaction between the wedge and the anchor. These results are also supported by the literature presented in Chapter 2. Therefore 0.3 is the most important test to compare. The strain limit for the 0.3 coefficient of friction was increased by 125% by the use of a modified short wedge. It can also be seen that for the majority of the friction coefficients tested, especially

the ones in the realistic range, 0.2 to 0.5, the modified short wedges preformed substantially better. This indicates that there is a detectable difference between the modified model and the standard model.

The stress comparison is less critical because both wedges should allow the strand to reach the elastic stress limit, when the rate of stress gain drops off dramatically. If a certain wedge had caused a failure at a significantly lower stress limit, this would signal an error in the base design of the model. If Tables 6.2 and 6.4 are reviewed it can be seen that there was no significant difference between the average stress value of the experimental tests and the stress value for any of the strands.

Another important comparison arises from the wedge displacement. A comparison of all the wedge displacements is shown in Figure 6.17. The experimental wedge displacement was roughly 0.2 in and was the same for both the modified and standard wedges. The wedge displacements for the standard and modified short wedges are separated by about 0.1 in at a coefficient of 0.3. However, for a coefficient of 0.2 the wedges experience the same displacement and are approximately equal to the experimental values. The chart also shows that there is not a substantial difference between the wedges displacements except at the higher less realistic coefficients of friction.

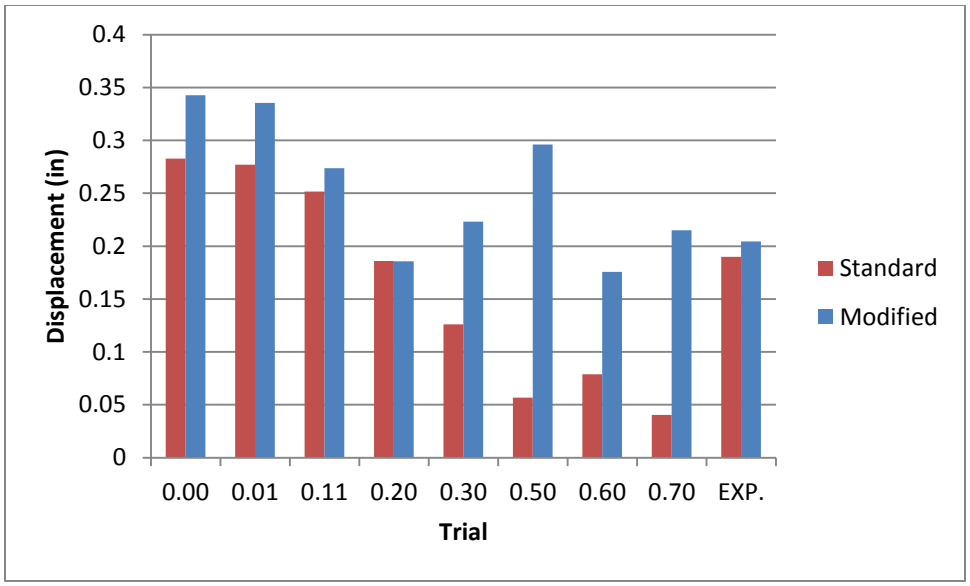

Figure 6.17: Displacement Comparison

The anchor strains are the final comparison criteria to be examined. It is important to note that the following conclusions should not be the main comparison because of the discrepancies between the experimental tests and the numerical models. Additionally, the results of the anchor strain can be drastically changed by the refining of the anchor material properties. It is still interesting to conduct a comparison of the strains experienced by the anchors that use different wedges. The strain comparison graphs are regenerated below in figure 6.18 in order to facilitate comparison.

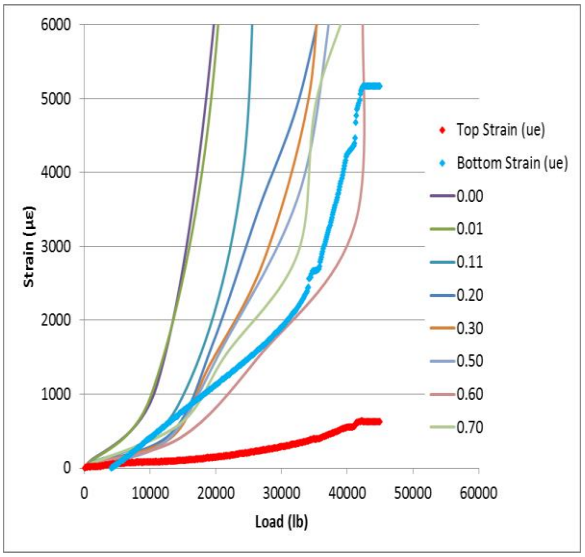

a) Modified short wedges

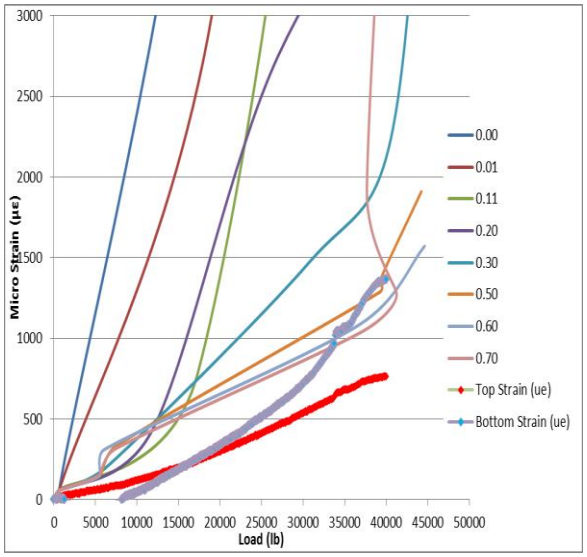

b)Standard Wedges

Figure 6.18: Anchor Strain Graphs

To determine that the anchors did indeed interact differently with each wedge type, the shape of the above graphs must be examined rather than the actual values. The modified short wedges had a quickly increasing slope trend throughout all the data samples, including the bottom strain of the experimental trials. The standard wedges had a trend of having lower slopes. This is reflected by the experimental trials. The two models seemed to generally follow this trend for each of the wedge types. The scale of the numerical values may be inaccurate; however the general shape of the experimental average is reflected throughout the trials. The reason for this accelerated strain growth is due to the fact that the modified short wedge focuses all of the early stress in the bottom of the anchor. (recall that bottom corresponds to the wide edge of the wedge or "back" of the wedge). This increased strain concentration is an indication that the slope differential mechanism is effective. Since this is represented in the numerical data, it is safe to say the model can detect the difference between the wedge shapes.

According to the above data, the program is able to detect differences in the models between the standard and modified short wedges. This means that finite modeling can be a

practical way to test different wedge configurations. Although the modified short wedge did not meet the experimental expectations, with refinement it should be possible to attain the expected values. It is viable to consider finite element modeling as path to developing new wedge geometries.

Chapter 7: Summary, Conclusion, Recommendations for Continued Study

This thesis presents the results from the experimental testing of three different wedge geometries; (1) standard, (2) modified, and (3) modified long. It also contains the results from analytical models of two of the wedges, (1) standard and (2) modified. The results were grouped into three criteria; (1) stress-strain data, (2) wedge displacement, and (3) anchor strain. The wedges and their respective models were compared using these criteria. Based on the results of these comparisons discussed in Chapter 6, conclusions about the feasibility of using an analytical model to test different wedge geometries were made. The following points are results from the interpretation of the data presented in this thesis.

(1) The gap control and angle differential geometric features substantially increase the strain capacity of a wedge-anchor system.

(2) Wedge geometry plays a substantial role in strain capacity.

(3) The coefficient of friction that should be used between the wedge and anchor is 0.3 as it returns the most accurate numerical results.

(4) Differences between wedge geometries can be observed using a numerical model.

(5) It is feasible to model experimental wedge designs using numerical models.

Conclusions 1 and 2 are based on the experimental results that show that the modified and modified long wedges were able to reach higher strains compared to the standard wedges. These conclusions are also supported by the studies discussed in the literature review. Conclusion 3 was derived from the comparison of the numerical results to the experimental results. The numerical model of the wedge best represented the experimental tests when a coefficient of 0.3 was used. Conclusions 4 and 5 are supported by the results of the numerical analysis as described in Section 6.3.

Despite the conclusions gathered above, there is significant room for improvement in future studies. If the numerical modeling the wedges is to be continued, the following recommendations should be utilized:

(1) Investigation of more precise friction coefficients ranging from 0.2 to 0.4.

(2) Experimental testing of the anchor material to acquire more accurate material properties.

(3) A refinement of the modified short geometry to better match the experimental results, specifically the dimensions.

These three recommendations would substantially improve the results from the numerical model. Once it is ensured that the experimental results from the modified short wedges can be obtained, the next step would be to begin modeling new wedge geometries to optimize the strand's capacity. Once the optimal geometry is obtained, production and experimental testing of the optimal geometry should be carried out. This final suggestion would involve much more experimental and numerical refinement, but should be the ultimate goal of a working numerical model.

The main objective of this study was to assess the feasibility of using a numerical model to represent two different wedge geometries. This objective was achieved because the numerical standard model generated represented the experimental model with a small margin of error. Additionally, there was a discernible difference between the standard numerical model and the modified numerical model that were consistent with experimental results. The model should undergo refinement in order to more accurately represent the experimental data, but numerical modeling of wedge geometry is feasible approach to designing new, more efficient wedges.

Works Cited

Abramson, Daniel A. *Comprehensive Evaluation of Multistrand Post-Tensioning Anchorage Systems for Seismic Resilient Rocking Wall Structures*. Thesis. University of Minnesota, 2013. Minneapolis: U of Minnesota, 2013. Print.

Acosta, Jose Antonio Arrellaga. Instrumentation Systems for Post-Tensioned Segmental Box Girder Bridges. Master's Thesis, Austin: University of Texas at Austin, 1991.

"AISI 12L14 Carbon Steel (UNS G12144)." *AISI 12L14 Carbon Steel (UNS G12144)*. Web. 30 Apr. 2014.

"AISI 12L14 Steel, Hot Rolled, 19-38 Mm round." *AISI 12L14 Steel, Hot Rolled, 19-38 Mm round*. Web. 30 Apr. 2014.

American Concrete Institute (2001). *Specification for Unbonded Single-Strand Tendons and Commentary* (ACI 423.6R-01)

ASTM Standard A370, 2012a, "Standard Test Methods and Definitions for Mechanical Testing of Steel Products," ASTM International, West Conshohocken, PA, 2012, Www.astm.org

ASTM Standard A416, 2012a, "Standard Specification for Steel Strand, Uncoated Seven-Wire for Prestressed Concrete," ASTM International, West Conshohocken, PA, 2012, Www.astm.org

Bastien, Josee, Daniel Marceau, Mario Fafard, and Hans R. Ganz. "Use of FEA for Design of Posttensioning Anchor Head." *Journal of Bridge Engineering ASCE* 12.2 (2007): 194-204. Print.

Chacos, Gregory P. "Wedge Forces on Post-Tensioning Strand Anchors." Ed. Bijan O. Aalami. *For Professionals Engaged in Post-Tensioning Design* 2 (1993). Rpt. in *PTI Technical Notes*. Phoenix: Post-Tensioning Institute, 1993. Print.

Hayes, Norris O., and Randy Draginis. Anchor System with Substantially Longitudinally Equal Wedge Compression. Hayes Et Al., assignee. Patent 20090205273A1. July-Aug. 2009. Print.

Itabashi, Masaaki, and Heikichi Koseki. "Mechanical Characterization of Pre-Fatigued Free-Cutting Steels Under Dynamic Tension." *Engineering Transactions* 61.2 (2012): 87-98. *Engineering Transactions*. Polish Academy of Science / National Engineering School of Metz. Web. 19 Feb. 2014.

Javadian, Siyamak, Sepehr E. Khatir, Mark Boots, and Charles Aire. *Tensile Testing Lab*. Report for ME843. Saskatoon: U of Saskatchewan. Print.

Madrazo, Geoff. *Post-tensioning and Anchorage Systems*. Student Report. Ed. David Roke. Bethlehem PA: Georgia Institute of Technology. Print.

Marceau, D., J. Bastien, M. Fafard, and A. Chabert. "Experimental and Numerical Studies of Mono-Strand Anchorages." *Structural Engineering and Mechanics* 12.2 (2001): 119-34. Print.

Marceau, D., M. Fafard, and J. Bastien. "Constitutive Law for Wedge-Tendon Gripping Interface in Anchorage Device - Numerical Modeling and Parameters Identification." *Structural Engineering and Mechanics* 15.6 (203): 609-28. Print.

Marceau, D., M. Fafard, and J. Bastien. "Numerical Study of Mono-Strand Anchorage Mechanism Under Service Load." *Structural Engineering and Mechanics* 18.4 (2004): 475-91. Print.

Slocum, Alexander H. *Lean and Agile Precision Manufacturing Systems*. N00014-95-1-G039. Washington D.C.: Naveal Research Laboratory. *Lean and Agile Precision Manufacturing Systems*. Web. 19 Feb. 2014.

Walsh, Kevin Q., and Yahya C. Kurama. *Behavior and Design of Unbonded Post-Tensioning Strand/Anchorage Systems for Seismic Applications*. Rep. no. NDSE-09-02. Notre Dame: U of Notre Dame, 2009. Print.

Walsh, Kevin Q., Randy L. Draginis, R. M. Estes, and Yahya C. Kurama. *Effects of Anchor Wedge Dimensional Parameters on Post-Tensioning Strand Performance*. Rep. no. NDSE-2013-02. Notre Dame: U of Notre Dame, 2013. Print.

Walsh, Kevin Q., Randy L. Draginis, R. M. Estes, and Yahya C. Kurama. *Effects of Anchor Wedge Dimensional Parameters on Post-Tensioning Strand Performance*. Rep. no. NDSE-2013-02. Notre Dame: U of Notre Dame, 2013. Print.

"What Is Post-tensioning." *Post-Tensioning Institute* (2000). Print.

Yates, D. L. *A Study of Fretting Fatigue in Post-Tensioned Concrete Beams.* M.S. Thesis, Austin, TX: The University of Texas at Austin, 1988.

"From Engineering to True Strain, True Stress." *LS-DYNA Support*. Web. 14 May 2014. <http://www.dynasupport.com/howtos/material/from-engineering-to-true-strain-true-stress>.

Appendix A: Strain Gage Application

Procedure for Application of Pre-wired Strain Gages to PT Strand using M-Bond 200 Adhesive from Micro-Measurements

Modified procedure adapted from Micro-Measurements Strain Gage Installations with M-Bond 200 Adhesive: http://www.vishaypg.com/docs/11127/11127_b1.pdf

The following products are used in this procedure:

- M-Bond 200 adhesive
- M-Bond 200 catalyst
- Degreaser (or isopropyl alcohol)
- Silicon-carbide paper (320- and 400-grit)
- M-Prep Conditioner A
- M-Prep Neutralizer 5A
- Gauze sponges
- Cotton applicators
- Gage installation tape

The following pre-wired Omega strain gages are recommended for this application:

- KFG-1N-120-C1-11L3M3R
- KFG-2N-120-C1-11L3M3R
- KFG-2N-120-C1-11L1M2R

Step 1
Thoroughly degrease the gaging area with degreaser or isopropyl alcohol. Simply spray the area of the strand where the gage will be applied and wipe dry with a clean rag or paper towel.

Step 2
Thoroughly wet the individual wire that the strain gage will be applied to with M-Prep Conditioner A and abrade with 320-grit silicon-carbide paper. This is followed by wiping dry with a gauze sponge. Repeat this wet abrading process with 400-grit silicon-carbide paper, and then dry by slowly wiping through with a gauze sponge.

Repeatedly apply M-Prep Conditioner A and scrub with cotton-tipped applicators until a clean tip is no longer discolored. Remove all residue and Conditioner by again slowly wiping through with a gauze sponge. Never allow any solution to dry on the surface because this invariably leaves a contaminating film and reduces chances of a good bond.

Step 3
Now apply a liberal amount of M-Prep Neutralizer 5A to the prepared wire and scrub with a cotton-tipped applicator. With a single, slow wiping motion of a gauze sponge, carefully dry this surface. Do not wipe back and forth because this may allow contaminants to be re-deposited.

Note: The cotton-tipped applicator should be clean after scrubbing since the conditioner was applied until the applicator was clean. If the applicator is not clean, repeat the second part of step two until the applicator is clean.

Step 4
Remove the pre-wired strain gage from the transparent envelope. Be careful not to touch the bonding surface of the strain gage directly as natural hand oils may contaminate the gage and reduce chances of a good bond.

Note: Gages have been treated for optimum bonding conditions and require no pre-cleaning before use unless contaminated during handling. If contaminated, the back of any gage can be cleaned with a cotton-tipped applicator slightly moistened with M-Prep Neutralizer 5A.

Step 5

The M-Bond **catalyst** can now be applied to the bonding surface of the gage. Very little catalyst is need, and it should be applied in a thin, uniform coat. Lift the brush-cap out of the catalyst bottle and wipe the brush approximately 10 strokes against the inside of the neck of the bottle to wring out most of the catalyst. Holding the strain gage by the lead wires with the bonding side up, set the brush down on the gage and swab the gage backing. Do not stroke the brush in a painting style, but slide the brush over the entire gage in a single motion. Allow the catalyst to dry at least **one minute** under normal ambient conditions before proceeding.

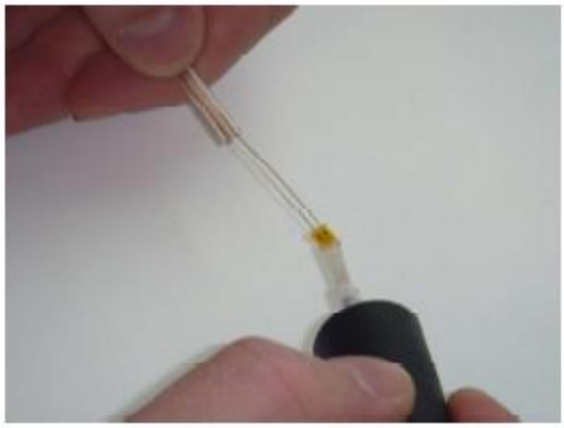

Step 6

Once the catalyst has been allowed to thoroughly dry for at least one minute, place the gage (bonding side down) on a chemically clean glass plate. Cut an approximately 2-in. long piece of gage installation tape in half the long way.

Apply the tape over the gage, slightly overlapping the lead wire insulation at one end and extending beyond the end of the strain gage at the other. Take care to center the gage on the tape. Holding the free end of the tape strip off of the glass plate, gently press on the top of the tape to ensure a good bond is formed between the tape and the gage.

Carefully lift the tape at a shallow angle (about 45 degrees to the glass surface), bringing the gage up with the tape and removing the assembly from the glass plate.

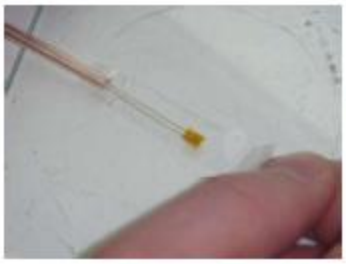

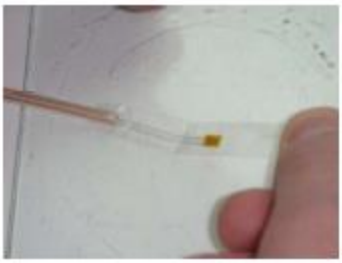

Step 7

Holding the assembly by the free end of the tape and strain gage lead wires, align the gage with the wire to be instrumented. Apply the free end of the tape to the individual strand wire so that the strain gage remains unattached and will be aligned with the individual wire once it is glued in place.

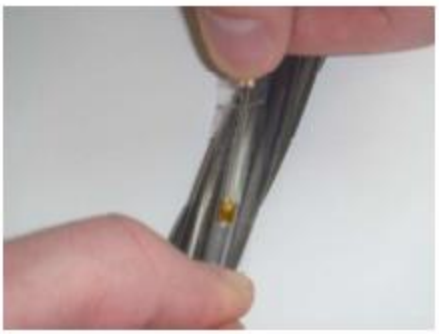

Note: The next three steps must be completed in the sequence shown, within 3 to 5 seconds. Read steps 8, 9, and 10 before proceeding.

Step 8

Lift the free end of the tape assembly so that a fold is formed in the tape approximately 0.5-in. from the strain gage. Holding in this position, apply one or two drops of M-Bond 200 **adhesive** at the fold formed by the junction of the tape and specimen surface. This adhesive application should be approximately 0.5-in. outside the actual gage installation area to ensure that local polymerization that takes place when the adhesive comes in contact with the specimen surface will not cause unevenness in the gage glueline.

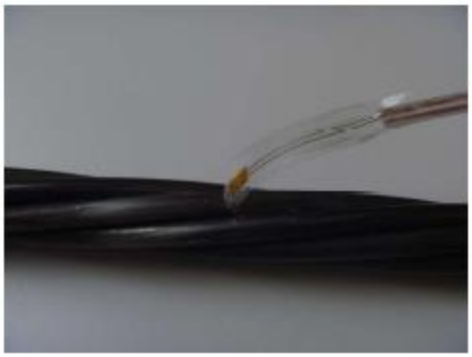

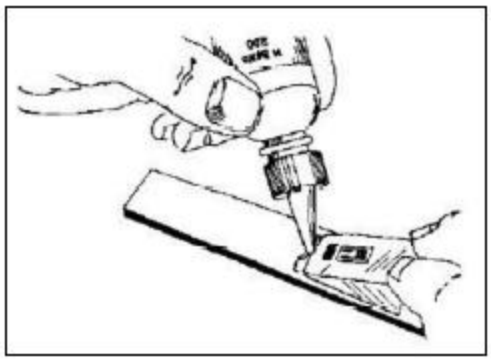

Step 9
Immediately rotate the tape to approximately a 30-degree angle so that the gage is bridged over the installation area. While holding the tape slightly taut, slowly and firmly make a single wiping stroke over the gage/tape assembly with your finger bringing the gage back down over the specimen. Use firm pressure when wiping over the gage. A very thin, uniform layer of adhesive is desired for optimum bond performance.

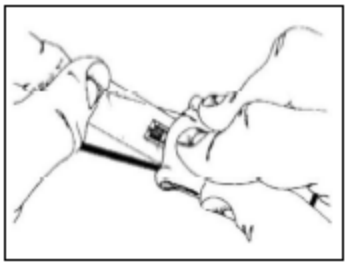

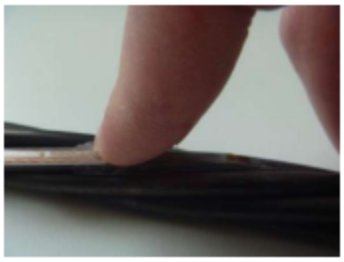

Step 10
Immediately upon completion of step 9, firm thumb pressure must be applied to the gage area. This pressure should be held for at least **one minute** (at room temperature conditions). Note that direct use of the thumb or finger rather than with a gauze pad is important because "thumb heat" helps to speed adhesive polymerization. If a gauze pad or other buffer is used, pressure-application time should be extended to ensure proper bond.

Step 11
Place a strip of masking tape around the gage lead wire insulation near its terminus. The tape should be placed tightly enough so that in the event that the lead wires are inadvertently tugged on or pulled, the force will be absorbed by the masking tape and lead wire insulation rather than the strain gage itself. Take care not to tug on the freshly glued strain gage while placing the masking tape.

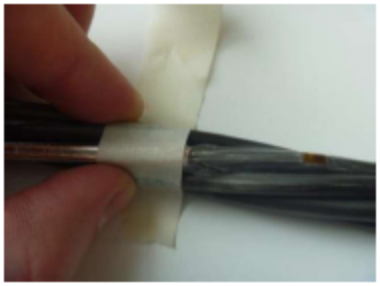
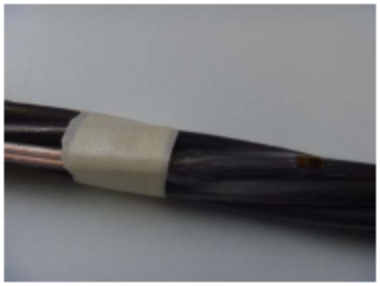

Note: Neither the masking tape nor the gage installation tape need to be removed prior to testing. Leaving them in place offers the best probability of a working (undamaged) strain gage at the time of testing.

Appendix B: Data Images

B.1 Scale Factor Graphs:

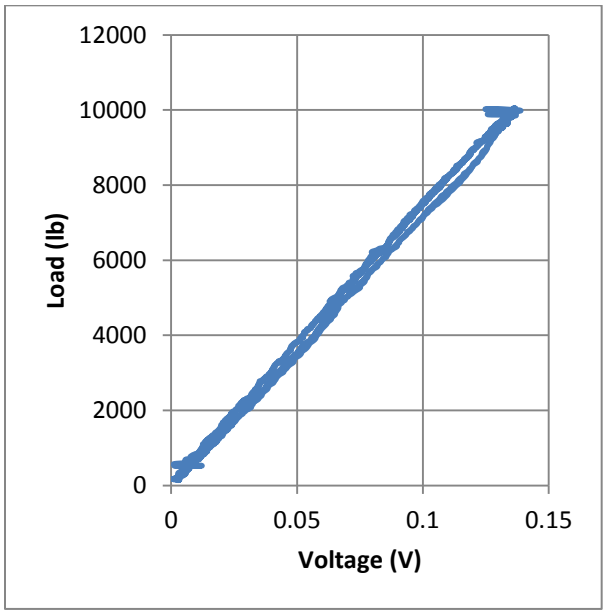

Figure B.1-1: Scale Factor #1

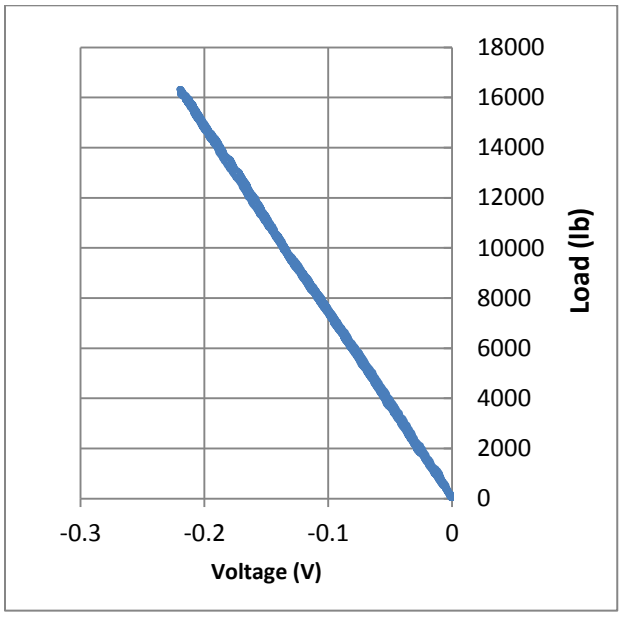

Figure B.1-2: Scale Factor #2

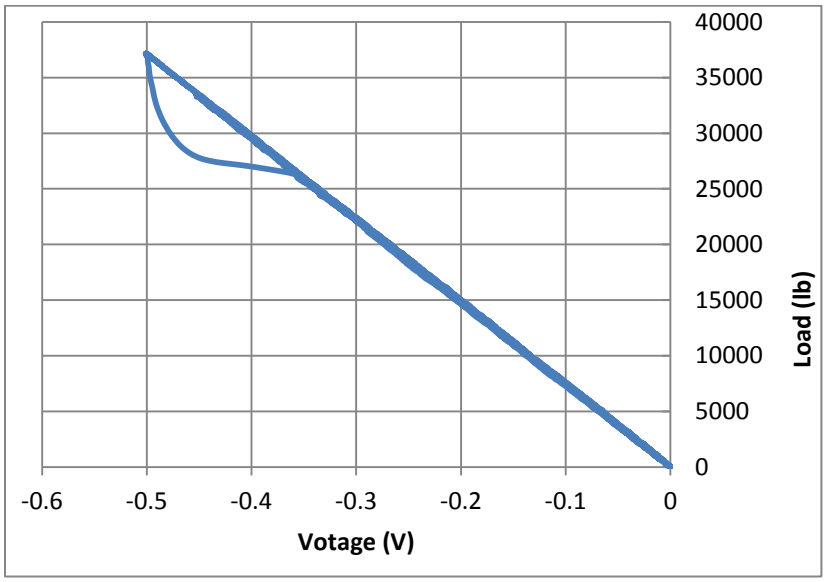

B.1-3: Scale factor #3

B.2 Free Length Fracture Data:

Table B.2-1: Values from Each Free Length Test

Strain (ε)	Strain (με)	Stress 1 (σ)	Stress 2 (σ)	Stress 3 (σ)	Average Stress (σ)
0.001	1000	31936	21956	27944	27279
0.002	2000	64371	51896	58882	58383
0.003	3000	93812	81337	89321	88157
0.004	4000	124750	110778	119760	118430
0.005	5000	155190	138723	150200	148037
0.006	6000	183633	167665	179641	176979
0.007	7000	213074	196108	208583	205921
0.008	8000	239521	223054	237026	233200
0.009	9000	255489	245509	255489	252162
0.01	10000	261976	255988	261976	259980
0.011	11000	264970	261477	265469	263972
0.012	12000	266467	263972	267465	265968
0.013	13000	266966	265968	267964	266966
0.014	14000	267465	266966	268463	267631
0.015	15000	267964	266966	268962	267964
0.016	16000	267964	267465	268962	268130
0.017	17000	267964	267465	268962	268130
0.018	18000	268463	267964	269461	268629
0.019	19000	268463	268463	269960	268962
0.02	20000	269461	268962	270459	269627
0.021	21000	269461	268962	270958	269794
0.022	22000	269960	269461	271457	270293
0.023	23000	270958	269960	272455	271124
0.024	24000	271956	270459	272954	271790
0.025	25000	271956	271457	273952	272455
0.026	26000	272954	271956	274451	273120
0.027	27000	273453	272954	275449	273952
0.028	28000	274451	273453	276447	274784
0.029	29000	274950	274451	276946	275449
0.03	30000	275948	274950	277944	276281
0.031	31000	276946	275948	278443	277112
0.032	32000	277445	276946	278942	277778
0.033	33000	278443	277445	279441	278443
0.034	34000	278443	277944	280439	278942
0.035	35000	278942	278942	280938	279607
0.036	36000	279441	278942	281437	279940
0.037	37000	279940	279441	281936	280439

0.038	38000	280439	280439	282435	281104
0.039	39000	280938	280439	282934	281437
0.04	40000	280938	281437	282934	281770
0.041	41000	281437	281437	283433	282102
0.042	42000	282435	282435	283932	282934
0.043	43000	282435	282435	284431	283100
0.044	44000	282435	282435	284431	283100
0.045	45000	282435	282934	284431	283267
0.046	46000	282934	283433	284431	283599
0.047	47000	283433	283433	284930	283932
0.048	48000	283433	283932	284930	284098
0.049	49000	283433	283932	284431	283932
0.05	50000	283433	283932	284930	284098
0.051	51000	283932	283932	284431	284098
0.052	52000	283932	284431	284930	284431
0.053	53000	283932	284431	285429	284597
0.054	54000	283932	284431	284930	284431
0.055	55000	284431	284431	284930	284597
0.056	56000	284431	284431	284930	284597
0.057	57000	283932	284431	284930	284431
0.058	58000	283932	284431	285429	284597
0.059	59000	283433	284431	284930	284265
0.06	60000	283932	284930	284930	284597
0.061	61000	283932	284431	284930	284431
0.062	62000	283932	284431	285429	284597
0.063	63000	283932	284431	284930	284431

B.3 Anchor Stress Charts

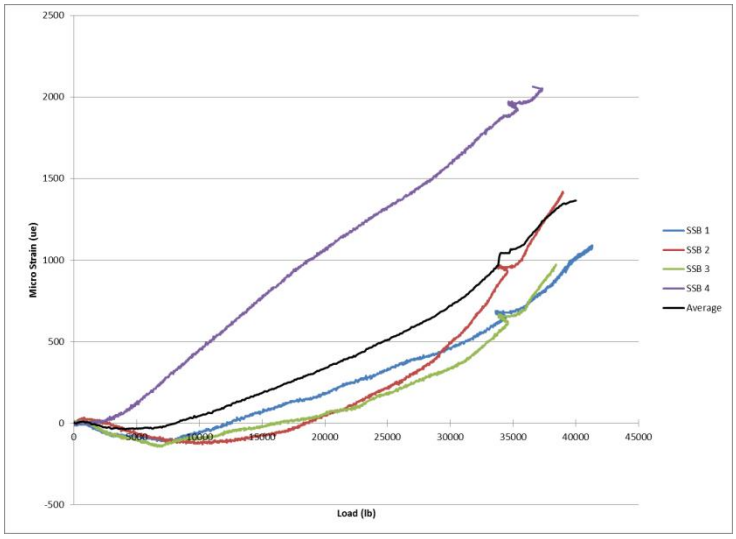

Standard Short Wedge Bottom Strain

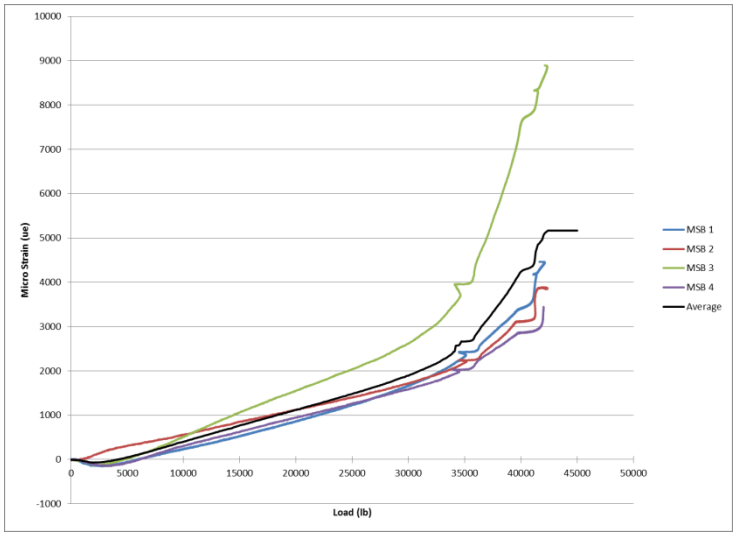

Modified Short Wedge Bottom Strain

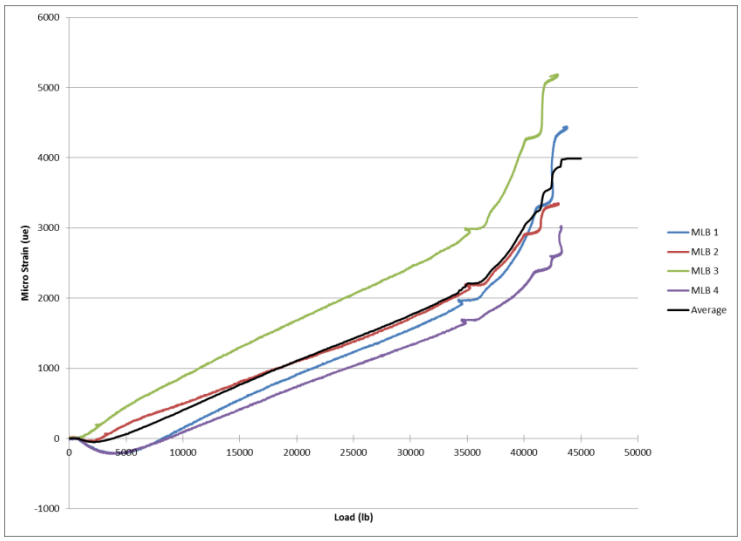

Modified Long Wedge Bottom Strain

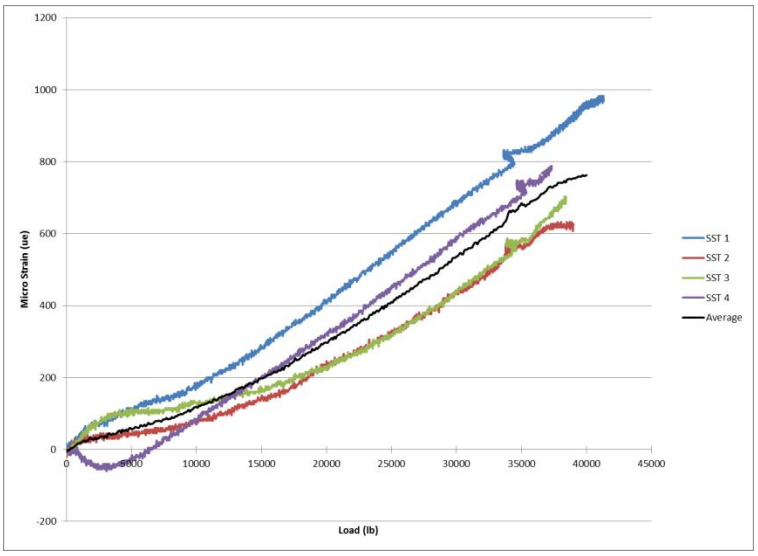

Standard Short Wedge Top Strain

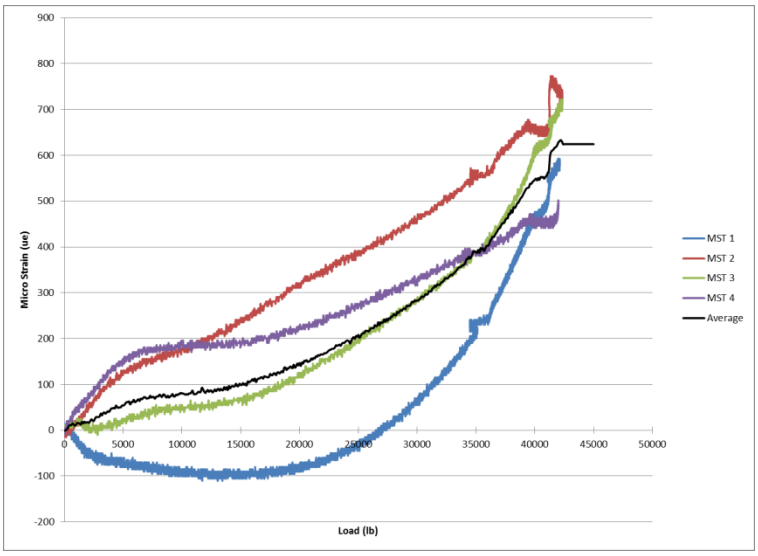

Modified Short Wedge Top Strain

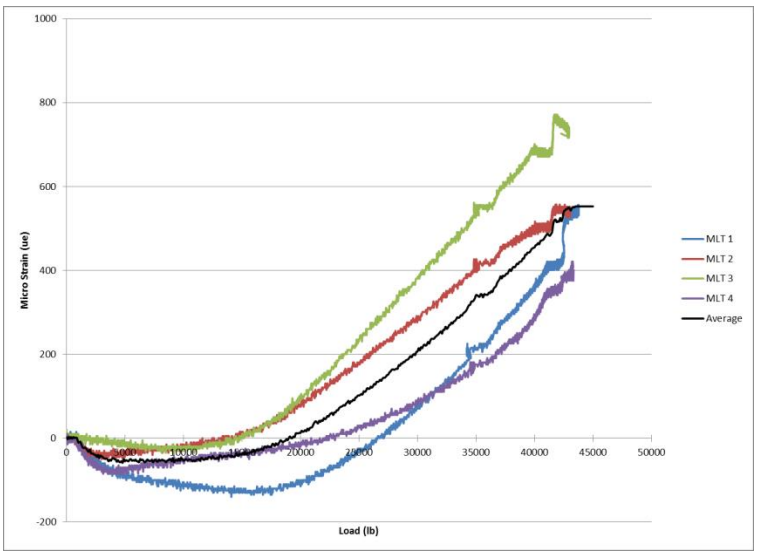

Modified Long Wedge Top Strain

B.4 Stress Strain Curves for Each Wedge Case

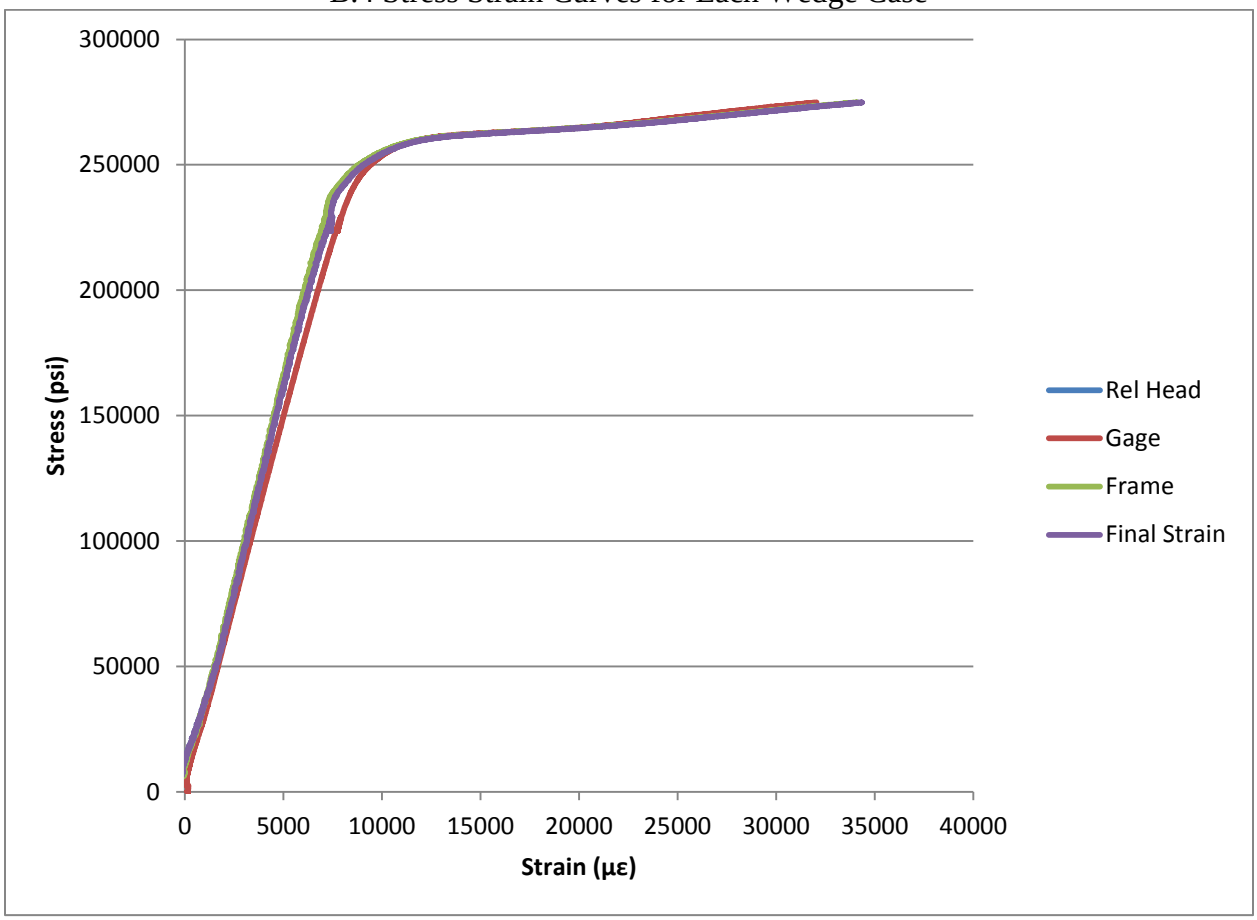

B.4-1: Standard Short #1

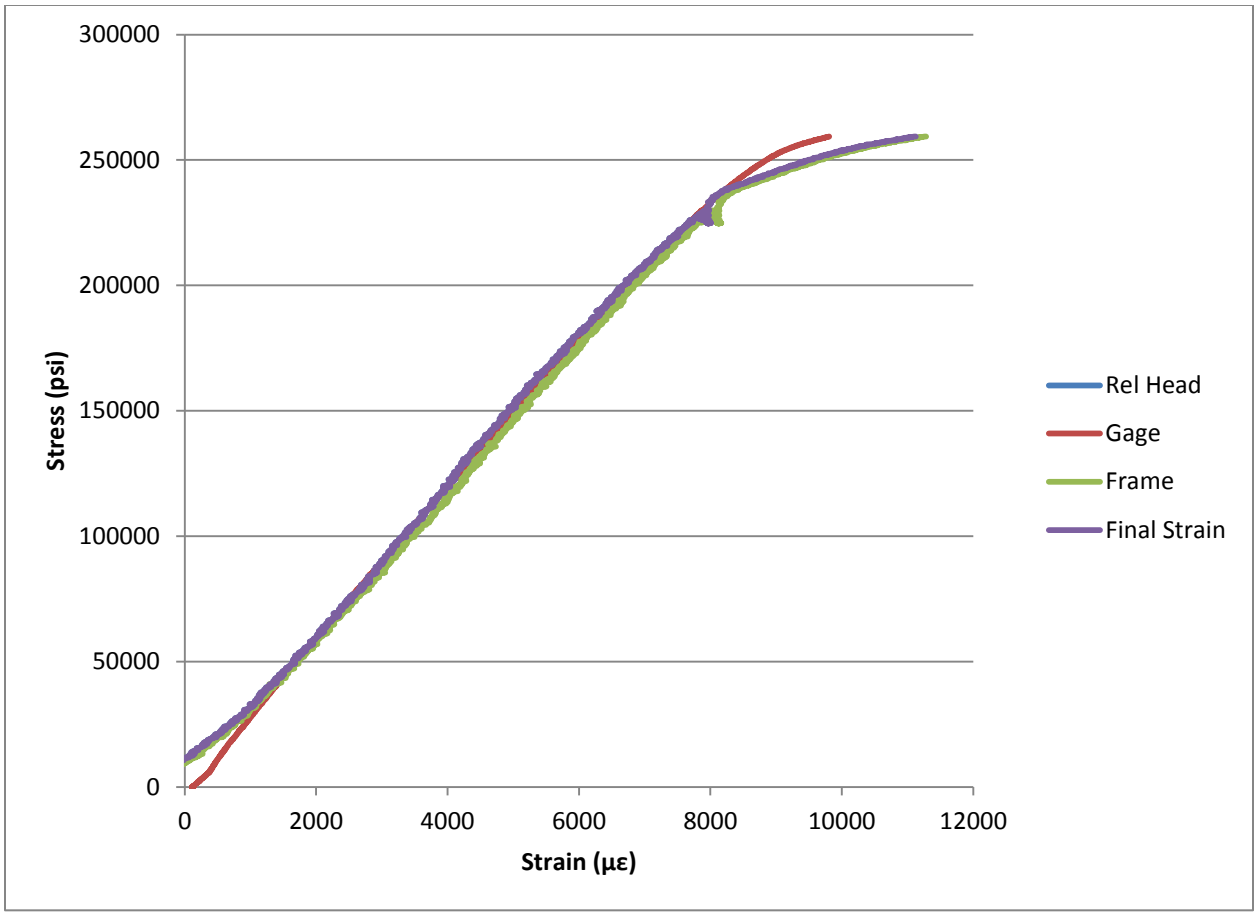

B.4-2: Standard Short #2

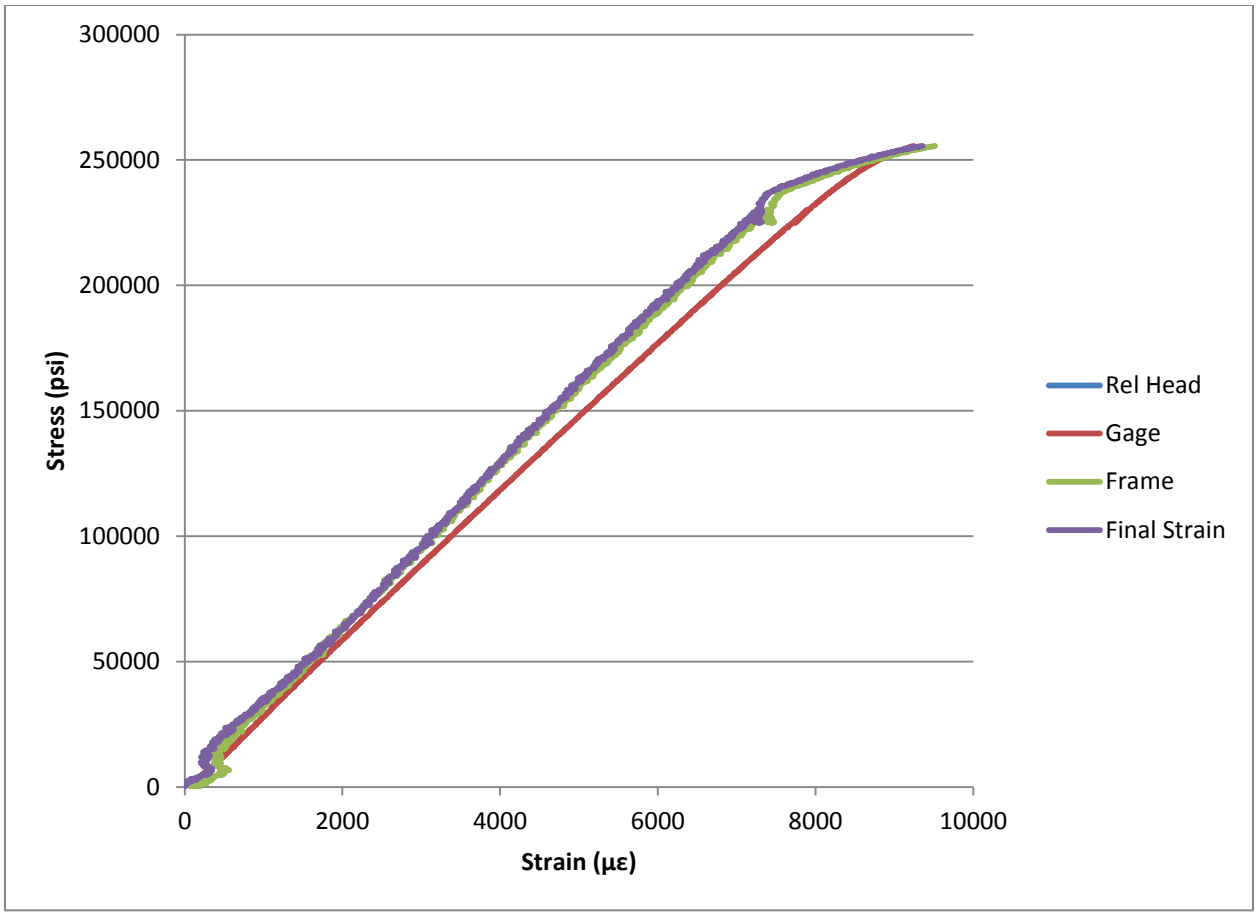

B.4-3: Standard Short #3

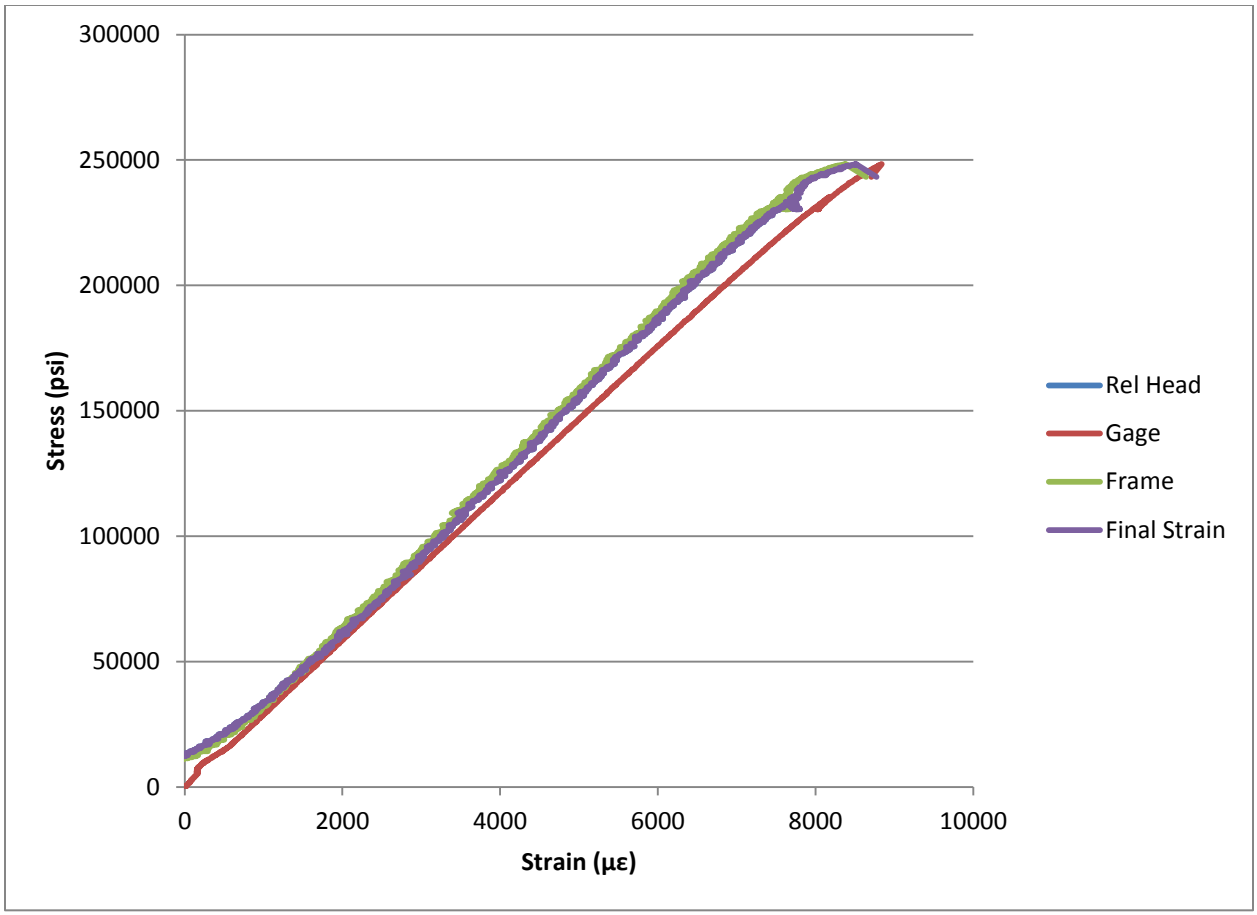

B.4-4: Standard Short #4

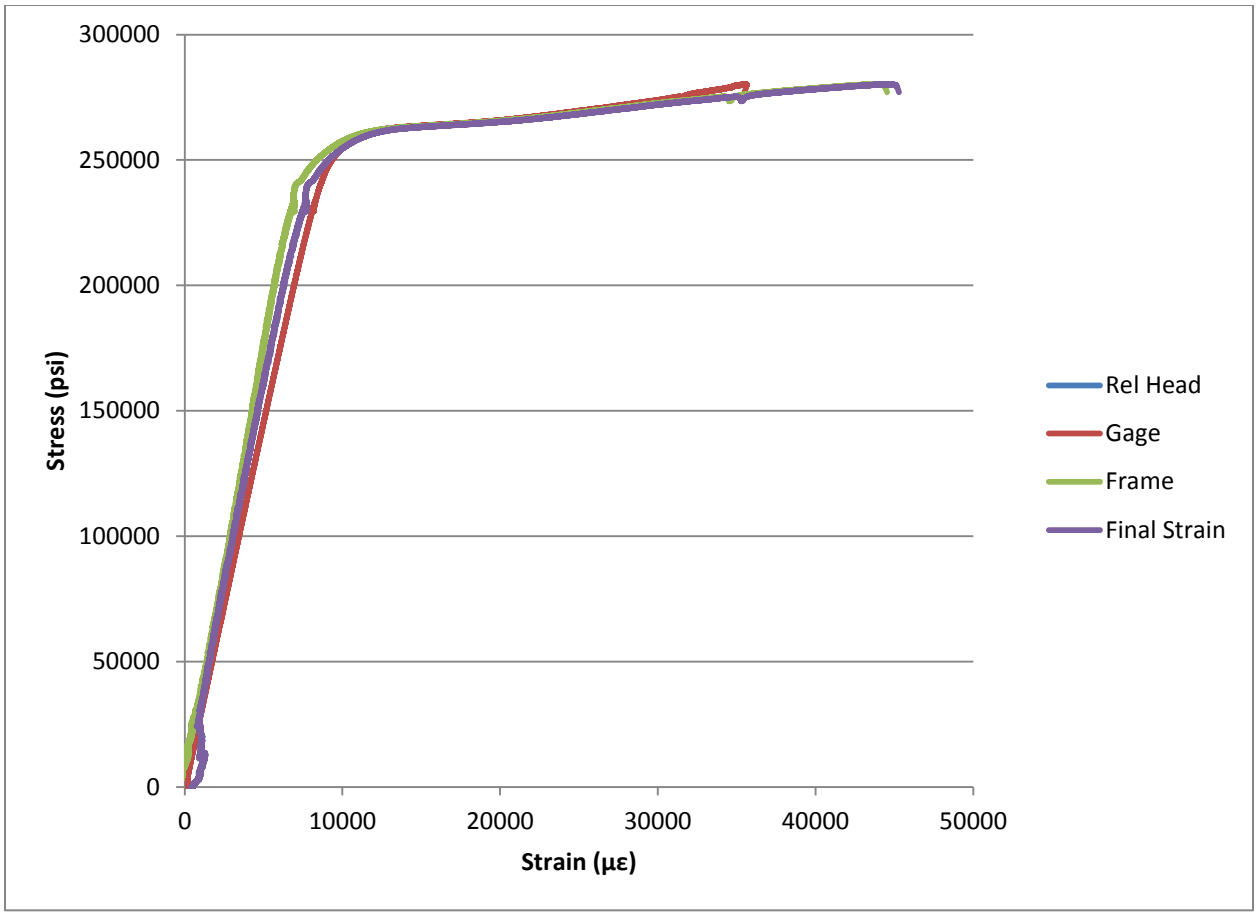

B.4-5: Modified Short #1

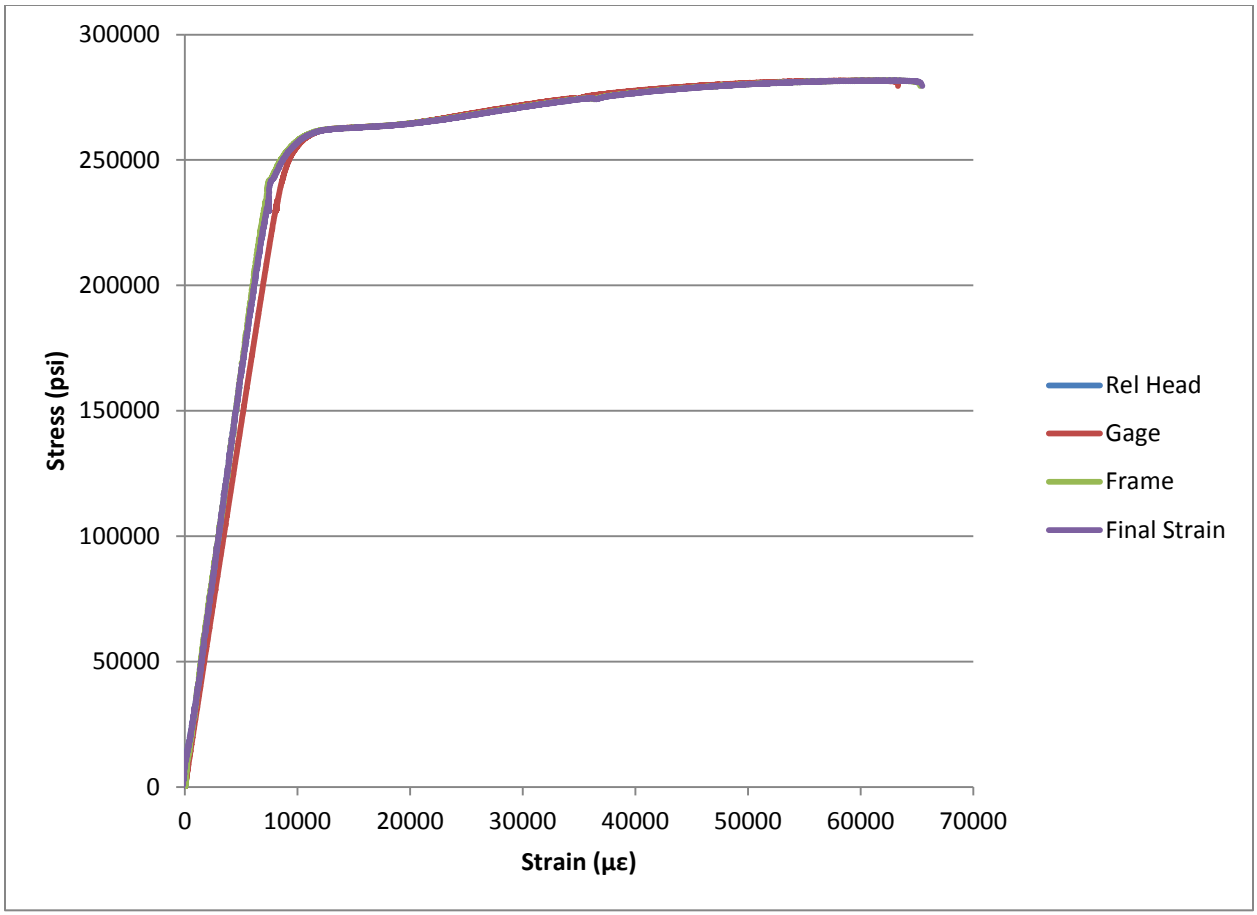

B.4-6: Modified Short #2

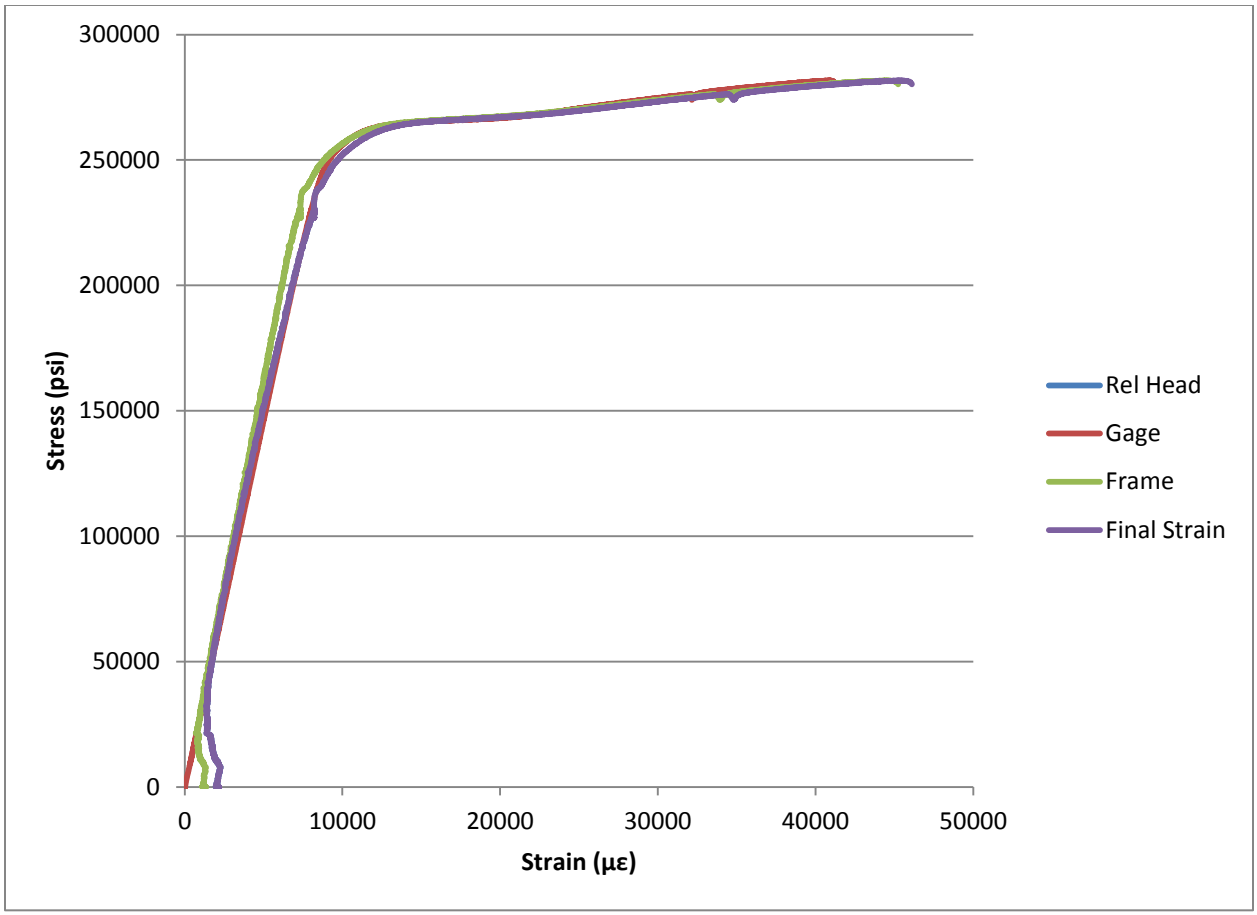

B.4-7: Modified Short #3

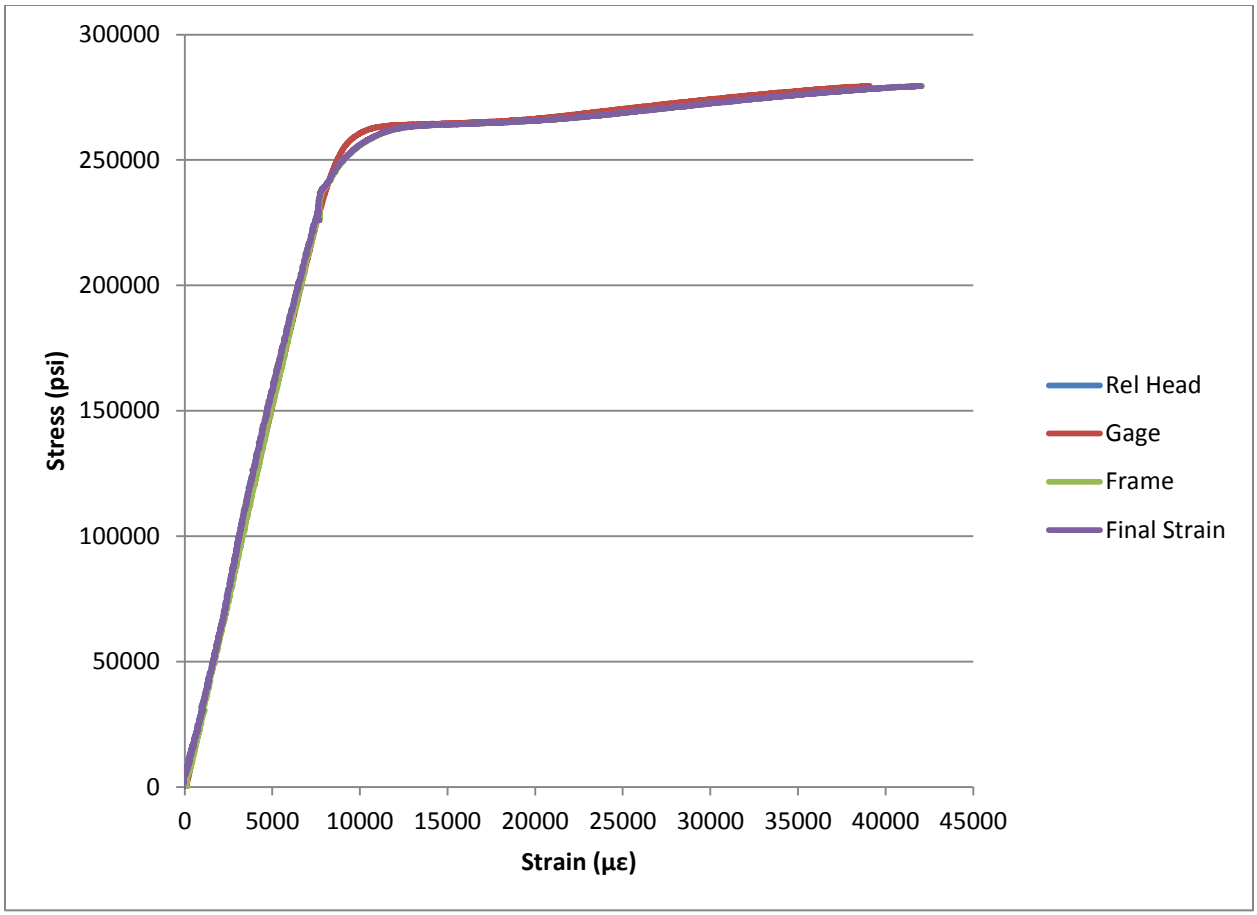

B.4-8: Modified Short #4

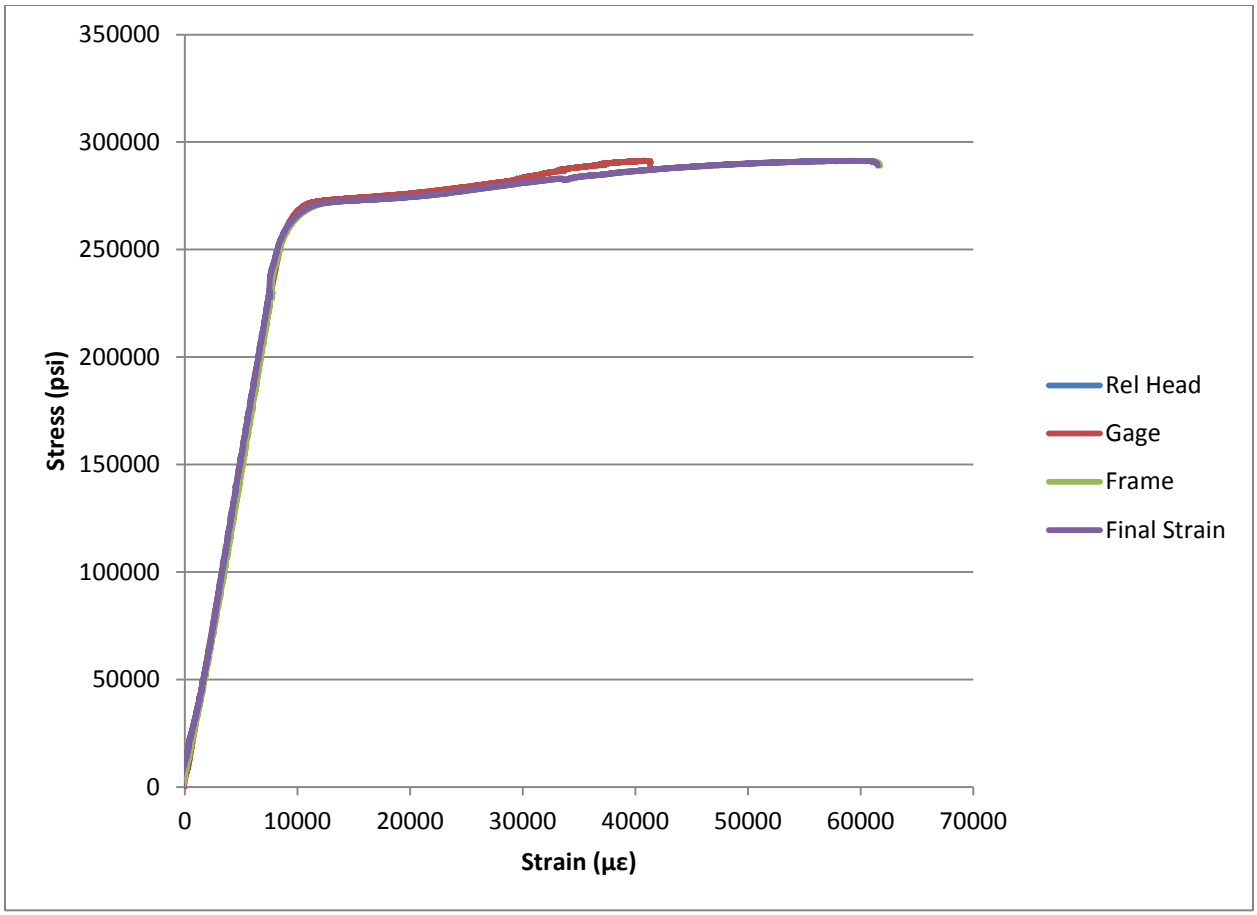

B.4-9: Modified Long #1

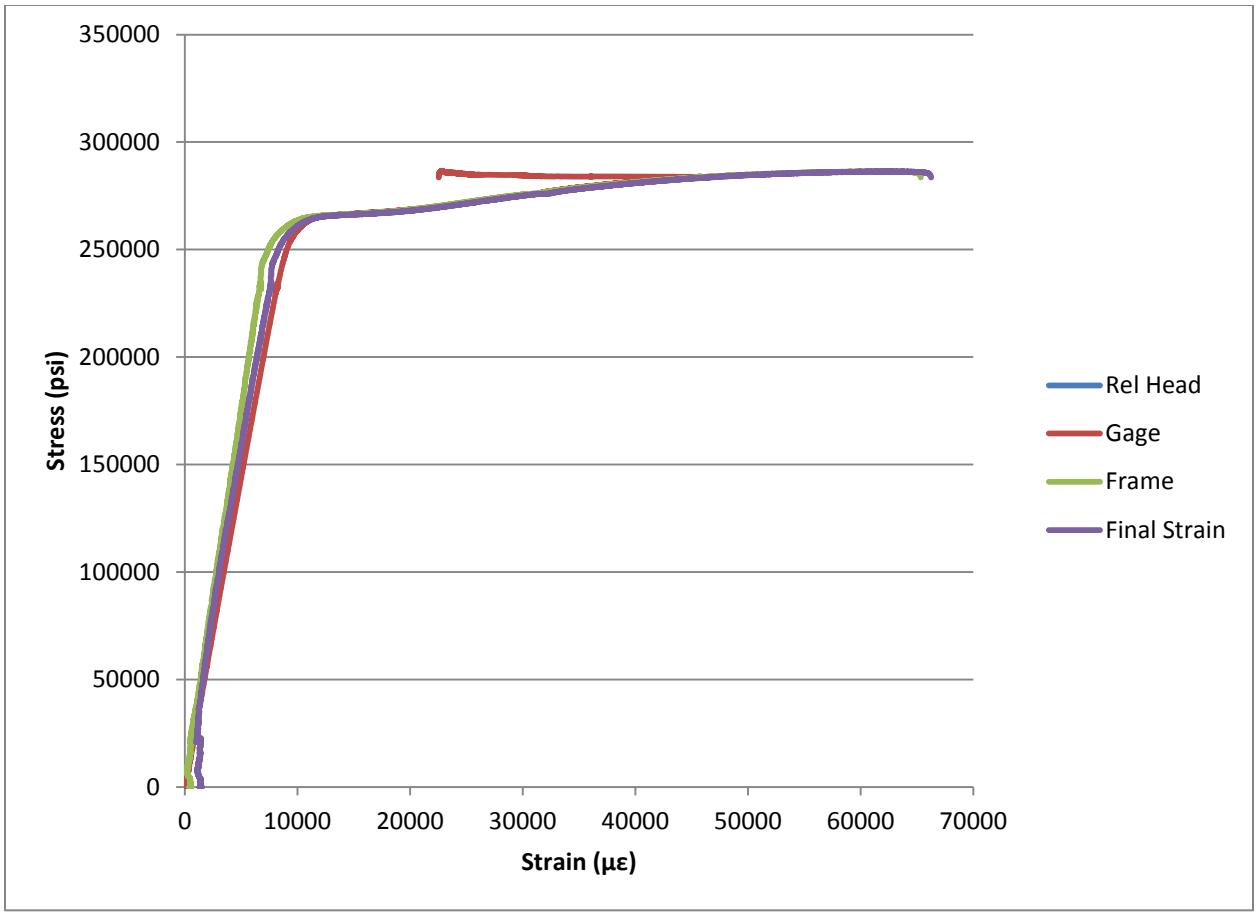

B.4-10: Modified Long #2

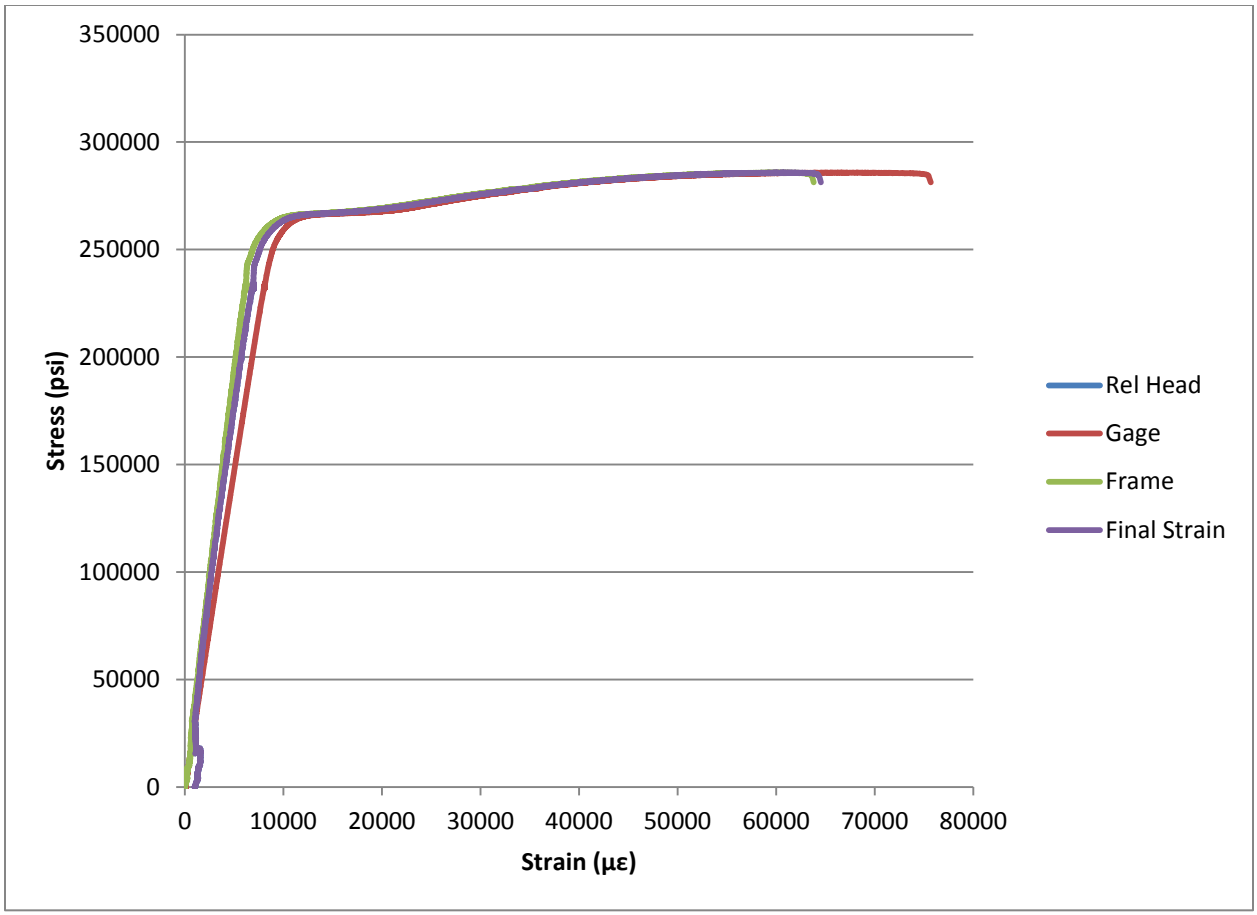

B.4-11: Modified Long #3

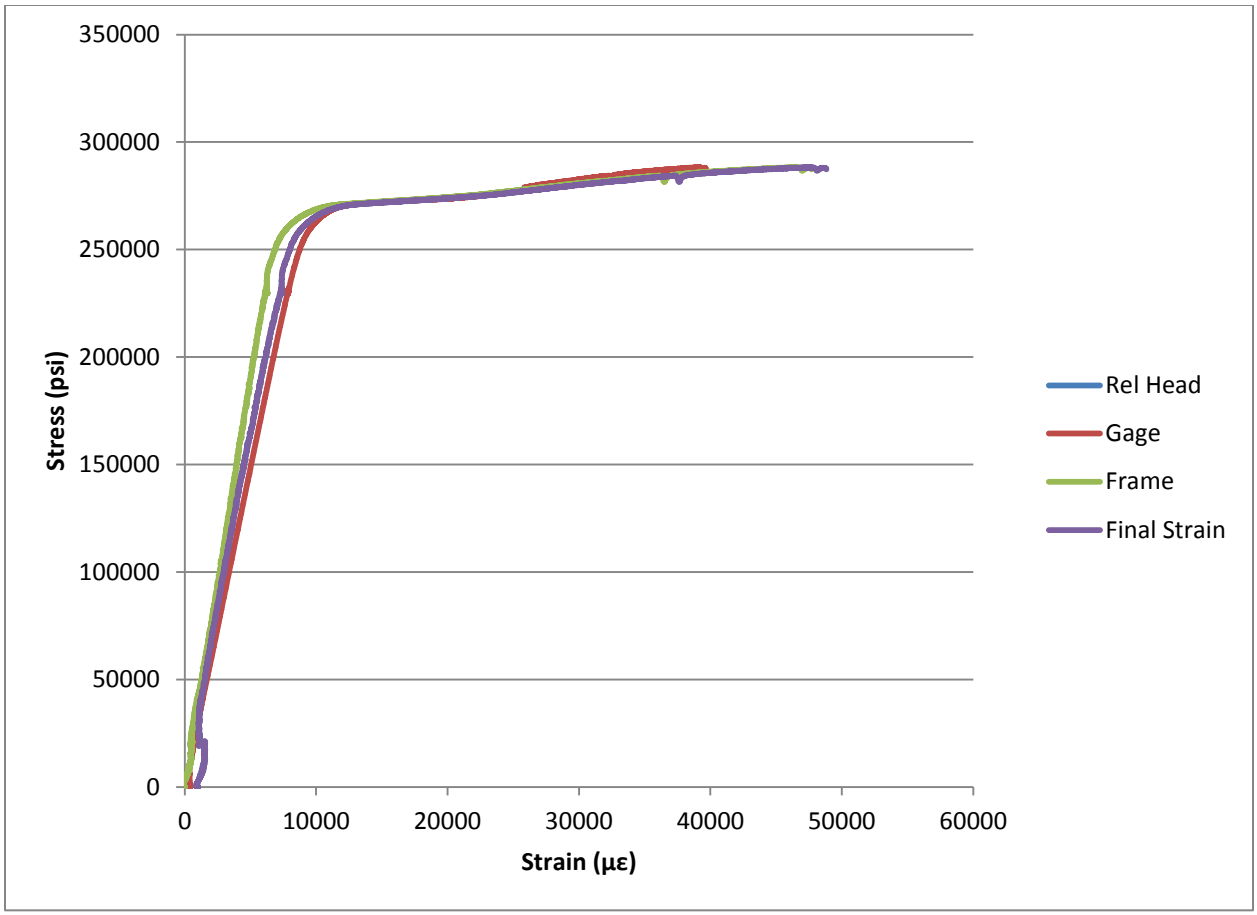

B.4-12: Modified Long #4

Appendix C: True Stress and True Plastic Strain

Table C.1: Strand Plastic Stress and True Plastic Strain

Strain	Averge Stress
0	163
0.001	26797
0.002	57353
0.003	86601
0.004	116340
0.005	145425
0.006	173856
0.007	202288
0.008	229085
0.009	247712
0.01	255392
0.011	259314
0.012	261275
0.013	262255
0.014	262908
0.015	263235
0.016	263399
0.017	263399
0.018	263889
0.019	264216
0.02	264869
0.021	265033
0.022	265523
0.023	266340
0.024	266993
0.025	267647
0.026	268301
0.027	269118
0.028	269935
0.029	270588
0.03	271405
0.031	272222
0.032	272876
0.033	273529
0.034	274020

E=	28635620.92

True Stress	True Strain	TP Strain
230918	0.008	0.000
249942	0.009	0.000
257946	0.010	0.001
262166	0.011	0.002
264410	0.012	0.003
265664	0.013	0.004
266589	0.014	0.005
267184	0.015	0.006
267613	0.016	0.007
267876	0.017	0.008
268639	0.018	0.008
269236	0.019	0.009
270167	0.020	0.010
270598	0.021	0.011
271364	0.022	0.012
272466	0.023	0.013
273401	0.024	0.014
274338	0.025	0.015
275276	0.026	0.016
276384	0.027	0.017
277493	0.028	0.018
278435	0.029	0.019
279547	0.030	0.020
280661	0.031	0.021
281608	0.031	0.022
282556	0.032	0.023
283336	0.033	0.024

0.035	274673	284287	0.034	0.024
0.036	275000	284900	0.035	0.025
0.037	275490	285683	0.036	0.026
0.038	276144	286637	0.037	0.027
0.039	276471	287253	0.038	0.028
0.04	276797	287869	0.039	0.029
0.041	277124	288486	0.040	0.030
0.042	277941	289615	0.041	0.031
0.043	278105	290063	0.042	0.032
0.044	278105	290341	0.043	0.033
0.045	278268	290790	0.044	0.034
0.046	278595	291410	0.045	0.035
0.047	278922	292031	0.046	0.036
0.048	279085	292481	0.047	0.037
0.049	278922	292589	0.048	0.038
0.05	279085	293039	0.049	0.039
0.051	279085	293318	0.050	0.039
0.052	279412	293941	0.051	0.040
0.053	279575	294393	0.052	0.041
0.054	279412	294500	0.053	0.042
0.055	279575	294952	0.054	0.043
0.056	279575	295231	0.054	0.044
0.057	279412	295338	0.055	0.045
0.058	279575	295791	0.056	0.046
0.059	279248	295724	0.057	0.047
0.06	279575	296350	0.058	0.048
0.061	279412	296456	0.059	0.049
0.062	279575	296909	0.060	0.050
0.063	279412	297015	0.061	0.051
0.064	279412	297294	0.062	0.052
0.065	279248	297400	0.063	0.053
0.066	279248	297679	0.064	0.054
0.067	279248	297958	0.065	0.054
0.06787692	279412	298377	0.066	0.055

Table C.2: Anchor Stress and Strain

% strain	Stress 1 (Mpa)	Stress 2 (Mpa)	Stress 3 (Mpa)	Avg Stress (Mpa)
0	0	0	0	0
0.003889	435	415	420.83	423.61
0.01	500	496.64	445.833	480.8243333
0.02	510.71	500	466.66	492.4566667
0.03	514.28	508.04	495.833	506.051
0.04	521.43	516.07	516.66	518.0533333
0.05		521.42	520.83	521.125
0.06		523.21	537.5	530.355
0.07		526.79	541.66	534.225
0.08		528.57	541.66	535.115
0.09		527.68	541.66	534.67
0.1		525	541.66	533.33
0.11		521.43	529.16	525.295
0.12		508.93	525	516.965
0.13		496.42	516.66	506.54
0.14			512.5	512.5
0.15			504.166	504.166
0.16		403.57		403.57

Table C.3: Anchor True Stress and True Plastic Strain

E=	15890971

Avg Stress (psi)	True Strain	Plastic Strain	True Stress
0	0	0	0
61439.44	0.003881	0	61678.37
69737.67	0.00995	0.005518	70435.05
71424.8	0.019803	0.015218	72853.3
73396.49	0.029559	0.024801	75598.39
75137.28	0.039221	0.034303	78142.77
75582.79	0.04879	0.043796	79361.93
76921.49	0.058269	0.053138	81536.78
77482.79	0.067659	0.062441	82906.58
77611.87	0.076961	0.071686	83820.82

77547.33	0.086178	0.080859	84526.59
77352.98	0.09531	0.089956	85088.27
76187.6	0.10436	0.099038	84568.23
74979.43	0.113329	0.108044	83976.97
73467.42	0.122218	0.116993	83018.18
74331.84	0.131028	0.125696	84738.3
73123.1	0.139762	0.13447	84091.56
58532.88	0.14842	0.144147	67898.14

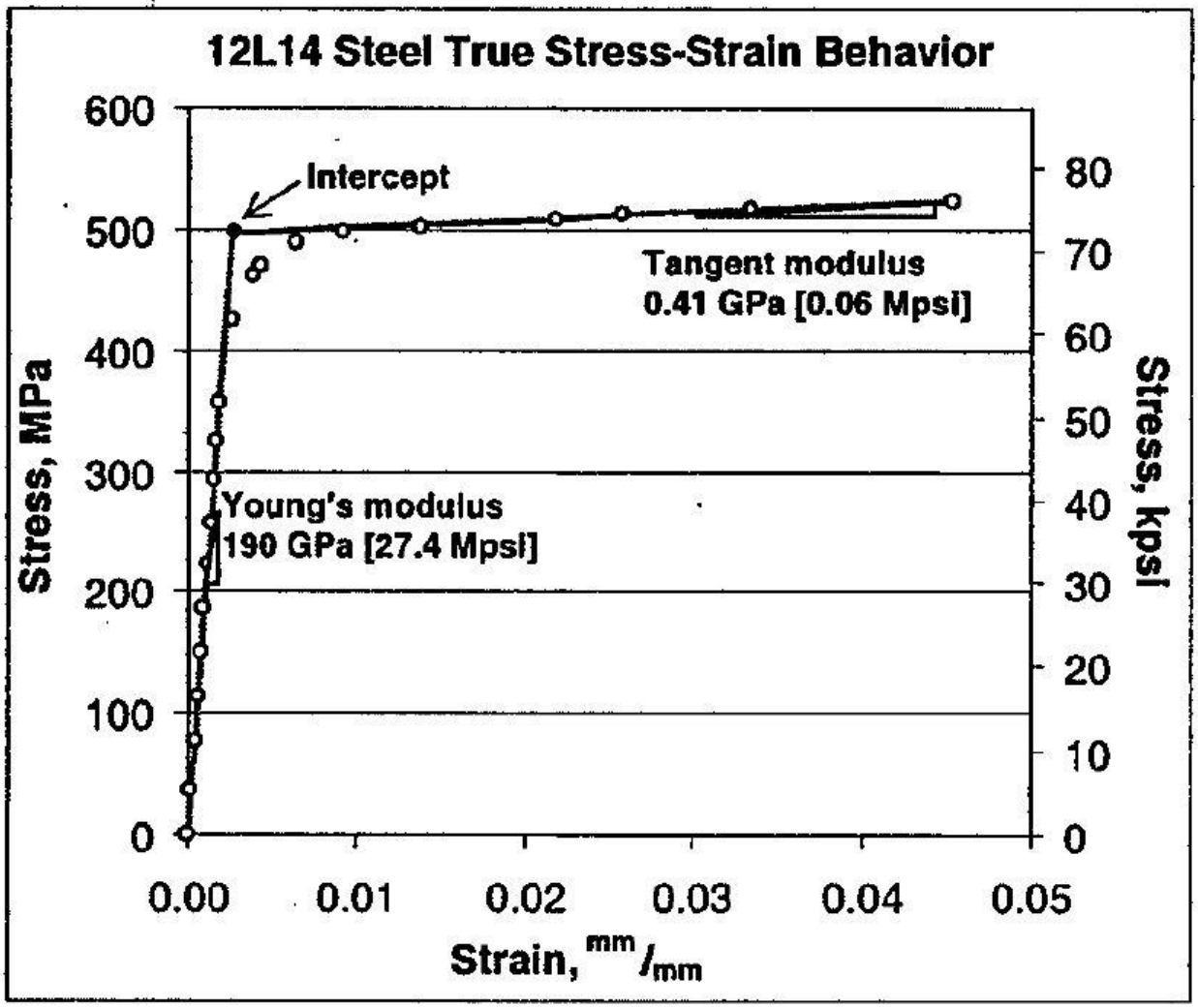

Lean and Agile Precision Manufacturing Systems
Office of Naval Research
Grant No. N00014-95-1-G039

Figure C.1: Anchor Stress Strain #1

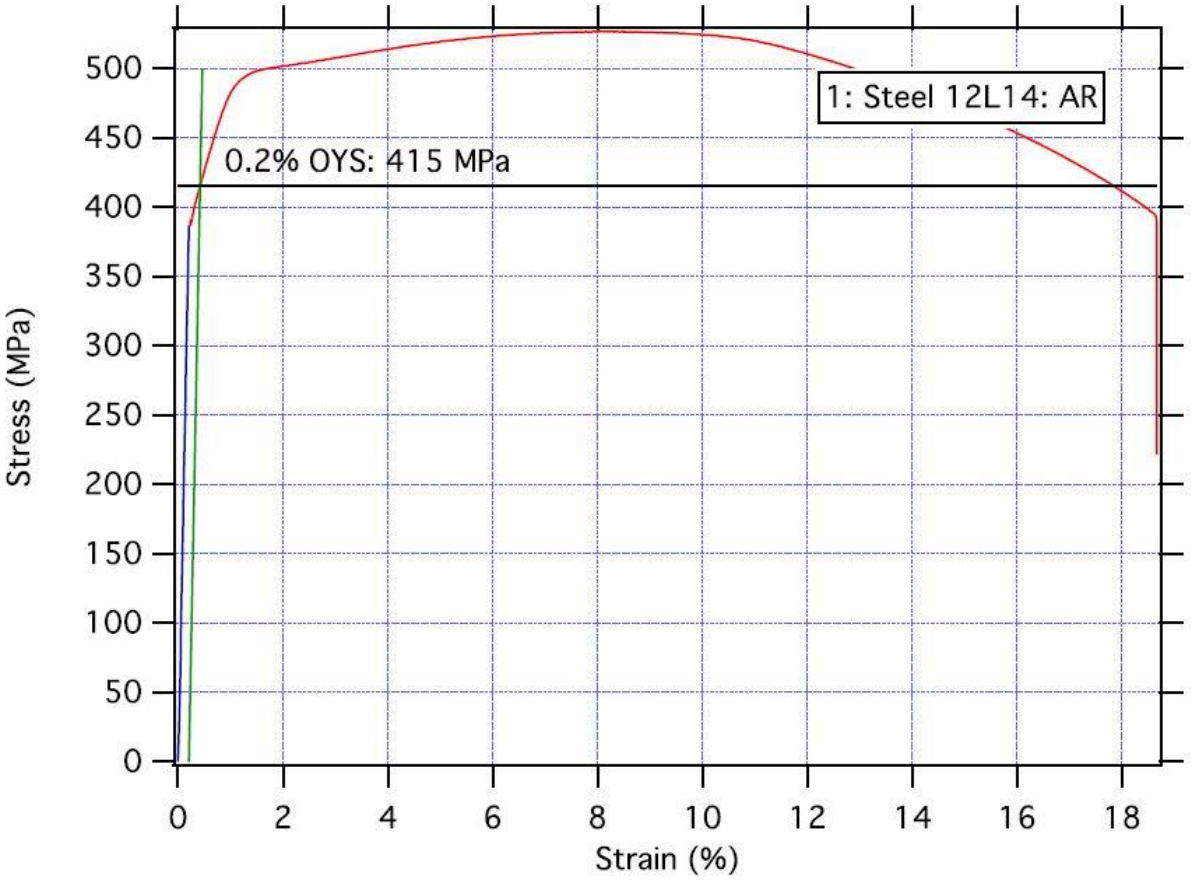

Tensile Testing Lab
ME843

Figure C.2: Anchor Stress Strain #2

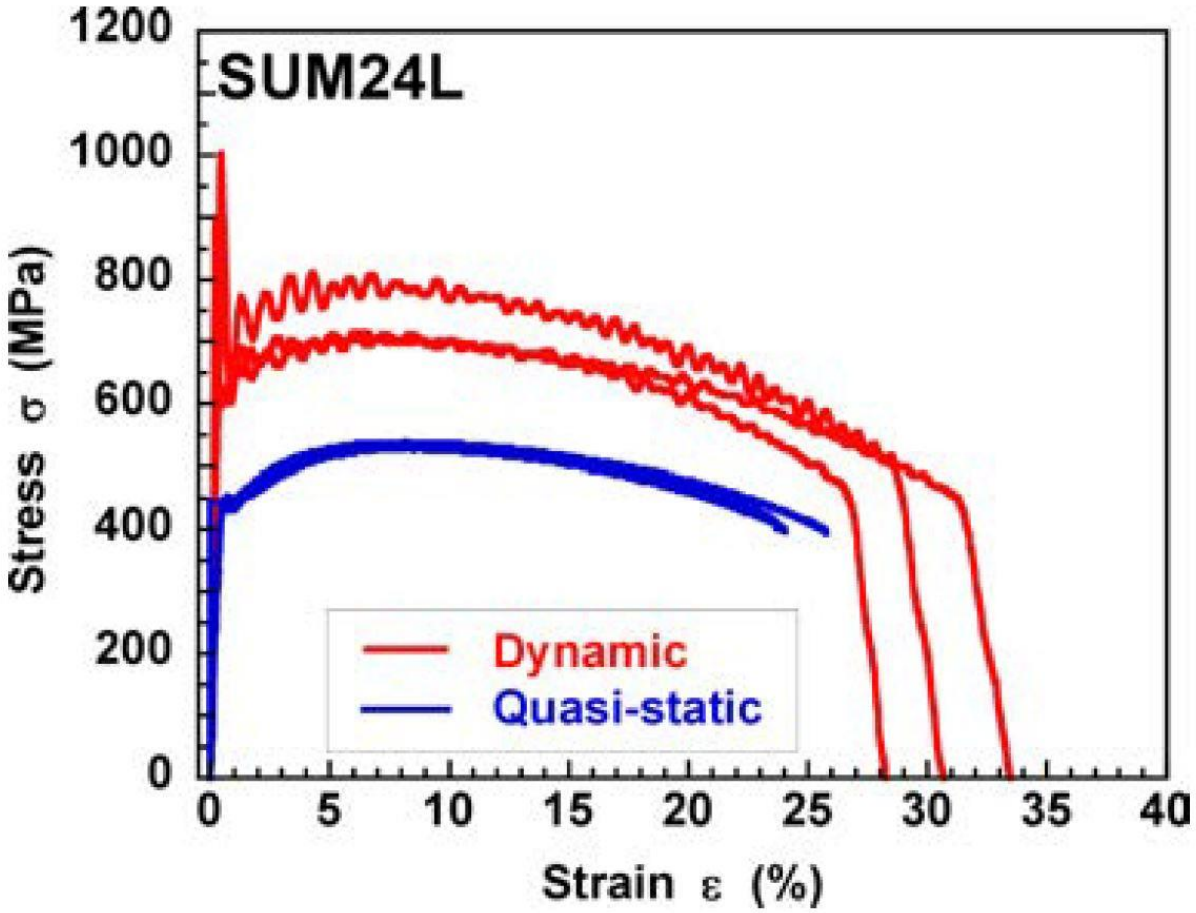

Mechanical Characterization of Pre-Fatigued Free-Cutting Steels under Dynamic Tension
Masaaki ITABASHI, Heikichi KOSEKI

Figure C.3: Anchor Stress Strain #3

Appendix D: Input Files

Basic Standard Model
(No Geometry)

```
*Nset, nset=StrandN
 8565,
*Nset, nset="Wedge  Displacement", generate
4172, 5116,   16
*Elset, elset="Wedge  Displacement", generate
3269, 3884,   15
*Elset, elset=_Surf-9_S2, generate
4529, 4569,   1
*Surface, type=ELEMENT, name=Surf-9
_Surf-9_S2, S2
*Elset, elset=_Surf-18_S6, generate
3269, 3884,   15
*Elset, elset=_Surf-18_S6, generate
3899, 4514,   15
*Surface, type=ELEMENT, name=Surf-18
_Surf-18_S6, S6
*Amplitude, name=Amp-2, definition=EQUALLY SPACED, fixed interval=1.
          0.,           1.
*Amplitude, name=Amp-3, definition=SMOOTH STEP
          0.,           0.,           1.,           1.
*Amplitude, name=Amp-4, time=TOTAL TIME, definition=EQUALLY SPACED, fixed
interval=1.
          0.,           1.
**
** MATERIALS
**
*Material, name=Anchor
*Density
 0.284,
*Elastic
 2.8891e+07, 0.35
*Plastic
 61678.4,        0.
 70435.1, 0.00551794
 72853.3,  0.0152181
 75598.4,  0.0248015
 78142.8,  0.0343033
 79361.9,   0.043796
 81536.8,  0.0531379
 82906.6,  0.0624414
 83820.8,  0.0716863
 84526.6,  0.0808585
```

```
 85088.3,  0.0899557
 84568.2,  0.0990382
  83977.,   0.108044
 83018.2,   0.116993
 84738.3,   0.125696
 84091.6,    0.13447
 67898.1,   0.144147
** Elasto-Plastic
*Material, name=Tendon
*Density
 0.28,
*Elastic
 2.8018e+07, 0.3
*Plastic
254432.,          0.
262580., 0.000578517
266876.,   0.0014148
269160.,  0.00232191
270437.,  0.00326399
271378.,  0.00421706
271984.,  0.00518117
272420.,  0.00615031
272689.,  0.00712451
273465.,  0.00807961
274072.,  0.00903976
275020.,  0.00998681
275459.,    0.010951
276239.,   0.0119022
277360.,   0.0128401
278313.,   0.0137832
279266.,   0.0147252
280222.,   0.0156663
281349.,   0.0166002
282478.,   0.0175332
283437.,   0.0184712
284569.,   0.0194022
285703.,   0.0203321
286667.,   0.0212672
287632.,   0.0222012
288426.,   0.0231405
289394.,   0.0240726
290018.,    0.025016
290815.,   0.0259524
291786.,   0.0268816
292413.,   0.0278221
293041.,   0.0287617
```

293669., 0.0297004
294817., 0.0306195
295274., 0.0315625
295557., 0.0325107
296014., 0.0334518
296645., 0.0343857
297277., 0.0353187
297735., 0.036257
297845., 0.0372069
298303., 0.0381433
298587., 0.0390851
299222., 0.0400135
299681., 0.0409472
299790., 0.0418925
300250., 0.0428244
300535., 0.0437617
300644., 0.0447043
301104., 0.0456335
301036., 0.0465807
301673., 0.0475018
301781., 0.0484409
302243., 0.0493665
302350., 0.0503038
297015., 0.0507229
297294., 0.0516534
297400., 0.0525892
297679., 0.0535179
297958., 0.0544458
298412., 0.0553667
** Elastic
*Material, name="Wedge Steel"
*Density
0.284,
*Elastic
2.9e+07, 0.35
**
** INTERACTION PROPERTIES
**
*Surface Interaction, name="Anchor Wedge"
*Friction
0.2,
*Surface Behavior, pressure-overclosure=HARD
*Surface Interaction, name="Strand Wedge Displacement"
*Friction, rough
*Surface Behavior, pressure-overclosure=HARD
*Surface Interaction, name="Strand Wedge Loading"

```
*Friction
0.,
*Surface Interaction, name="Wedge Wedge"
*Surface Behavior, pressure-overclosure=HARD
**
** BOUNDARY CONDITIONS
**
** Name: BC-1 Type: Displacement/Rotation
*Boundary
"Bottom of Anchor", 1, 1
"Bottom of Anchor", 2, 2
"Bottom of Anchor", 3, 3
"Bottom of Anchor", 4, 4
"Bottom of Anchor", 5, 5
"Bottom of Anchor", 6, 6
** ----------------------------------------------------------------
**
** STEP: seatingload
**
*Step, name=seatingload, nlgeom=YES
*Dynamic, Explicit
, 0.5
*Bulk Viscosity
0.06, 1.2
**
** LOADS
**
** Name: Load-1   Type: Pressure
*Dsload
Surf-18, P, 1000.
**
** INTERACTIONS
**
** Interaction: Anchor Wedge 2
*Contact Pair, interaction="Anchor Wedge", mechanical constraint=KINEMATIC,
cpset="Anchor Wedge 2"
"Standard sweep-2_Outer wedge", "Anchor-1_inner anchor"
** Interaction: CP-3-Tendon-1-Standard sweep-1 (Load)
*Contact Pair, interaction="Strand Wedge Loading", mechanical constraint=KINEMATIC,
cpset="CP-3-Tendon-1-Standard sweep-1 (Load)"
Tendon-1_Tendon, "Standard sweep-1_InnerWedge"
** Interaction: CP-4-Tendon-1-Standard sweep-2 (Load)
*Contact Pair, interaction="Strand Wedge Loading", mechanical constraint=KINEMATIC,
cpset="CP-4-Tendon-1-Standard sweep-2 (Load)"
Tendon-1_Tendon, "Standard sweep-2_InnerWedge"
** Interaction: Wedge Anchor 1
```

*Contact Pair, interaction="Anchor Wedge", mechanical constraint=KINEMATIC,
cpset="Wedge Anchor 1"
"Standard sweep-1_Outer wedge", "Anchor-1_inner anchor"
**
** OUTPUT REQUESTS
**
*Restart, write, number interval=1, time marks=NO
*Output, field, number interval=0
*Output, history, frequency=0
*End Step
** --
**
** STEP: Step-1
**
*Step, name=Step-1, nlgeom=YES
*Dynamic, Explicit
, 1.
*Bulk Viscosity
0.06, 1.2
**
** BOUNDARY CONDITIONS
**
** Name: displacement Type: Displacement/Rotation
*Boundary, amplitude=Amp-2
"Bottom Of Strand", 1, 1
"Bottom Of Strand", 2, 2
"Bottom Of Strand", 3, 3, -2.
"Bottom Of Strand", 4, 4
"Bottom Of Strand", 5, 5
"Bottom Of Strand", 6, 6
**
** LOADS
**
** Name: Load-1   Type: Pressure
*Dsload, op=NEW
**
** INTERACTIONS
**
** Interaction: CP-3-Tendon-1-Standard sweep-1 (Disp)
*Contact Pair, interaction="Strand Wedge Displacement", mechanical constraint=KINEMATIC,
cpset="CP-3-Tendon-1-Standard sweep-1 (Disp)"
Tendon-1_Tendon, "Standard sweep-1_InnerWedge"
** Interaction: CP-3-Tendon-1-Standard sweep-1 (Load)
*Contact Pair, op=DELETE, cpset="CP-3-Tendon-1-Standard sweep-1 (Load)"
Tendon-1_Tendon, "Standard sweep-1_InnerWedge"
** Interaction: CP-4-Tendon-1-Standard sweep-2 (Disp)

*Contact Pair, interaction="Strand Wedge Displacement", mechanical constraint=KINEMATIC, cpset="CP-4-Tendon-1-Standard sweep-2 (Disp)"
Tendon-1_Tendon, "Standard sweep-2_InnerWedge"
** Interaction: CP-4-Tendon-1-Standard sweep-2 (Load)
*Contact Pair, op=DELETE, cpset="CP-4-Tendon-1-Standard sweep-2 (Load)"
Tendon-1_Tendon, "Standard sweep-2_InnerWedge"
** Interaction: Wedge to Wedge
*Contact, op=NEW
*Contact Inclusions, ALL EXTERIOR
*Contact Property Assignment
, , "Wedge Wedge"
**
** OUTPUT REQUESTS
**
*Restart, write, number interval=1, time marks=NO
**
** FIELD OUTPUT: F-Output-1
**
*Output, field
*Node Output
A, AR, AT, CF, RF, RM, RT, U
UR, UT, V, VR, VT
*Element Output, directions=YES
BF, CTSHR, E, EFABRIC, ER, ERV, GRAV, HP, IWCONWEP, LE, MISES, MISESMAX, MISESONLY, NE, NFORC, NFORCSO
P, PE, PEEQ, PEEQMAX, PEEQT, PEEQVAVG, PEMAG, PEQC, PEVAVG, PRESSONLY, PS, S, SBF, SE, SF, SFABRIC
SSAVG, STAGP, SVAVG, TRIAX, TRNOR, TRSHR, TSHR, VE, VEEQ, VP, VS
**
** HISTORY OUTPUT: AnchorN
**
**
** HISTORY OUTPUT: displacement
**
*Output, history
*Node Output, nset="Bottom Of Strand"
U3,
**
** HISTORY OUTPUT: Force
**
*Node Output, nset="Bottom of Anchor"
CF1, CF2, CF3, CM1, CM2, CM3, RF1, RF2
RF3, RM, RM1, RM2, RM3, RT, RWM
*Element Output, elset="Bottom of Anchor"
NFORC, NFORCSO, SF1, SF2, SF3, SM1, SM2, SM3
**

```
** HISTORY OUTPUT: Reaction
**
*Node Output, nset="Bottom of Anchor"
RF3,
**
** HISTORY OUTPUT: StrandN
**
**
** HISTORY OUTPUT: Wedge displacement
** This took too long
*Node Output, nset="Wedge  Displacement"
U3,
*End Step
```

Basic Modified Model
(No Geometry)

*Nset, nset=StrandN
 6645,
*Nset, nset="Top of Wedges"
9884,9886,9903,9904,9944,9946,9963,9964,10004,10006,10023,10024,10064,10066,10083,100
84
10124,10126,10143,10144,10184,10186,10203,10204,10244,10246,10263,10264,10304,10306,1
0323,10324
10364,10366,10383,10384,10424,10426,10443,10444,10484,10486,10503,10504,10544,10546,1
0563,10564
10604,10606,10623,10624,10664,10666,10683,10684,10724,10726,10743,10744
*Nset, nset="Top of Wedges"
10784,10786,10803,10804,10844,10846,10863,10864,10904,10906,10923,10924,10964,10966,1
0983,10984
11024,11026,11043,11044,11084,11086,11103,11104,11144,11146,11163,11164,11204,11206,1
1223,11224
11264,11266,11283,11284,11324,11326,11343,11344,11384,11386,11403,11404,11444,11446,1
1463,11464
11504,11506,11523,11524,11564,11566,11583,11584,11624,11626,11643,11644
*Elset, elset="Top of Wedges"
7823,7835,7836,7865,7877,7878,7907,7919,7920,7949,7961,7962,7991,8003,8004,8033
8045,8046,8075,8087,8088,8117,8129,8130,8159,8171,8172,8201,8213,8214,8243,8255
8256,8285,8297,8298,8327,8339,8340,8369,8381,8382
*Elset, elset="Top of Wedges"
8411,8423,8424,8453,8465,8466,8495,8507,8508,8537,8549,8550,8579,8591,8592,8621
8633,8634,8663,8675,8676,8705,8717,8718,8747,8759,8760,8789,8801,8802,8831,8843
8844,8873,8885,8886,8915,8927,8928,8957,8969,8970
*Nset, nset="Wedge Displacement"
10784,10786,10803,10804,10844,10846,10863,10864,10904,10906,10923,10924,10964,10966,1
0983,10984
11024,11026,11043,11044,11084,11086,11103,11104,11144,11146,11163,11164,11204,11206,1
1223,11224
11264,11266,11283,11284,11324,11326,11343,11344,11384,11386,11403,11404,11444,11446,1
1463,11464
11504,11506,11523,11524,11564,11566,11583,11584,11624,11626,11643,11644
*Elset, elset="Wedge Displacement"
8411,8423,8424,8453,8465,8466,8495,8507,8508,8537,8549,8550,8579,8591,8592,8621
8633,8634,8663,8675,8676,8705,8717,8718,8747,8759,8760,8789,8801,8802,8831,8843
8844,8873,8885,8886,8915,8927,8928,8957,8969,8970
*Elset, elset=_Surf-3_S4, generate
7823, 8369,   42
*Elset, elset=_Surf-3_S4, generate
8411, 8957,   42

```
*Elset, elset=_Surf-3_S5
7835,7836,7877,7878,7919,7920,7961,7962,8003,8004,8045,8046,8087,8088,8129,8130
8171,8172,8213,8214,8255,8256,8297,8298,8339,8340,8381,8382
*Elset, elset=_Surf-3_S5
8423,8424,8465,8466,8507,8508,8549,8550,8591,8592,8633,8634,8675,8676,8717,8718
8759,8760,8801,8802,8843,8844,8885,8886,8927,8928,8969,8970
*Surface, type=ELEMENT, name=Surf-3
_Surf-3_S4, S4
_Surf-3_S5, S5
*Elset, elset=_Surf-9_S2, generate
3269, 3309,  1
*Surface, type=ELEMENT, name=Surf-9
_Surf-9_S2, S2
*Amplitude, name=Amp-2, definition=EQUALLY SPACED, fixed interval=1.
        0.,          1.
*Amplitude, name=Amp-3, definition=SMOOTH STEP
        0.,          0.,          1.,          1.
*Amplitude, name=Amp-4, time=TOTAL TIME, definition=EQUALLY SPACED, fixed
interval=1.
        0.,          1.
**
** MATERIALS
**
*Material, name=Anchor
*Density
 0.284,
*Elastic
 2.8891e+07, 0.35
*Plastic
 61678.4,        0.
 70435.1, 0.00551794
 72853.3,  0.0152181
 75598.4,  0.0248015
 78142.8,  0.0343033
 79361.9,   0.043796
 81536.8,  0.0531379
 82906.6,  0.0624414
 83820.8,  0.0716863
 84526.6,  0.0808585
 85088.3,  0.0899557
 84568.2,  0.0990382
  83977.,   0.108044
 83018.2,   0.116993
 84738.3,   0.125696
 84091.6,    0.13447
 67898.1,   0.144147
```

** Elasto-Plastic
*Material, name=Tendon
*Density
 0.28,
*Elastic
 2.8018e+07, 0.3
*Plastic
254432.,   0.
262580., 0.000578517
266876.,   0.0014148
269160., 0.00232191
270437., 0.00326399
271378., 0.00421706
271984., 0.00518117
272420., 0.00615031
272689., 0.00712451
273465., 0.00807961
274072., 0.00903976
275020., 0.00998681
275459.,   0.010951
276239.,   0.0119022
277360.,   0.0128401
278313.,   0.0137832
279266.,   0.0147252
280222.,   0.0156663
281349.,   0.0166002
282478.,   0.0175332
283437.,   0.0184712
284569.,   0.0194022
285703.,   0.0203321
286667.,   0.0212672
287632.,   0.0222012
288426.,   0.0231405
289394.,   0.0240726
290018.,   0.025016
290815.,   0.0259524
291786.,   0.0268816
292413.,   0.0278221
293041.,   0.0287617
293669.,   0.0297004
294817.,   0.0306195
295274.,   0.0315625
295557.,   0.0325107
296014.,   0.0334518
296645.,   0.0343857
297277.,   0.0353187

297735., 0.036257
297845., 0.0372069
298303., 0.0381433
298587., 0.0390851
299222., 0.0400135
299681., 0.0409472
299790., 0.0418925
300250., 0.0428244
300535., 0.0437617
300644., 0.0447043
301104., 0.0456335
301036., 0.0465807
301673., 0.0475018
301781., 0.0484409
302243., 0.0493665
302350., 0.0503038
297015., 0.0507229
297294., 0.0516534
297400., 0.0525892
297679., 0.0535179
297958., 0.0544458
298412., 0.0553667
** Elastic
*Material, name="Wedge Steel"
*Density
0.284,
*Elastic
2.9e+07, 0.35
**
** INTERACTION PROPERTIES
**
*Surface Interaction, name="Anchor Wedge"
*Friction
0.2,
*Surface Behavior, pressure-overclosure=HARD
*Surface Interaction, name="Strand Wedge Displacement"
*Friction, rough
*Surface Behavior, pressure-overclosure=HARD
*Surface Interaction, name="Strand Wedge Loading"
*Friction
0.,
*Surface Interaction, name="Wedge Wedge"
*Surface Behavior, pressure-overclosure=HARD
**
** BOUNDARY CONDITIONS
**

```
** Name: BC-1 Type: Displacement/Rotation
*Boundary
"Bottom of Anchor", 1, 1
"Bottom of Anchor", 2, 2
"Bottom of Anchor", 3, 3
"Bottom of Anchor", 4, 4
"Bottom of Anchor", 5, 5
"Bottom of Anchor", 6, 6
** ----------------------------------------------------------------
**
** STEP: seatingload
**
*Step, name=seatingload, nlgeom=YES
*Dynamic, Explicit
, 0.5
*Bulk Viscosity
0.06, 1.2
**
** LOADS
**
** Name: Load-1   Type: Pressure
*Dsload
Surf-3, P, 1100.
**
** INTERACTIONS
**
** Interaction: Anchor Wedge 2
*Contact Pair, interaction="Anchor Wedge", mechanical constraint=KINEMATIC,
cpset="Anchor Wedge 2"
"Modified Sweep-2_OuterWedgeM", "Anchor-1_inner anchor"
** Interaction: CP-3-Tendon-1-Standard sweep-1 (Load)
*Contact Pair, interaction="Strand Wedge Loading", mechanical constraint=KINEMATIC,
cpset="CP-3-Tendon-1-Standard sweep-1 (Load)"
Tendon-1_Tendon, "Modified Sweep-1_Inner WedgeM"
** Interaction: CP-4-Tendon-1-Standard sweep-2 (Load)
*Contact Pair, interaction="Strand Wedge Loading", mechanical constraint=KINEMATIC,
cpset="CP-4-Tendon-1-Standard sweep-2 (Load)"
Tendon-1_Tendon, "Modified Sweep-2_Inner WedgeM"
** Interaction: Wedge Anchor 1
*Contact Pair, interaction="Anchor Wedge", mechanical constraint=KINEMATIC,
cpset="Wedge Anchor 1"
"Modified Sweep-1_OuterWedgeM", "Anchor-1_inner anchor"
**
** OUTPUT REQUESTS
**
*Restart, write, number interval=1, time marks=NO
```

```
*Output, field, number interval=0
*Output, history, frequency=0
*End Step
** ----------------------------------------------------------------
**
** STEP: Step-1
**
*Step, name=Step-1, nlgeom=YES
*Dynamic, Explicit
, 1.
*Bulk Viscosity
0.06, 1.2
**
** BOUNDARY CONDITIONS
**
** Name: displacement Type: Displacement/Rotation
*Boundary, amplitude=Amp-2
"Bottom Of Strand", 1, 1
"Bottom Of Strand", 2, 2
"Bottom Of Strand", 3, 3, -2.
"Bottom Of Strand", 4, 4
"Bottom Of Strand", 5, 5
"Bottom Of Strand", 6, 6
**
** LOADS
**
** Name: Load-1   Type: Pressure
*Dsload, op=NEW
**
** INTERACTIONS
**
** Interaction: CP-3-Tendon-1-Standard sweep-1 (Disp)
*Contact Pair, interaction="Strand Wedge Displacement", mechanical constraint=KINEMATIC,
cpset="CP-3-Tendon-1-Standard sweep-1 (Disp)"
Tendon-1_Tendon, "Modified Sweep-1_Inner WedgeM"
** Interaction: CP-3-Tendon-1-Standard sweep-1 (Load)
*Contact Pair, op=DELETE, cpset="CP-3-Tendon-1-Standard sweep-1 (Load)"
Tendon-1_Tendon, "Modified Sweep-1_Inner WedgeM"
** Interaction: CP-4-Tendon-1-Standard sweep-2 (Disp)
*Contact Pair, interaction="Strand Wedge Displacement", mechanical constraint=KINEMATIC,
cpset="CP-4-Tendon-1-Standard sweep-2 (Disp)"
Tendon-1_Tendon, "Modified Sweep-2_Inner WedgeM"
** Interaction: CP-4-Tendon-1-Standard sweep-2 (Load)
*Contact Pair, op=DELETE, cpset="CP-4-Tendon-1-Standard sweep-2 (Load)"
Tendon-1_Tendon, "Modified Sweep-2_Inner WedgeM"
** Interaction: Wedge to Wedge
```

```
*Contact, op=NEW
*Contact Inclusions, ALL EXTERIOR
*Contact Property Assignment
 ,  , "Wedge Wedge"
**
** OUTPUT REQUESTS
**
*Restart, write, number interval=1, time marks=NO
**
** FIELD OUTPUT: F-Output-1
**
*Output, field
*Node Output
A, AR, AT, CF, RF, RM, RT, U
UR, UT, V, VR, VT
*Element Output, directions=YES
BF, CTSHR, E, EFABRIC, ER, ERV, GRAV, HP, IWCONWEP, LE, MISES, MISESMAX,
MISESONLY, NE, NFORC, NFORCSO
P, PE, PEEQ, PEEQMAX, PEEQT, PEEQVAVG, PEMAG, PEQC, PEVAVG, PRESSONLY,
PS, S, SBF, SE, SF, SFABRIC
SSAVG, STAGP, SVAVG, TRIAX, TRNOR, TRSHR, TSHR, VE, VEEQ, VP, VS
**
** HISTORY OUTPUT: AnchorN
**
**
** HISTORY OUTPUT: displacement
**
*Output, history
*Node Output, nset="Bottom Of Strand"
U3,
**
** HISTORY OUTPUT: Force
**
*Node Output, nset="Bottom of Anchor"
CF1, CF2, CF3, CM1, CM2, CM3, RF1, RF2
RF3, RM, RM1, RM2, RM3, RT, RWM
*Element Output, elset="Bottom of Anchor"
NFORC, NFORCSO, SF1, SF2, SF3, SM1, SM2, SM3
**
** HISTORY OUTPUT: Reaction
**
*Node Output, nset="Bottom of Anchor"
RF3,
**
** HISTORY OUTPUT: StrandN
**
```

```
**
** HISTORY OUTPUT: Wedge displacement
** This took too long
*Node Output, nset="Wedge  Displacement"
U3,
*End Step
```

Appendix E: Comparison Data

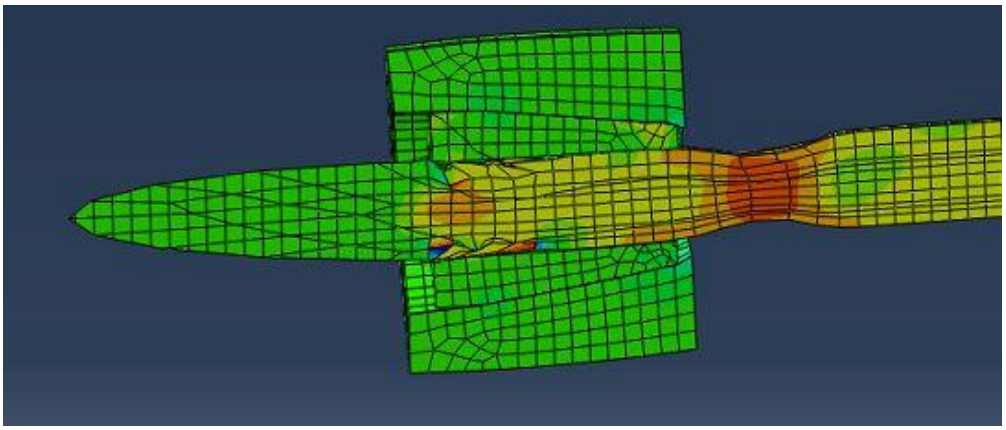

Figure E.1: Modified short wedge Friction = .01

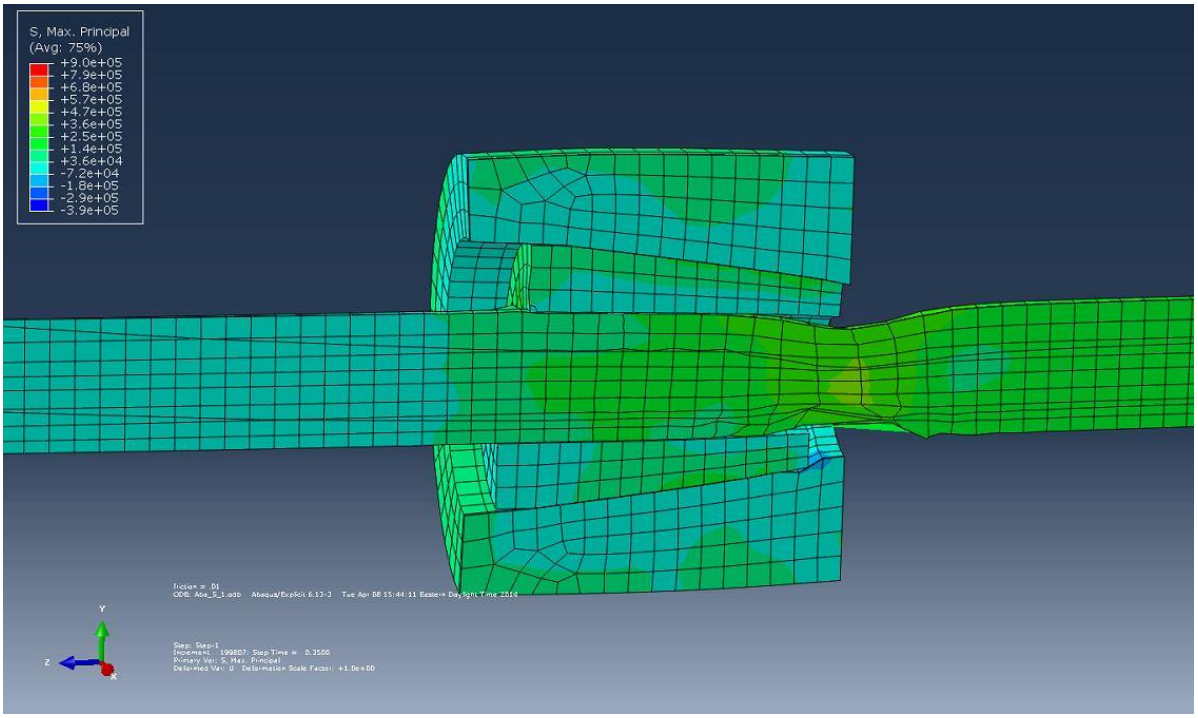

Figure E.2: Standard Wedge Friction = .01

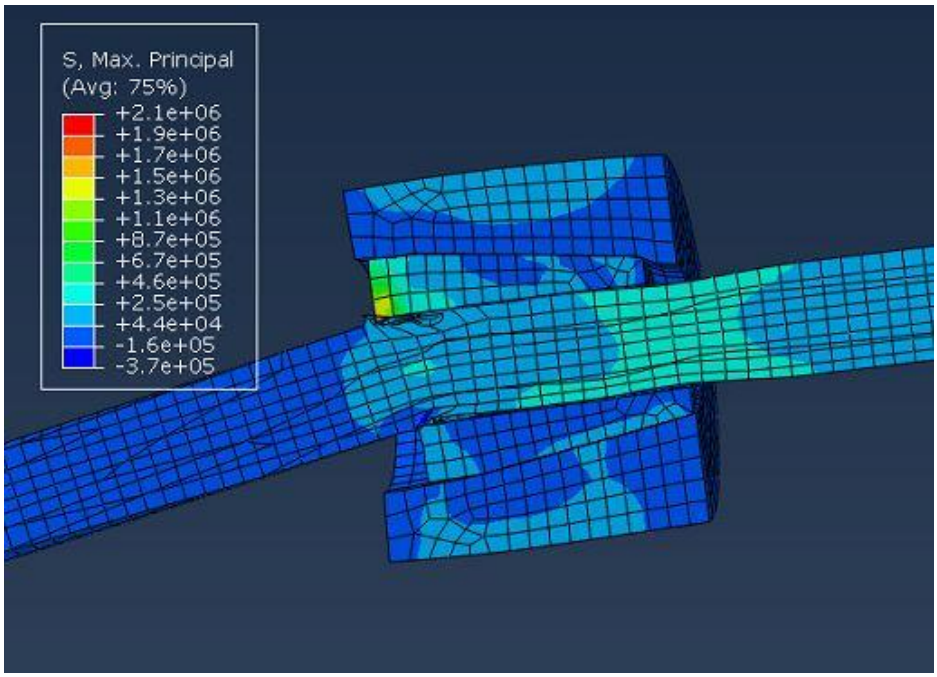

Figure E.3: Modified short wedge Friction = .11

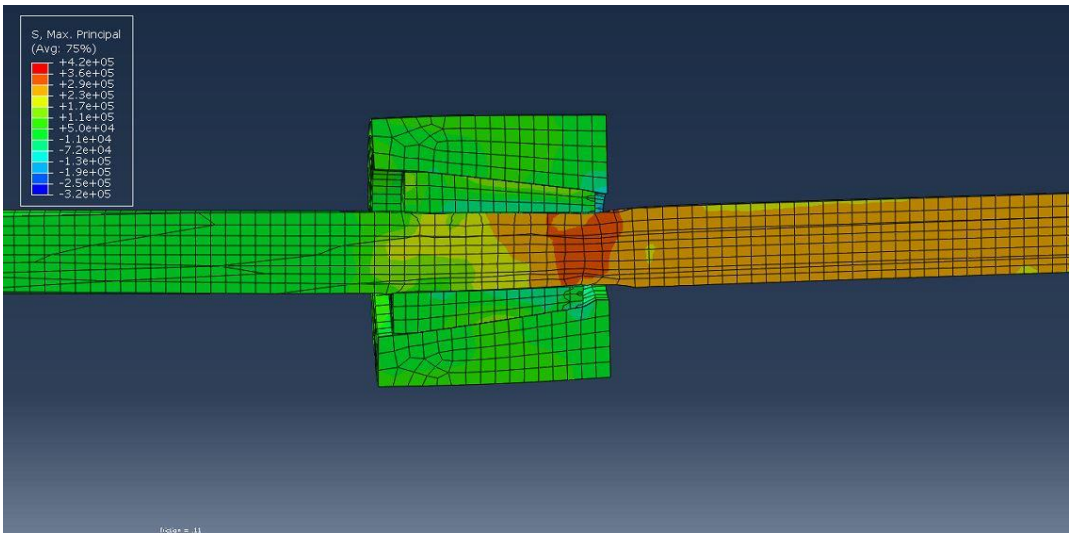

Figure E.4: Standard Wedge Friction = .11

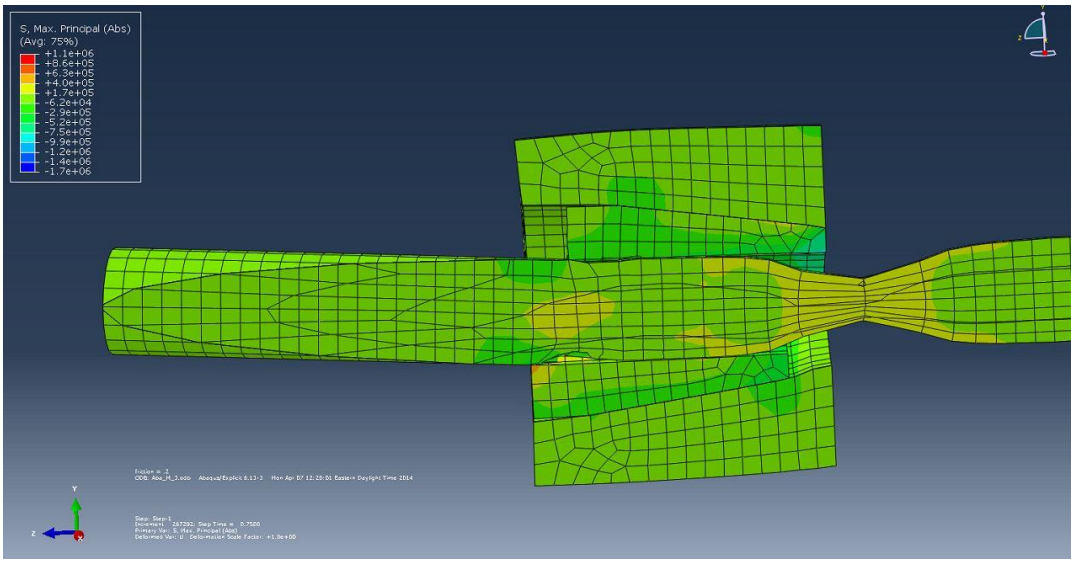

Figure E.5: Modified short wedge Friction = .2

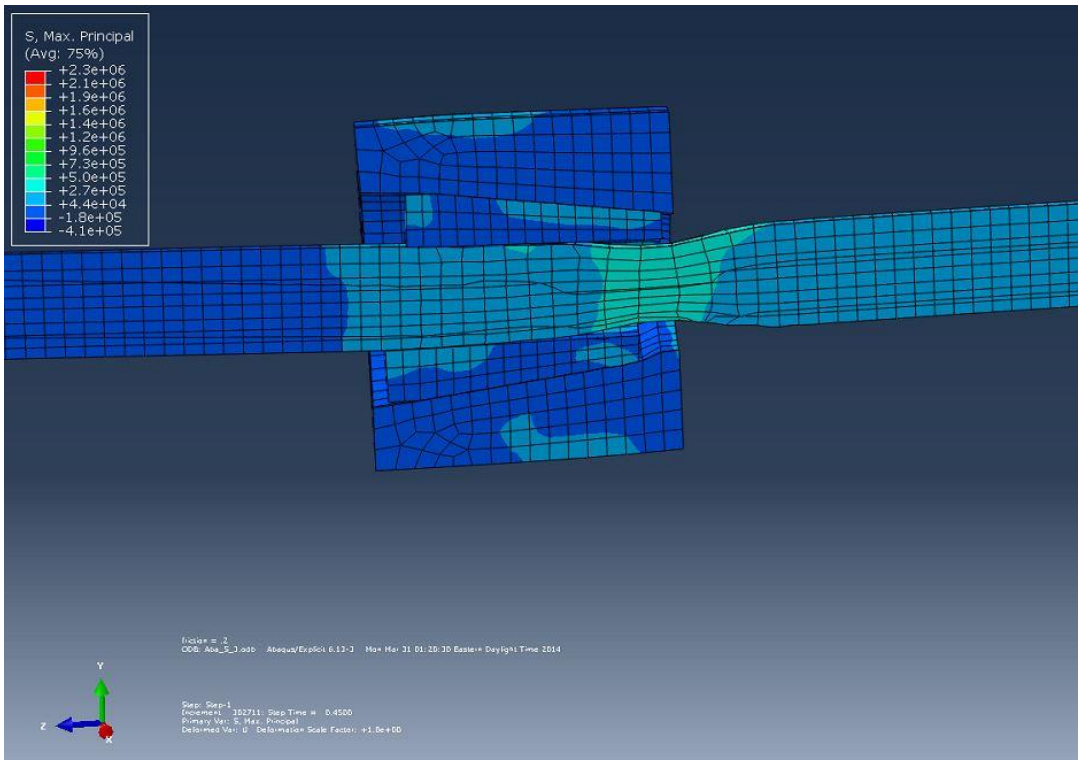

Figure E.6: Standard Wedge Friction = .2

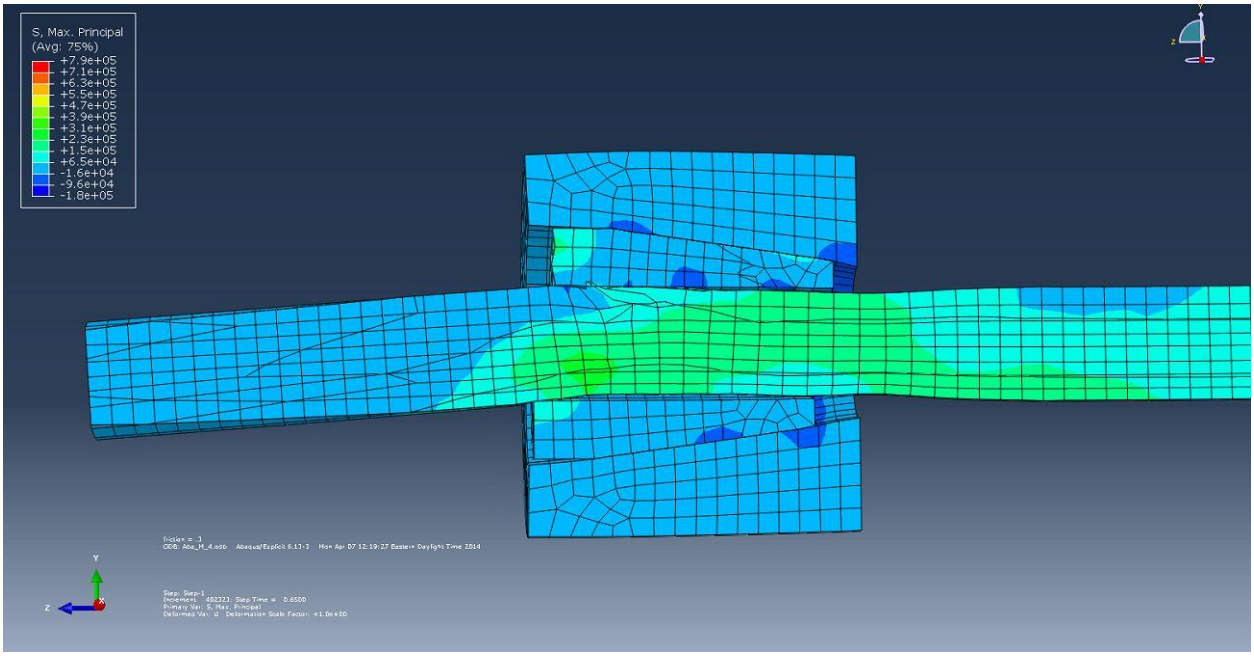

Figure E.7: Modified short wedge Friction = .3

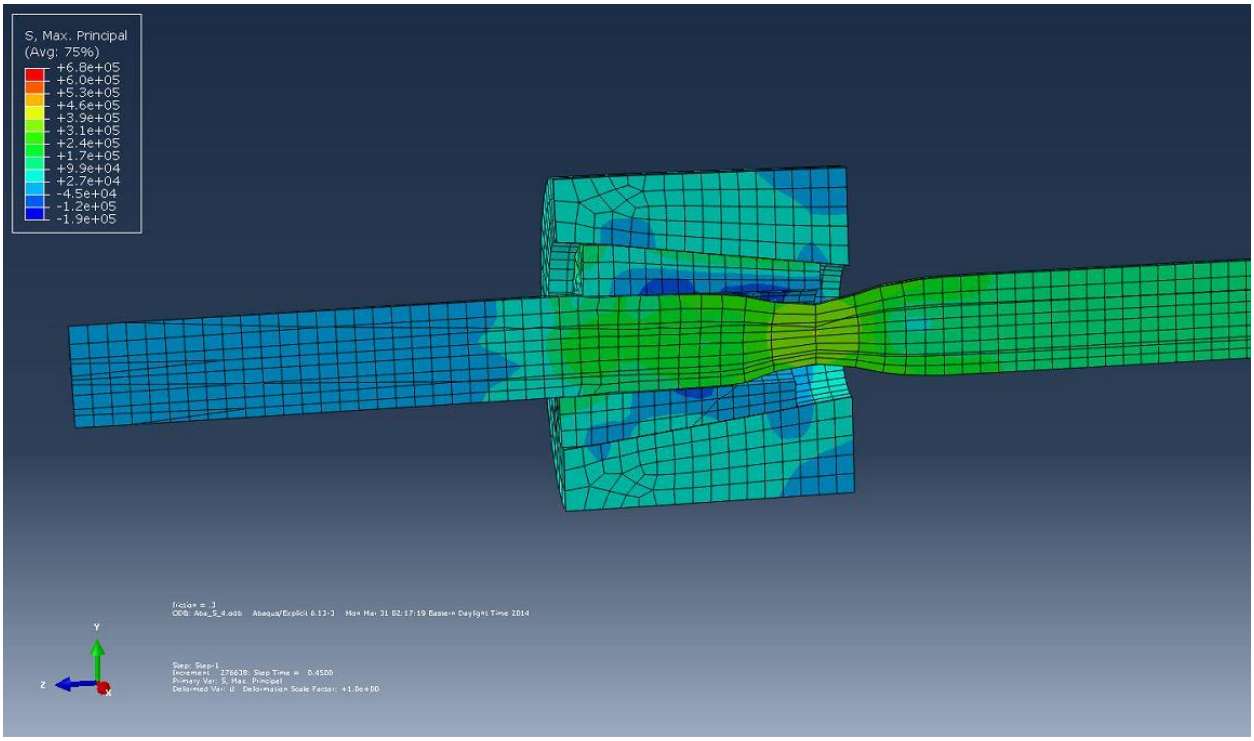

Figure E.8: Standard Wedge Friction = .3

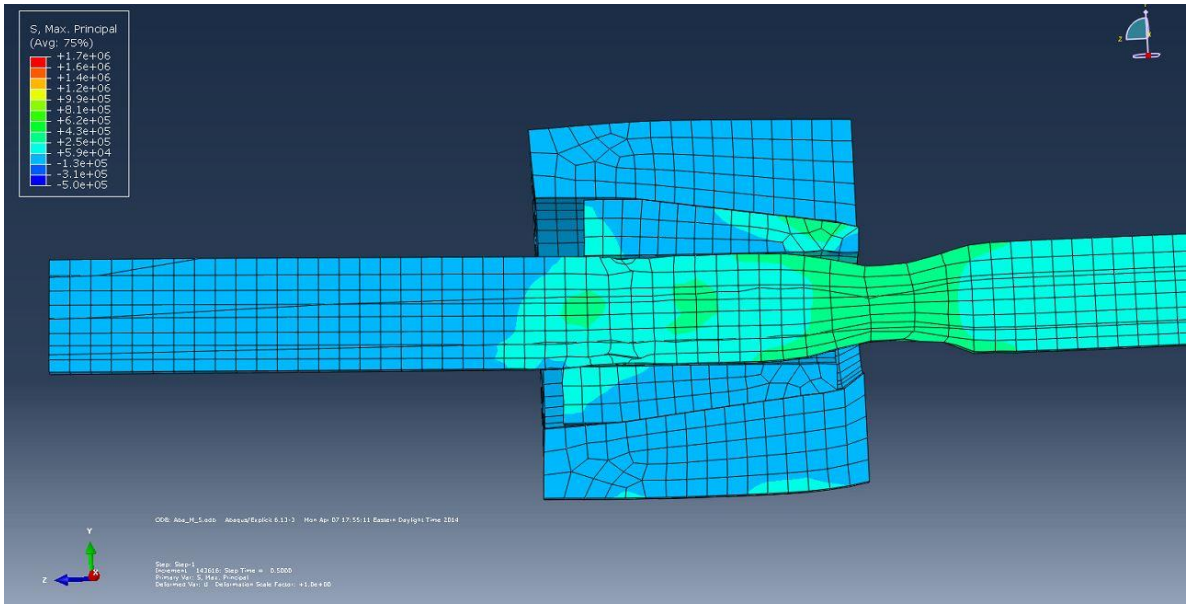

Figure E.9: Modified short wedge Friction = .00

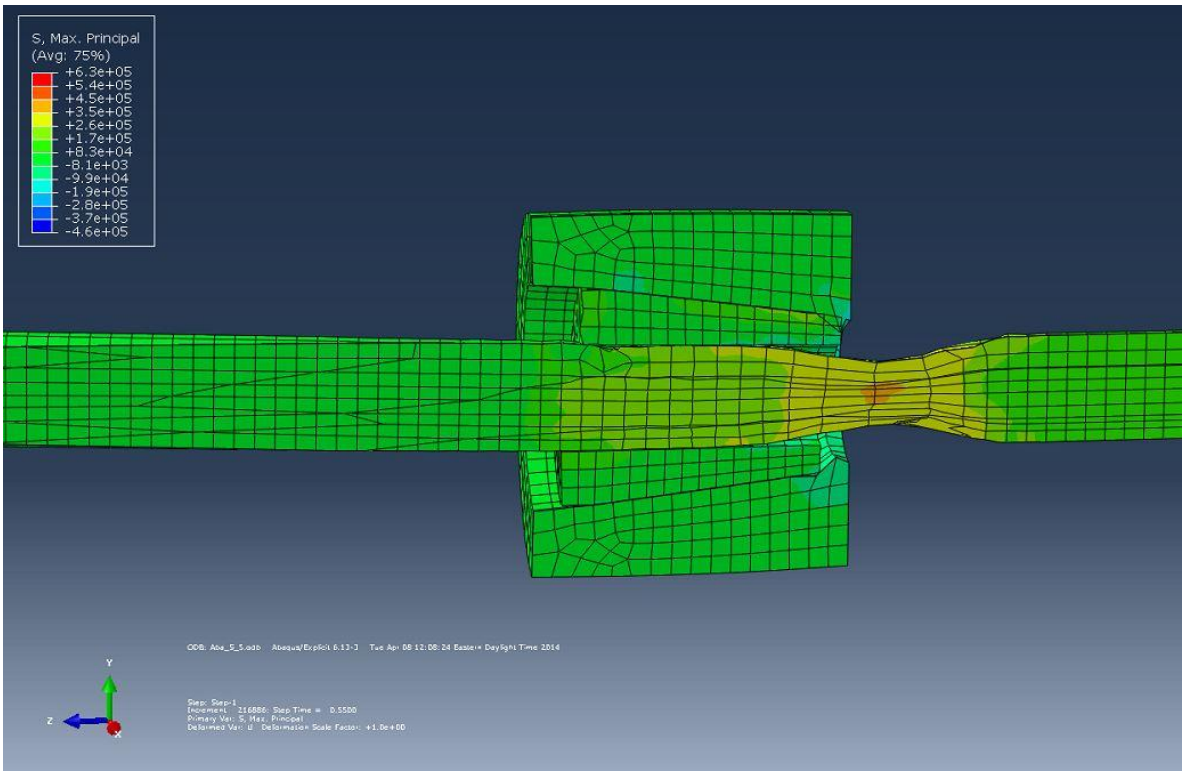

Figure E.10: Standard Wedge Friction = .00

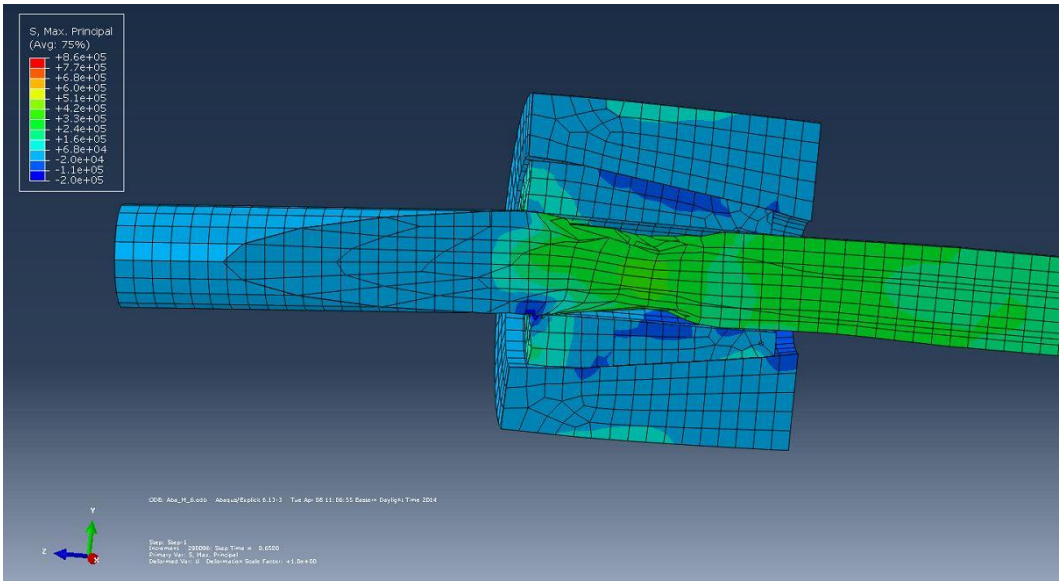

Figure E.11: Modified short wedge Friction = .5

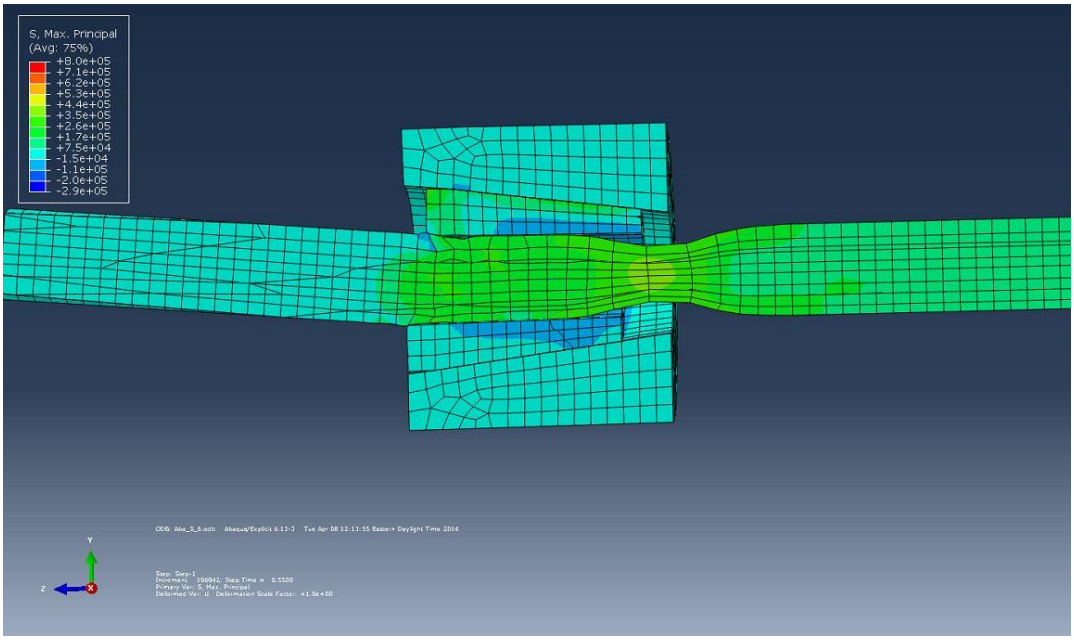

Figure E.12: Standard Wedge Friction = .5

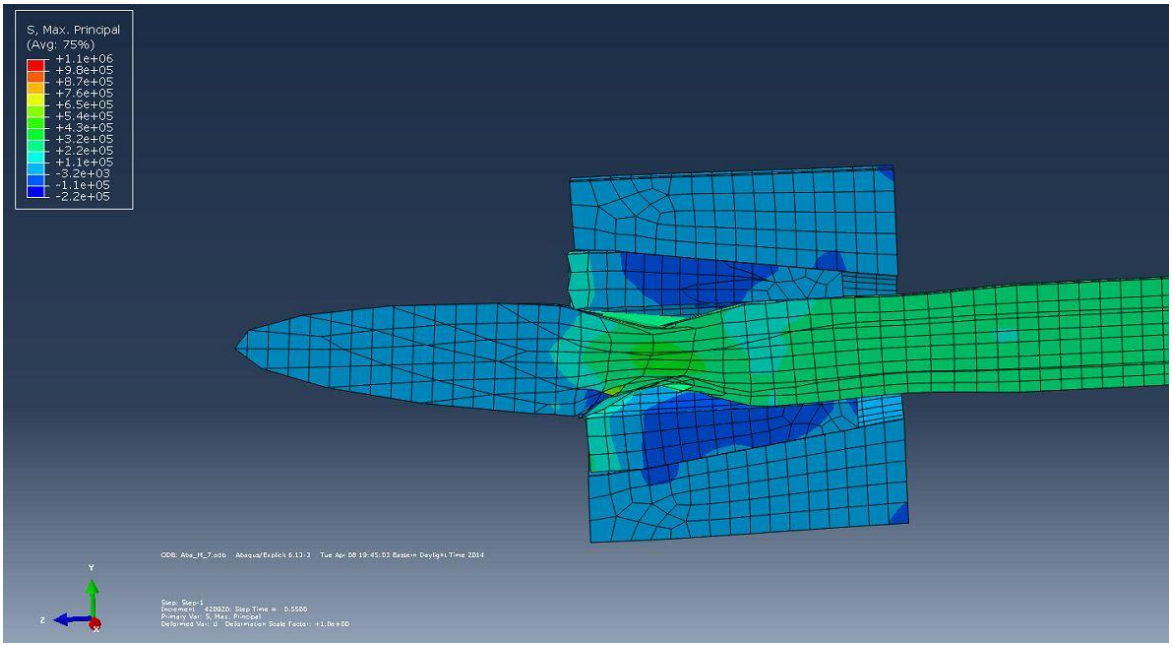

Figure E.13: Modified short wedge Friction = .6

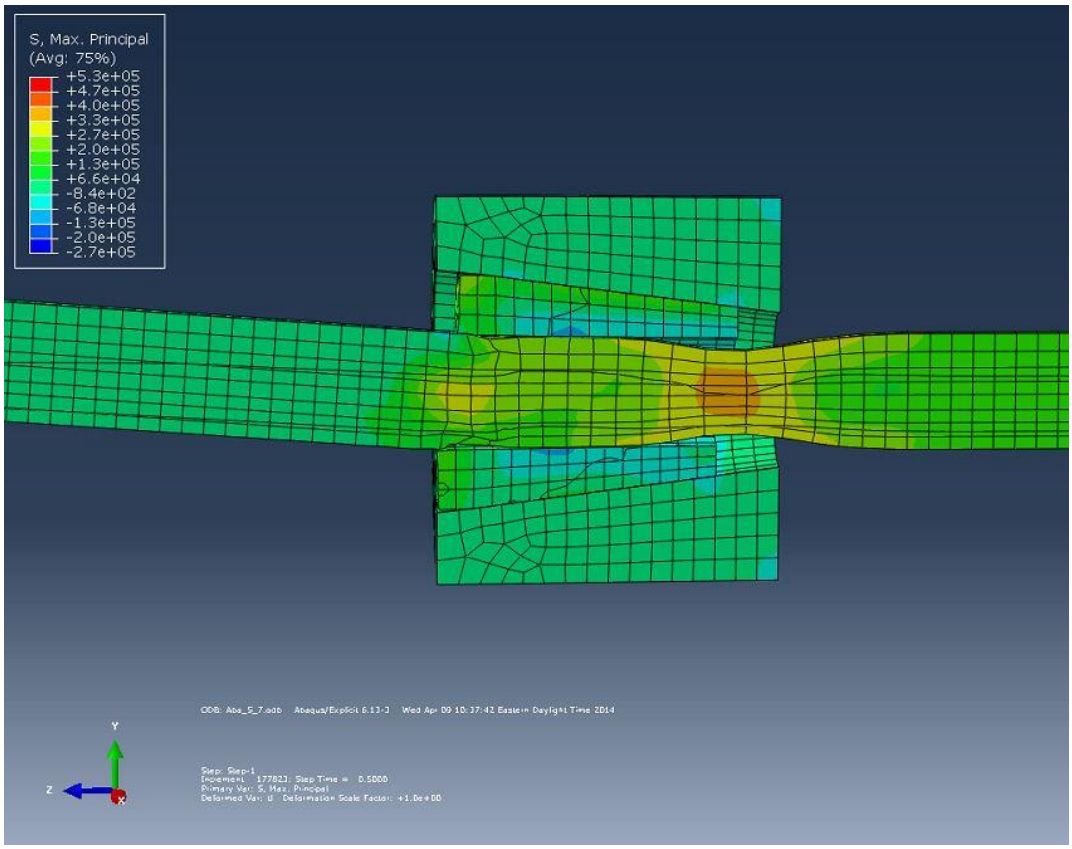

Figure E.14: Standard Wedge Friction = .6

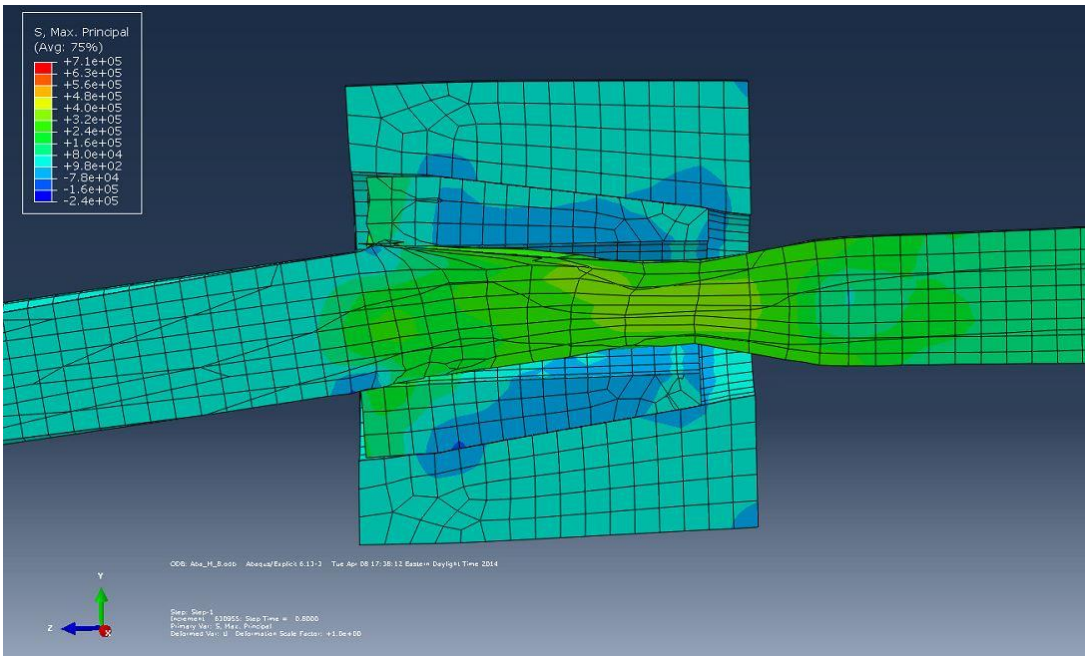

Figure E.15: Modified short wedge Friction = .7

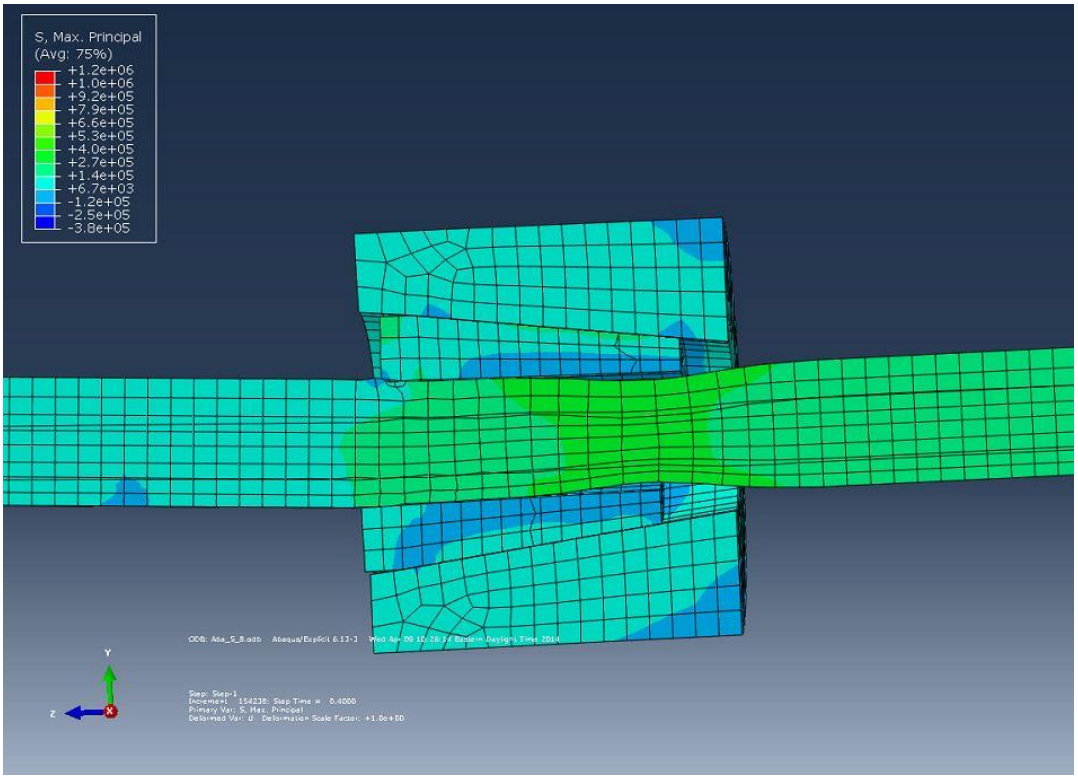

Figure E.16: Standard Wedge Friction = .7